RAY-TRACING WIRELESS CHANNEL MODELING AND VERIFICATION IN COORDINATED MULTI-POINT SYSTEMS

BY

MOHAMMAD HASAN SULEIMAN AMRO

A Thesis Presented to the
DEANSHIP OF GRADUATE STUDIES

KING FAHD UNIVERSITY OF PETROLEUM & MINERALS

DHAHRAN, SAUDI ARABIA

In Partial Fulfillment of the
Requirements for the Degree of

MASTER OF SCIENCE

In

TELECOMMUNICATION ENGINEERING

JANUARY 2014

KING FAHD UNIVERSITY OF PETROLEUM & MINERALS

DHAHRAN- 31261, SAUDI ARABIA

DEANSHIP OF GRADUATE STUDIES

This thesis, written by **MOHAMMAD HASAN SULEIMAN AMRO** under the direction of his thesis advisor and approved by his thesis committee, has been presented and accepted by the Dean of Graduate Studies, in partial fulfillment of the requirements for the degree of **MASTER OF SCIENCE IN TELECOMMUNICATION ENGINEERING.**

6-1-2014

Dr. Mohamed Adnan Landolsi
(Advisor)

Dr. Ali Ahmad Al-Shaikhi
Department Chairman

Dr. Salam Adel Zummo
(Co-Advisor)

Dr. Salam A. Zummo
Dean of Graduate Studies

Dr. Maan Abdulgader Kousa
(Member)

20/1/14
Date

6-1-2014

Dr. Samir Al-Ghadhban
(Member)

Dr. Wessam Mesbah
(Member)

To My Parents, My Wife and My Daughter

&

To My Late Grandfather (*Abu Amin*), My Teachers and My Family

ACKNOWLEDGMENT

All Praises be to Allah the Almighty, Who helped me to do this milestone beside the commitments towards my family, work, and other life obligations.

I would like to express my gratitude to both Dr. Adnan Landolsi & Prof. Salam Zummo who were my thesis advisors. This thesis work could not be achieved without their guidance, support, and encouragement. I also thank my thesis Committee members: Dr. Maan Kousa, Dr. Samir Al-Ghadhban, and Dr. Wessam Mesbah for their supportive comments and efforts that made this work of a better quality.

This thesis work was done in cooperation with Vodafone Chair for Mobile Communications Systems, Faculty of Electrical and Computer Engineering in Technical University of Dresden (TUD), and Actix GmbH, in Germany. My gratitude to Michael Grieger who was my main advisor in TUD, thanks to Prof. Gerhard Fettweis for allowing me to be a visiting student in his chair and for his encouragement. I also thank both Dr. Jens Voigt and Carsten Jandura from Actix for allowing me to work on Actix GmbH properties and for their support.

I am deeply grateful to my wife for her support, patience, and sacrifices of family time during my master program.

TABLE OF CONTENTS

LIST OF TABLES

LIST OF FIGURES

LIST OF ABBREVIATIONS

3G	:	3rd Generation
3GPP	:	3rd Generation Partnership Project
AWGN	:	Additive White Gaussian Noise
BS	:	Base Station
BER	:	Bit Error Rate
BLER	:	BLock Error Rate
BSC	:	Base Station Controller
BSS	:	Base Station Subsystem
C/I	:	Carrier-to-Interference ratio
CDF	:	Cumulative Distribution/Density Function
CDMA	:	Code Division Multiple Access
CE	:	Channel Element
CIR	:	Channel Impulse Response
CSI	:	Channel State Information
CoMP	:	Coordinated MultiPoint
COST	:	European COoperation in the field of Scientific and Technical research
DL	:	DownLink
DoA	:	Direction of Arrival
DS	:	Delay Spread
Easy-C	:	Enablers for Ambient Services and Systems, Part C

Ec/I0	:	Chip Energy over Interference
EDGE	:	Enhanced Data rates for GSM Evolution
eNB	:	Evolved NodeB
EPM	:	Empirical Propagation Model
EVM	:	Error Vector Magnitude
FBI	:	FeedBack Information
GPS	:	Global Positioning System
GO	:	Geometrical Optics
GSM	:	Global System for Mobile communication
ICT	:	Information and Communication Technology
IEEE	:	The Institute of Electrical and Electronics Engineers
ITU	:	International Telecommunication Union
Iub	:	Interface between an RNC and a Node B
JP	:	Joint Processing
JD	:	Joint Detection
Kbps	:	Kilo bits per second
KPI	:	Key Performance Indicator
LOS	:	Line Of Sight
NLOS	:	Non-Line of Sight
LTE-	:	Long Term Evolution
LTE-A	:	Long Term Evolution Advanced
MPC	:	Multi-Path Component
Mbps	:	Mega bits per second

MED	:	Mean Excess Delay
MIMO	:	Multiple Input Multiple Output
MISO	:	Multiple Input Single Output
MRC	:	Maximal Ratio Combining
MCS	:	Modulation and Coding Scheme
MS	:	Mobile Station
MU		Multi-User
NF	:	Noise Figure
NLOS	:	Non-LOS
NodeB	:	WCDMA BS
OFDM	:	Orthogonal Frequency Division Multiplexing
OFDMA	:	Orthogonal Frequency Division Multiple Access
OSS	:	Operations Support System
P-CPICH	:	Primary CPICH
QoS	:	Quality of Service
RPS	:	Radio Propagation Simulator
RSCP	:	Received Signal Code Power
RSSI	:	Received Signal Strength Indicator
RT	:	Ray Tracing
Rx	:	Receive
SaTO	:	Sample Time Offset
SIC	:	Successive Interference Cancellation
SCM	:	Spatial Channel Model

SCME	:	Spatial Channel Model Extension
SINR	:	Signal to Interference plus Noise Ratio
SNR	:	Signal to Noise Ratio
STO	:	Symbol Time Offset
SU	:	Single-User
TDMA	:	Time Division Multiplex
TDoA	:	Time Difference of Arrival
Theo.	:	Theoretical
UE	:	User Equipment
UL	:	UpLink
UMTS	:	Universal Mobile Telecommunications Systems
UTD	:	Uniform Theory of Diffraction
WINNER	:	Wireless World Initiative New Radio
WCDMA	:	Wideband Code Division Multiple Access
WGS-84	:	World Geodetic System 84
WiMAX	:	Worldwide interoperability for Microwave Access

THESIS ABSTRACT (English)

Full Name: MOHAMMAD HASAN SULEIMAN AMRO

Thesis Title: RAY-TRACING WIRELESS CHANNEL MODELING AND VERIFICATION USING COORDINATED MULTI-POINT SYSTEMS

Major Field: TELECOMMUNICATION ENGINEERING

Date of Degree: JANUARY 2014

Coordinated Multi-Point (CoMP) Multiple Input Multiple Output (MIMO) transmission improves user's coverage and data throughput particularly on the cell edges. Interference under CoMP is an advantage instead of being a disadvantage in traditional communication systems. In this work one of the world's largest CoMP testbeds is modelled in a Ray Tracing (RT) simulator. The main contribution of this thesis is to evaluate how close RT simulations can predict end to end system performance compared to the real-world measured performance. Both measured and RT simulated channels are processed in an offline tool chain that represents a Long Term Evolution (LTE) Advanced (LTE-A) system. CoMP and conventional MIMO systems performances are evaluated and compared for measured and simulated channels. The results show that the RT matches the measurements for the inter-site CoMP scenario by 88%. The deviations come from real hardware errors and the shortage of very detailed 3D objects in the RT model. Field measurements rates show high CoMP gain by around 43%, while RT CoMP gain is around 18%. Successive Interference Cancellation (SIC) approach improves the performance by around 10% at low Signal to Interference plus Noise Ratio (SINR). Field measurements had 10%

higher rates when using theoretical post-equalization schemes compared to Error Vector Magnitude (EVM) rates, while RT rates had around 5%. Geometrical analyses showed that an Inter-Carrier-Interference (ICI) is unlikely due to short inter-site distance in the testbed. Unlike field measurements, the RT Channel State Information (CSI) is known and therefore, channel estimation is eliminated for RT channels, which resulted in a low complexity CSI signal processing. This simplification increases RT accuracy by around 5%. These gave us confidence in the currently used channel estimator and open a door to investigate deeper in the future in tuning the estimator based on channels type and number of mobiles. The research covered analyses of Empirical Propagation Model (EPM) compared to RT model and discuss the advantages and disadvantages of each model.

ملخص الرسالة

الاسم: محمد حسن سليمان عمرو

عنوان الرسالة: نمذجة القنوات اللاسلكية بطريقة تتبع الشعاع والتحقق من خلال الانظمة المتعاونة متعددة النقاط

التخصص: ماجستير في علوم هندسة الاتصالات

تاريخ الدرجة العلمية: ربيع الأول 1435 الموافق لينار 2014

الانظمة التراسلية المتعاونة متعددة النقاط (CoMP) متعددة المدخلات متعددة المخرجات (MIMO) تحسن من تغطية وسرعة نقل البيانات لمستخدمين الشبكات الخلوية وخاصة على أطراف الخلية. التداخل في الاشارات هي ميزة تستغل من قبل الانظمة التراسلية المتعاونة متعددة النقاط بدلا من أن تكون مشكلة كما هو الحال في أنظمة الاتصالات الحاليه التقليدية. في هذه الرسالة تم نمذجة ومحاكاة القنوات اللاسلكية بطريقة تتبع الشعاع لإحدى أكبر الشبكات التجريبية في العالم للأنظمة المتعاونة متعددة النقاط. المساهمة الرئيسية لهذه الأطروحة هو تقييم مدى دقة محاكاة القنوات اللاسلكية بطريقة تتبع الشعاع وذلك من خلال مقارنة أدائها مع أداء القنوات اللاسلكية الناتجة من قياسات ميدانية في العالم الحقيقي. تمت التحقيقات والمقارنات بين هذين النوعين من القنوات اللاسلكية (المحاكاة والحقيقية) في بيئة معالجة مماثله للجيل الرابع المتقدم للاتصالات الخلوية والمعروف باسم التطور طويل الأمد المتقدم (LTE-Advanced). أظهرت النتائج تطابق القنوات اللاسلكية المحاكاة بطريقة تتبع الشعاع مع القنوات المقاسة حقيقيا بنسبة 88 ٪ وذلك عندما تكون محطات الارسال للأنظمة التراسلية المتعاونة متعددة النقاط متباعدة (Inter-Site CoMP). وجد بأن الاختلافات في النتائج تأتي من أخطاء الأجهزة الحقيقة أثناء القياسات الميدانيه من جهة ومن جهة أخرى بسبب نقص دقة مكونات الخرائط ثلاثية الأبعاد في بيئة المحاكاة بطريقة تتبع الشعاع. وجد أن الانظمة التراسلية المتعاونة متعددة النقاط تحقق مكاسب عالية في سرعة نقل البيانات بنحو 43 ٪ مقارنة بأنظمة الاتصالات التقليديه غير المتعاونة عندما تمت معالجة القياسات الميدانية، في حين انخفضت فائدة هذه الانظمة الى حوالي 18 ٪ عند معالجة القنوات اللاسلكية الناتجة بطريقة تتبع الشعاع. هذا الفرق يوضح أن المكاسب القادمة من القياسات الميدانيه التجريبية هي مبالغ فيها. اضافة تم معالجة القنوات اللاسلكية بطريقة الغاء التداخل المتعاقبة (SIC) وقد تحسن الأداء بنحو 10 ٪ عند تحقيق ومقارنة قوة الاشارة المفيدة الى التداخل بالإضافة إلى نسبة الضوضاء (SINR). كان القنوات الميدانية تعطي مؤشرا أعلى بنسبة 10 ٪ مقارنة مع القيمه الحقيقية المقاسة بطريقة قيمة الخطأ الاتجاهي (EVM)، في حين كانت المعدلات لقنوات اللاسلكية بطريقة تتبع الشعاع حوالي 5 ٪. أظهرت التحليلات الهندسية أن التداخل المشترك بين الترددات (ICI) هو من غير المحتمل حصوله بسبب المسافة القصيرة بين محطات الاستقبال (الخلايا) في الميدان وعلى غراره بيئة المحاكاة. على عكس القياسات الميدانية ، القنوات اللاسلكية بطريقة تتبع الشعاع تتميز بمعرفة حالتها بشكل تام (Perfect CSI) وبالتالي لاتوجد حاجه لتقدير القنوات (Estimation) مما أدى إلى تبسيط دوائر معالجة الإشارات. هذا التبسيط زاد من دقة النتائج للقنوات اللاسلكية بطريقة تتبع الشعاع بنحو 5 ٪. هذه النتيجة أوضحت مدى دقة معالج تقدير القناة (Channel Estimator) والمستخدم لكل من القنوات الميدانية والمحاكاة. اضافة الى ذلك من الممكن في المستقبل العمل على ضبط معالج تقدير القناة بحسب نوع بيئة الاتصال وعدد الهواتف الخلوية المستخدمه. نهاية تطرق البحث الى مقارنة بين نموذج محاكاة آخر مع نموذج طريقة تتبع الشعاع لمحاكاة القنوات اللاسلكية.ويسمى نموذج انتشار الموجات التجريبي (EPM) . تم تلخيص هذين النموذجين وتم مناقشة مزايا وعيوب كل نموذج.

CHAPTER 1

INTRODUCTION

The International Telecommunication Union (ITU) statistical report of Information and Communication Technology (ICT) issued on February, 2013 highlights that there are almost as many mobile subscriptions as people in the world, (around 7 billion) [1]. This steadily increasing demand for mobile communication services, mainly data services, is being addressed through the latest data oriented technologies. These started to evolve in the last decade, such as Universal Mobile Telecommunications System (UMTS), Worldwide interoperability for Microwave Access (WiMAX) and Long Term Evolution (LTE). The big obstacle facing this growth is the limited frequency spectrum, which has become the most precious resource [2].

In [3], a comparison between Orthogonal Frequency Division Multiple Access (OFDMA) and Code Division Multiple Access (CDMA) systems (both have frequency reuse factor of one) gives superiority to OFDMA systems on CDMA ones due to their higher spectral efficiencies. Spectral efficiency is defined as the maximum achievable throughput per bandwidth in (bits/Sec/Hz) [4].

LTE is an example of an OFDM based system that uses Multiple-Input Multiple-Output (MIMO) technique. MIMO can greatly increase communications channel capacity without the expansion of bandwidth, therefore it has recently received high interest in research [5],[4]. In [6] and [7], LTE can effectively increase the throughput and reduce Block Error Rate (BLER) of the users. However, if the targeted user is located at the edge

of the cell, MIMO will not get a good performance due to the high co-channel interference and poor SINR in both uplink and downlink directions.

Therefore, a technique called Coordinated Multi-Point (CoMP) has proven to increase the utilization of the spectrum and at the same time the user throughput at the cell-edge [6],[7]. CoMP communications (transmission and reception) is a hot research area and was addressed by the Third Generation Project Partnership (3GPP) as a future mechanism for interference mitigation in the future LTE releases (release-10 and beyond), known as LTE-Advanced [6],[7],[8].

In [9], field measurements showed that CoMP could improve up to 50% of the spectral efficiency and 55% of the cell-edge user throughput compared to non-CoMP MIMO systems. CoMP is also known as cooperative MIMO, and coordinated multi-cell processing [10]. CoMP technique is adopted by 3GPP for 4^{th} Generation wireless systems.

As known in both theory and practice, and before implementing designs and plans of such wireless communication systems, accurate predictions for propagation environments and system capacity have to be performed [11]. The fast evolution of wireless cellular communications, such as MIMO based systems, and the demand of higher data rates have led to the use of higher frequency bands, smaller cell sizes, and smart antenna systems. All of these advancements made propagation and capacity predictions issues more challenging [11].

Propagation predictions cover two main categories, large-scale path loss, and small scale fading statistics. Capacity simulations cover Signal to Noise Ratio (SNR), throughput, spectral efficiency, and interference calculations. Without predictions, these

parameters can only be obtained by field measurements which are time consuming and costly. Prediction tools can be divided into three types, i.e., empirical, theoretical, and site-specific models. Empirical and theoretical (stochastic) models describe the characteristics of radio channels by means of statistical parameters. These parameters are usually estimated from extensive measurement campaigns, or inferred from geometrical assumptions. Stochastic models usually need less information than deterministic ones, and they produce more general results, as many repetitions are considered [12]. Many prediction models representing MIMO channels have been published, but most of these models assume specific scenarios and did not consider enough parameters that can affect MIMO channel performance [5].

A well-known deterministic prediction model is the RT model and it is of big interest recently [13]. The RT model is essential for the simulation of the performance of new MIMO based radio systems such as LTE and WiMAX [14]. In RT models, the Channel Impulse Response (CIR) is obtained by tracing the reflected, diffracted, and scattered rays, based on databases that provide information about the size and location of the physical structures. Besides, the database contains information about the electromagnetic properties of structure materials [11].

RT offers the possibility of detailed characterization of all multipath and investigation on propagation effects without any constraint concerning the antenna or the measurement equipment [15]. RT models have the advantage of providing accurate site-specific information that is easily reproducible without the need of on-site measurements for model tuning [12].

1.1 Background

1.1.1 Wireless Channel Characterization

Wireless channel between a transmitter and a receiver is usually presented by its impulse response. A Channel Impulse Response (CIR) for fading multipath channels can be written as [16]

$$h(\tau, t) = \sum_{i} a_i(t) \cdot \delta(t - \tau_i(t)) \,, \tag{1.1}$$

where a is the amplitude of the transmitted signal. δ is the Dirac delta function and τ i

the transmitted signal delay at the receiver.

Therefore, CIR defined as the response of a channel when the input is a unit impulse [17]. The channel often represents the most stressful impairment to wireless communications. Typically, there is a large number of objects in the environment, and some of these object positions vary with time. The transmitted signal can be reflected, diffracted, and scattered from those objects leading to multiple replicas of signal arriving at the receiver. These replicas are called multipath components. The impulse response of a wireless channel is generally time varying and spatially varying, so a comprehensive analysis often addresses both dimensions.

CIR provides a linear system perspective, but also includes information regarding the nature of propagation delays due to the reflections and diffractions from various sources, the delays and the path loss associated with all multipath components.

Reliable transmission of a signal through a communication channel faces challenges such as path loss, delay and phase shift, shadowing, noise and interference [18].

1.1.2 Channel Modeling

Channel Impulse Response (CIR) Statistics

Channel statistics are being calculated from the CIR or Power Delay Profiles (PDP). PDP is a plot of the power of each multipath component versus delay. CIR statistics are measured by but not limited to the mean excess delay (MED) and RMS delay spread (RMS DS).

Mean Excess Delay (MED)

MED is the first moment of the PDP. MED can be expressed as follows [17]

$$\mu_\tau = \frac{\int_0^\infty \tau \cdot \emptyset_g(\tau)\, d\tau}{\int_0^\infty \emptyset_g(\tau)\, d\tau} \cong \frac{\sum_k(\tau_k \cdot {\alpha_k}^2)}{\sum_k({\alpha_k}^2)}, \tag{1.2}$$

where τ represents the delay associated with each multipath component, $\emptyset_g$ represents the PDP and α_k represents the amplitude associated with each multipath (k).

Root Mean Square Delay Spread (RMS DS)

Delay spread is the time delay difference between the first and the last arriving signal components associated with a single transmitted pulse.

DS is also defined as the second central moment of the noise-free PDP as follows

$$\sigma_t = \sqrt{\bar{\tau^2} - (\bar{\tau})^2}\ , \tag{1.3}$$

where τ is the delay of any propagation tap and $\bar{\tau}$ is the average delay.

RMS DS quantifies the spread in delays from the average delay (MED) [17].

$$\sigma_\tau = \sqrt{\frac{\int_0^\infty (\tau - \mu_\tau)^2 \cdot \emptyset_g(\tau)\, d\tau}{\int_0^\infty \emptyset_g(\tau)\, d\tau}} \cong \sqrt{\frac{\sum_k (\tau_k{}^2 \cdot \alpha_k{}^2)}{\sum_k (\alpha_k{}^2)} - \mu_\tau{}^2} \ . \quad (1.4)$$

1.1.3 Propagation Models

Propagation prediction usually provides two types of parameters corresponding to the large-scale path loss and small-scale fading statistics. The path-loss prediction models can be roughly divided into three types, i.e., the empirical, theoretical, and site-specific [11]. The outdoor radio wave propagates through reflections from vertical walls and ground, diffractions from vertical and horizontal edges of buildings and scattering from non-smooth surfaces, and all possible combinations.

Empirical models are usually a set of equations derived from extensive field measurements. The empirical propagation model (EPM) is derived from Hata model. EPM models are simple and efficient to use. They are accurate for environments with the same characteristics as those where the measurements were made. The input parameters for the EPM models are usually qualitative and not very specific, e.g., a dense urban area, a rural area, and so on. One of the main drawbacks of empirical models is that they cannot be used for different environments without modification [11].

Theoretical models are derived physically by assuming some ideal conditions. In this model, the path loss in decibels is the sum of free-space loss and the so-called excess loss.

Site-specific models offer a fast and inexpensive means of obtaining channels information without the need for on-site measurements. In the outdoor environment, it is essential to include diffracted fields in making predictions. Diffraction is a very important

propagation mechanism in this environment, whether it is diffraction around corners into non-line-of-sight streets or diffraction over rooftops down to street level [19]. Site-specific models are based on numerical methods such as the ray-tracing method and the finite-difference time-domain (FDTD) method [11]. All site-specific models combine some type of ray-tracing procedure with one of the high frequency methods for calculating diffracted field amplitudes. The most popular method is the Uniform Theory of Diffraction (UTD) originally developed by Joseph Keller in 1962 [19].

1.1.4 Ray Tracing (RT) Basics

A RT model is a multidimensional characterization of radio propagation environment. This model outputs time delay, Direction of Arrival (DoA), Direction of Departure (DoD) and time variance of the radio channel such as the Delay Spread (DS). Therefore, a RT propagation model is capable of simulating the actual multipath propagation environment [11]. Any RT model depends on basic principles in operations, such as Maxwell's equations, Geometrical Optics (GO), Uniform Theory of Diffraction (UTD), and efficiency increasing schemes.

GO refers mainly to ray tracing techniques that have been used for centuries at optical frequencies. Some of the basic postulates of GO are:

- Wave fronts are locally plane and waves are transverse electromagnetic (TEM) mode
- Wave direction is specified by the normal to the equiphase planes
- Rays travel in straight lines in a homogeneous medium

- Polarization is constant along a ray in an isotropic medium (e.g. free space)
- Power in a flux tube (bundle of rays) is conserved
- Reflection and refraction obey Snell's law
- The reflected field is linearly related to the incident field at reflection point by a reflection coefficient

UTD is a complementary part for GO topics. Where the diffracted fields (rays) arise from edges need to be considered in the total field at an observation point (P). Therefore, the field ($\vec{E}$) at that point is decomposed into GO and diffracted components as

$$\overrightarrow{E_r}(P) = \vec{E}_{GO}(P) \quad + \vec{E}_{UTD}(P)\,. \tag{1.5}$$

Some of the basic postulates of UTD are:

- Wave fronts are locally plane and waves are transverse electromagnetic (TEM) mode
- Diffracted rays emerge radially from an edge
- Rays travel in straight lines in a homogeneous medium
- Polarization is constant along a ray in an isotropic medium (e.g. free space)
- The diffracted field strength is inversely proportional to the cross sectional area of the flux tube
- The diffracted field is linearly related to the incident field at the diffraction point by a diffraction coefficient

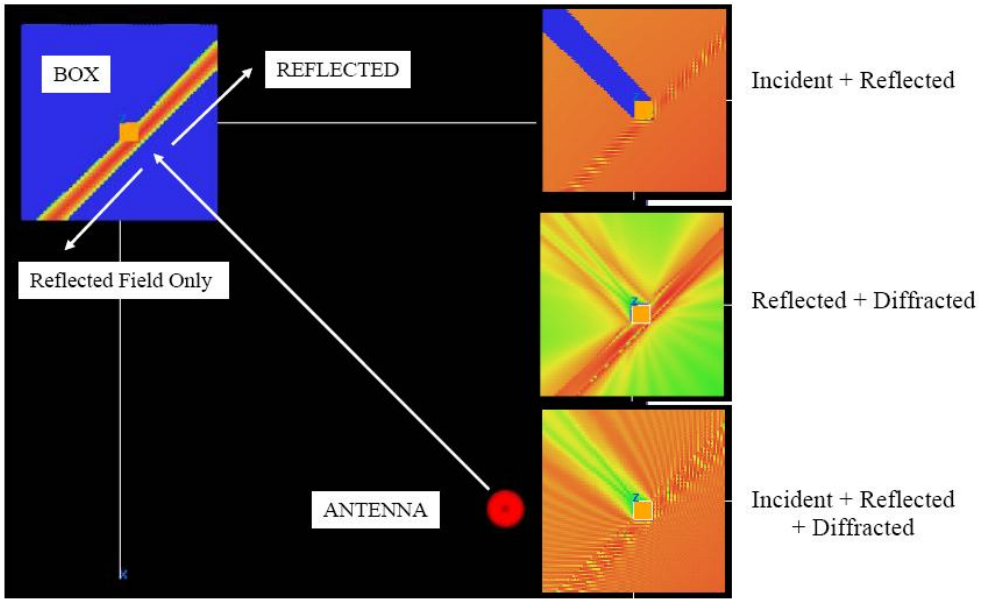

Figure 1.1 An example of fields scattered from a box. Field strength from -100 dBm (blue) to -35 dBm (red). Antenna power is zero dBm [20].

Figure 1.1 shows light fields scattered from a box (the orange square box in the center of each sub-graph). There are multiple combinations of reflected and diffracted rays from multiple scenarios. Reflections only are shown in the top right corner graph, reflections and diffractions are shown in middle right sub-graph and all combinations are shown in the bottom right corner sub-graph including incident light, reflections and diffractions.

GO and UTD are not only used for LOS rays, but reflected, diffracted, scattered and combined ones, too. GO and UTD are implemented in ray tracing models such as in the simple two-ray and in the multi-ray models. A simple two-ray model is defined as a model with one line of sight (LOS) and one dominant reflected ray as in the below graph.

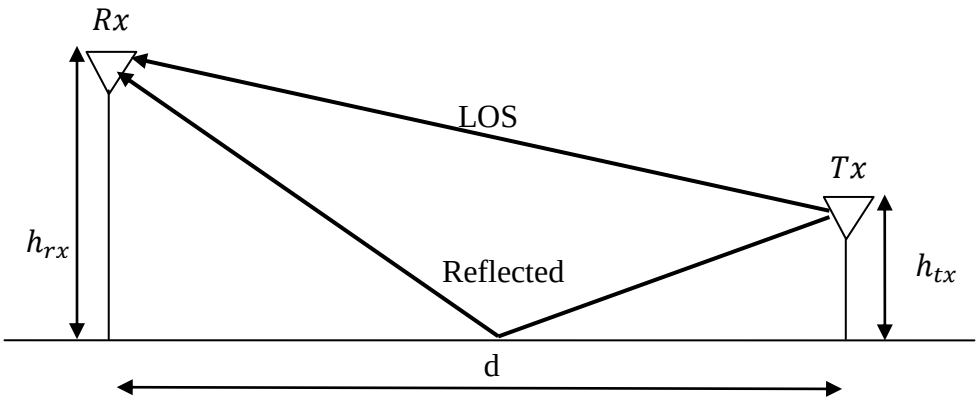

Figure 1.2 Two-Ray model.

The LOS component is the signal from transmitter to receiver through free space directly. The reflected ray can be a reflection from the ground or from an object. A simple two-ray model shown in Figure 1.2 requires the heights of both antennas, the distance between them and the location of the main reflector. A simple two-ray approximation for path loss can be written as in [18]

$$P_r = P_t\left(\frac{G_t \cdot G_r \cdot {h_{tx}}^2 \cdot {h_{rx}}^2}{d^4}\right). \quad (1.6)$$

Here h_{tx} and h_{rx} are the antenna heights of the transmitter (Tx) and the receiver (Rx), respectively. G_t and G_r are the transmit and receive antenna field radiation patterns respectively, and d is the distance between Tx and Rx. This equation assumes that the reflection is nearly perfect and that $d >> h_t h_r$ [18].

A multi-ray tracing model consists of a larger number of reflected, refracted, and diffracted rays. In this thesis work, this model is used to characterize the channels.

Figure 1.3 illustrates a multi-ray model that contains multipath components from various objects e.g. ground, buildings, trees, and cars. This is closer to the real world environment than the simple Two-Ray model.

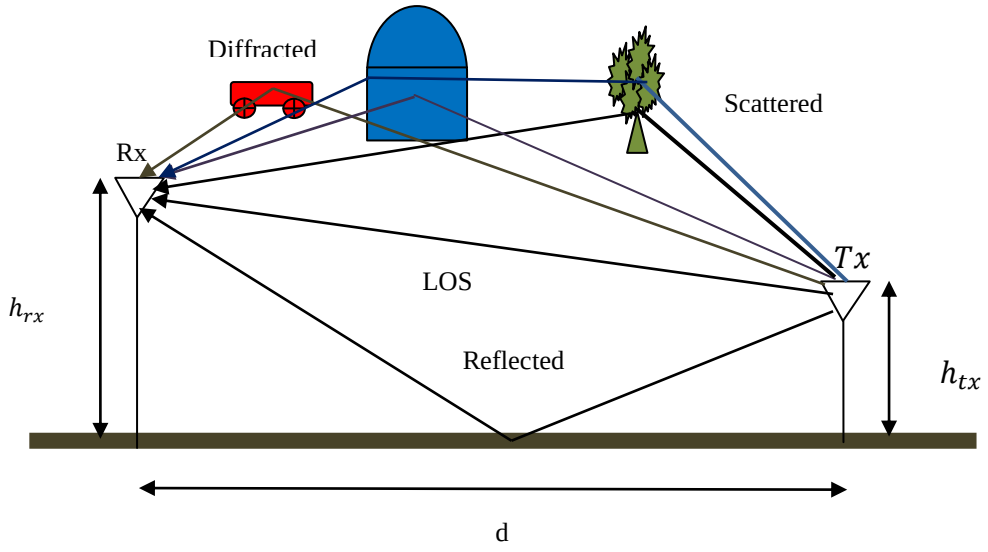

Figure 1.3 Multi-Ray model (adapted and modified from [21]).

RT model is based on solving Maxwell's equations that provides the interrelationship between the electric and the magnetic fields [22]. RT will be more and more important for the design and the implementation of future mobile radio and broadcasting systems. In a basic RT algorithm, the main task is to determine the trajectory of a ray launched from a transmitting antenna. As in [23], a ray-tracing method is Shooting-and-Bouncing Ray (SBR) launching algorithm. First, a ray, which is actually a ray tube or a cone, is launched from the transmitting antenna (Tx), then the ray is traced to see if it hits any object or is received by the receiving antenna. When an object is being hit, reflection, transmission, diffraction, or scattering will occur, depending on the geometry and the electric properties of that object. When a ray is received by an antenna, the electric field (power) associated with the ray is calculated.

The complexity of the ray-tracing model depends on the number of multipath components used. A simple environment with a small number of multipath components can be modeled easily and accurately compared to one with a large number of compo-

nents because of locations, size and the properties of all the materials that can potentially be determined more accurately for a small number of objects unlike in the latter case.

Many studies were performed to optimize an efficient approach. Such approaches should be accurate with reasonable processing time. An example is the ray launching and reception approach [24], [25], and the ray intersection test with an object approach [25], [26]. Other RT approaches are the image method and the hybrid method [11].

The computation efficiency is the biggest obstacle against the application of RT methods [11], [22], [27],[28]. Many publications are focusing on the acceleration of the RT algorithms. There are several ways to achieve this acceleration [11], [22]. The first way is to reduce the number of objects on which actual ray-object intersection will be performed. The second one is to accelerate the calculation of the intersection point. Methods for RT accuracy enhancement are mentioned in [29], e.g. by implementing various optimization techniques, one of those is the pre-creation of the trees in the 3D map. Another optimization technique is the use of the spatial averaging technique to avoid the inaccuracy of receiving antenna positions and therefore the computation error [30].

Polarized Antenna Systems

The use of orthogonal polarization to provide two communications channels for each frequency band has led to interest in the polarization purity of antenna patterns [31]. The IEEE standard definitions [32] provides two definitions for the antenna polarization pattern. The first one is the spatial distribution of the polarizations of a field vector excited by an antenna taken over its radiation sphere. The second one is the response of a given antenna to a linearly polarized plane wave incident from a given direction. Its direction of polarization is rotating about an axis parallel to its propagation vector, the re-

sponse is a function of the angle that the direction of polarization makes with a given reference direction. The polarization is usually resolved into a pair of orthogonal polarizations, the co-polarization and the cross polarization.

As per [33], we can represent any signal field strength vector by either one of two coordinate systems that have the same preciseness. One is the polarized system and the other is the linear system. This is to say, a co-polarized (E_{+45}) antenna pattern is composed of adding linear horizontal (E_x) vector to a linear vertical vector (E_y) and a cross-polarized (E_{-45}) antenna pattern is composed of subtracting the linear horizontal (E_x) vector from a linear vertical vector (E_y). Figure 1.4 shows four types of linear polarizations. The vector components on the left side are the linear horizontal and the linear vertical. The vector components on the right side are the linear co-polar and the linear cross-polar components. As a practical example, if the polarization is almost +45°, the radiation patterns measured in the vertical polarization E_y and in the horizontal polarization E_x will be quite close to each other, or as in [33] the cross-polar value $E_{-45°}$ of the field strength will be much smaller than the co-polar one $E_{+45°}$.

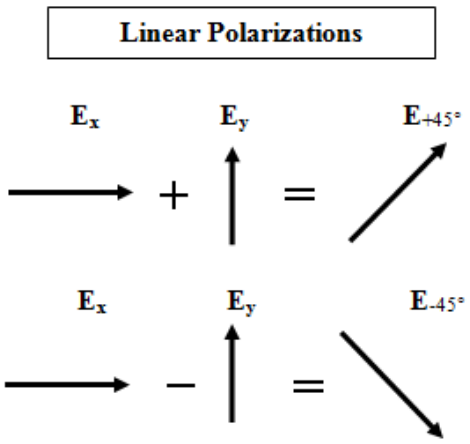

Figure 1.4 Linear polarization types: horizontal, vertical, co-polar and cross-polar.

Polarized antennas technology has enabled antennas manufacturers to produce compact antennas as shown in Figure 1.5, where, e.g., instead of installing three dual +/-45 degree polarized antennas for a complete three-sector site, previously, six or nine vertically polarized antennas had to be installed. For polarization diversity to function properly, it is very important that the different polarized signals are as independent as possible from each other (principle of uncorrelated signals). The most important point is the "Cross-polar ratio (CPR)", i.e. the ratio of the signal levels of similar polarizations compared to dissimilar polarizations [34].

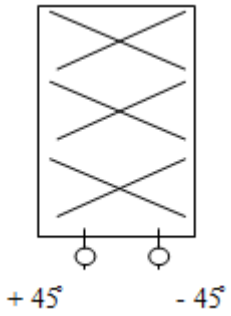

Figure 1.5 A simplified cross-polar (XP) antenna components.

The table in appendix A shows the results of channel impulse response magnitudes for 3 radio transmission taps (rays) after varying the configuration of a transmitting polarized antenna that has both co-polarized and cross-polarized elements for four times. Each simulation time shows the result of using one of the following polarizations:

Linear Polarization with +45° arbitrary angle (L+45), linear polarization with -45° arbitrary angle (L-45), Linear Horizontal (LH) polarization and Linear Vertical (LV) polarization. In appendix A, we can see that by changing the antenna polarization by 90°, e.g. from Linear +45° to Linear -45°, the values in the CIR (three taps) are the same but shifted from

the co-polarized element to the cross-polarized element as highlighted there for two instances in the dashed red rectangles.

1.1.5 Multiple-Input-Multiple-Output (MIMO) Systems

A MIMO communication system uses multiple antennas at the same time at the transmitter and the receiver of the system. A MIMO system uses the Multi-Path Components (MPC) to provide a higher system capacity [11]. Many OFDM based systems use MIMO scheme that offer large spectral efficiencies compared to Single Input Single Output (SISO) traditional systems [35]. Assuming that the number of transmitting antennas is M_T , the transmitted signals are, $S_j(t), j = 1, \dots, M_T$, and the number of receiving antennas is M_R , the received signals are, $y_i(t), i = 1, \dots, M_R$. A basic description for a MIMO channel for the relation between the transmitted and received signals can be modeled as [36]

$$y_i(t) = \sum_{j=1}^{M_T} h_{i,j}(t) \cdot S_j(t) + n_i(t), \quad i = 1, \dots, M_R \ , \tag{1.7}$$

where $h_{i,j}(t)$: is the Channel Impulse Response (CIR) between the transmitting antenna of number j and the receiving antenna of number i.

The receiver with multi-antenna can separate and decode the data stream by using advanced space-time coding and get the best processing method [37].

In a MIMO system with (M_T) transmitting antennas and (M_R) receiving antennas, the channel capacity (C) at high SNR, if the sub-channels are independent Rayleigh fading channel (i.i.d), depends on $M_m \leq \min(M_T, M_R)$., Channels matrix can be expressed as

$$H(t,\tau) = \begin{bmatrix} h_{11}(t,\tau) & h_{12}(t,\tau) & \dots & h_{1M_R}(t,\tau) \\ h_{21}(t,\tau) & h_{22}(t,\tau) & \dots & h_{2M_R}(t,\tau) \\ \vdots & \vdots & \ddots & \vdots \\ h_{M_T1}(t,\tau) & h_{M_T2}(t,\tau) & \dots & h_{M_TM_R}(t,\tau) \end{bmatrix}, \quad (1.8)$$

where H is the MIMO channel represented by the MxN channel matrix, $h_{M_TM_R}(t,\tau)$ is the impulse response between a single transmit antenna and a single receive antenna [38]. The higher the rank of (HH^H) is the higher the capacity of the MIMO system, where H^H is the conjugate transpose.

1.2 Literature Survey

1.2.1 Coordinated Multi-Point (CoMP) Communications

The capacity of cellular mobile communications systems is mainly limited by inter-cell interference [35]. In order to overcome this limitation, many authors have proposed cooperation among base stations as a means to actively exploit signal propagation across cell borders rather than treating it as noise, yielding in large spectral efficiency and fairness gain [39],[40],[41],[42]. CoMP techniques in general refer to any kind of interference-aware transceiver technique, which enables the exploitation of interference rather than treating it as noise [39]. CoMP is not an isolated communication MIMO link as in Bell Laboratories Layered Space-Time (BLAST) scheme [43]. CoMP is a coordinated MIMO scheme. In [44], two types of CoMP are possible, intra-eNB CoMP, which involves multiple points within a single base station, and inter-eNB CoMP, which involves transmitter (UL CoMP) points or receiver (DL CoMP) points associated with different

base stations. The term eNB refers to evolved NodeB, which is the base station terminology used in LTE system [4]. In [4], LTE current systems will only use intra-eNB CoMP technique, in order to avoid the backhaul load and synchronization requirements between eNBs.

CoMP communication technique has proven through many practical studies to improve the user throughput located at the edge of the cell, in addition to the overall spectral efficiency [4], [10]-[45]. CoMP communication technique inherits the benefits of MIMO channels that enable spatial multiplexing, array gain and interference mitigation by making use of the spatial signature of interference [4]. In CoMP systems, a group of users, cells or base stations coordinate to decode a particular signal by exploiting inter-cell interference [10],[40],[41]. This interference is caused by the neighboring cells when using the same frequency band, eventually leading to severe performance degradation or loss of connection [46]. CoMP results in an increase in the fairness among the users in the same cell, defined as having the same throughput regardless of user equipment location in a cell [10]. Uplink CoMP technique allows UEs transmitted signals to be properly demodulated at several involved NodeBs (eNBs) as a cooperating cluster [42]. UL Single-User (SU) MIMO or Multi-User (MU) MIMO may spread out over different base station sectors at the network side (inter-eNB). Most of the information exchange between cooperating cells is caused by sharing the quantized baseband samples received in each cell [4]. Channel State Information (CSI) and resource allocation tables are shared in the cooperation cluster. In [9], it is highlighted that UL CoMP techniques promise average cell throughput gains about 80% and roughly a threefold cell edge throughput improvements. There are two basic types of CoMP techniques detection schemes: Joint Pro-

cessing (JP) also known as Joint Detection (JD) and Coordinated Beamforming/Scheduling (CS/BS) [9]. UL CoMP JD scheme indicates that multiple signals are received by multiple BSs from a Single-User (SU) or Multiple-Users (MU) and are jointly processed [45]. CS/BS type indicates performing link adaptation based on predicted signal to-interference-plus-noise ratio (SINR) values that are likely to occur during the associated data transmissions. Prediction is enabled by exchange of resource allocation information within a cluster of cooperating cells.

1.2.2 Ray Tracing Channels and. Field Measurements

Multiple simulation models were used to characterize CoMP channels. Well-known models are the 3GPP Spatial Channel Model (SCM), COST 273, the Wireless World Initiative New Radio (WINNER) model and the RT model [4]. Two main models are extensively used in the literature, which are the SCM model and the RT model.

In [45], the 3GPP SCM standard model was used to simulate MIMO channels and calculate their capacities in an UL CoMP system. The UL CoMP system considered only intra-eNB scenario. The results showed that UL CoMP has better results compared to non-cooperative MIMO in terms of BLER, SINR and spectral efficiencies. Capacities (bps/Hz) and user throughput (Kbps) were improved by 20%. Furthermore, it was observed that the actual performance is dependent on the receiver type, scheduling algorithms and other design scenarios. In this scenario, both UL CoMP JD and link adaptation detection schemes were used.

In [47], MIMO channel measurements using HyEff channel sounder were performed in order to record the channel impulse response (CIR). MIMO predictions using SCM mod-

el were performed. The measurement results composed of Multi-Path Components (MPC), delay profile (delay spread and excess delay) were significantly different compared to SCM predictions model. As per [47], the main reason for the difference is that the SCM model assumes a fixed number equals to six taps in the CIR. This assumption is fine when simulating a single site case, but not with a multi-site case such as inter-eNB CoMP scenario. Moreover, SCM assumes an antenna spacing of zero meter, therefore the correlation between channels is high, and consequently the MIMO performance is less. As a conclusion, when SCM is used to evaluate the performance of CoMP JD technique, results regarding the throughput are considered as a lower bound for the field achievable capacity. In [48], a criticism was directed towards the SCM model and its extension the Spatial Channel Extended Model (SCME), due to the lack of precise modeling for polarization properties of the MIMO channel. This issue becomes worse especially when using in reality cross-polarized antennas, because SCM is based on 2D predictions approach but not 3D ones. This widely used 3GPP model is criticized by being inaccurate and forms a lower bound to evaluate the performance of CoMP techniques [49]. In [47], SCM model simulations results were significantly different from the measurement results.

In [50], good predictions for complicated radio environments should combine a composition of site-specific RT and theoretical over-rooftop model [50].

Using RT simulation schemes for modeling MIMO channels and their performance is a well-known approach and increasingly arising in recent works, e.g., [22], [28].

A major advantage of that is the flexibility of modeling almost any scenario and keeping high efficiency in terms of time and cost without the need of doing field measurements [5]. There have been many publications describing the use of RT models to characterize,

predict, and verify the capacity and performance of MIMO channels. Some of these publications were based only on comparing MIMO theoretical capacities with RT simulated channels capacities without verifying the results with field measurements.

In [48], CoMP field measurements and 3D RT simulations were performed on four BSs testbed. Results in terms of channel matrices such as were compared for LOS and NLOS elements and were found comparable. The focus was on singular values in channel matrices, which can affect the channel rank. The small deviations in the results observed were assumed to be due to slightly different antennas patterns used in simulations compared to measurements ones. It was observed that the path loss gains and channel singular values (due to LOS) in the simulation model were very sensitive to the distances between the BSs and UEs. Rates were enhanced by a factor of five in the measurement scenario if BS cooperation is enabled i.e., using CoMP technique.

In [51], verifications of field measurements in a MIMO setup using a developed RT model were performed. The model used image theory for tracking reflections and used UTD for diffractions. The field measurements were collected using RUSK MIMO channel sounder measurement that is a real-time system for radio CIR measurement, for multiple transmit and receive antenna elements configurations. The measurements setup used multiple types of MIMO antennas and sophisticated sampling rate through measurements routes. A conclusion was drawn that the RT spatio-temporal outputs, such as delay spread, have a very good agreement with the measurements based on mean and standard deviation measures.

Moreover, it was shown that the diffuse scattering non-specular components could contribute a considerable part of the signal energy. In the conclusion, the RT predictions

showed a very good agreement with measurements. In [27], an indoor environment consists of two MIMO approaches distinguished by their radiant elements. One is using Conventional Systems (CS) MIMO where the antennas are separated by some multiples of wavelengths varies between ($\lambda/2$ to 2λ). The second approach is Distributed Systems (DiS) where the antennas are widely spread in the environment with four different configurations. The results of these MIMO approaches were compared with RT simulations. MIMO capacity results in bits/sec/Hz under fixed signal to noise ratio (SNR) were obtained. Apparently, MIMO DiS approach under all configurations showed better capacities than the CS approach. RT simulations matched with CS measurement capacities but underestimated the DiS capacities. However, RT results were slightly better than the CS case. An important observation was that the DiS case exceeded the RT simulations when assuming independent and identical distributed (i.i.d) fading channels. In [52], an RT model was used in a dense urban environment to characterize MIMO channels and capacity estimates were driven from the simulated channels. The study emphasized the importance of the diffuse scattering model and its importance in order to have a matched predicted MIMO capacities compared to theoretical Rayleigh (i.i.d) full scattering channels. Two MIMO configurations were taken in consideration, in terms of transmitters and receivers as 2x2 MIMO and 8x8 MIMO. As a result, the angular spread of receiving UEs showed that the bigger the spread the more scattered are the signals and the higher the MIMO achieved gain. This was also shown in the measurements at particular points. In [5], a method for MIMO channel estimation based on an analytical RT model was analyzed, this model considered various electric properties of antennas such as pattern and structure, polarization, and mutual coupling. The study showed that correlated channels

due to LOS are contributing less to the capacity, if SNR was fixed to a particular value. In [29], the authors compared RT simulated MIMO and SIMO systems with theoretical expressions and measurements only for the SIMO setup. Simulations were done by an enhanced RT approach using a virtual point concept. In RT, a virtual point concept implies that multiple antennas at transmitter and receiver can be merged into a single point that is equidistant to all antennas, so that the system looks like a point-to-point system. The virtual point concept is meant to reduce the computational complexity for RT model in predicting MIMO channels. The results covered the path loss and capacities. A main conclusion was that the virtual point approximation in RT simulations works well in most cases and the difference errors were negligible such as few dBs in case of path loss calculations and a fraction of bps/Hz for capacities case. At the same time, the RT computation complexity was reduced in the study by a factor approaching 10.

1.3 Thesis Contributions

The focus in this thesis work is to answer the question how close RT simulations can predict end-to-end system performance compared to real-world measured performance. Analysis and evaluation of MIMO channels performance, both conventional and CoMP MIMO schemes using ray traced simulated channels and field measured ones are performed. SNR, SINR, spectral efficiencies, and some of channel geometries were analyzed.

1. **Modeling an LTE-Advanced testbed using ray tracing techniques, with applying a real-world 3D map for the city of Dresden, Germany.**

   Description: The starting point in this thesis is to build the LTE-A testbed in the ray-tracing simulator. This required building carefully a project that composes all radio components like eNBs, UEs, antenna pattern, and other RT simulator parameters. The RT model has variable set of parameters fitting different radio environments. The RT simulator involves big number of parameters used in calculating penetration, reflection, diffraction, and diffuses scattering algorithms. Moreover, designing the ray launching algorithms parameters is critical in the RT model in terms of accuracy versus complexity. An example of this design challenge is the step size for RT launched rays. This completed milestone was planned in the thesis initial proposal.

2. **Verification of the ray traced channels through evaluating MIMO systems, conventional and CoMP performance and comparing it to field measured channels.**

   Description: An LTE-Advanced based simulator was exploited and amended to evaluate the MIMO channels. Ray traced channels were verified through the perfor-

mance of both CoMP and non-CoMP (conventional) schemes. Field measured channels were verified too and compared to RT channels results. Analysis for twenty-four scenarios including matching factors between RT and field measurements results were presented. CoMP gain ratios compared to conventional MIMO were shown when using measured channels or RT channels were shown. Few issues related to hardware limitations or RT model errors are explained. A short comparison between EPM and RT models in terms of accuracy and complexity is highlighted. This completed milestone was planned in the thesis initial proposal.

3. **Verification of CoMP channel estimator through RT modeled channels.**

   Description: The signal processing in the CoMP tool chain includes channel estimation for both measured channels and RT channels (both setups go under the same signal processing). As we are completely aware of the RT simulated channels, we have available Channel State Information (CSI) that allows us to get rid of the channel estimator for the RT transmission. An effort is done to bypass any channel estimation for RT channels. The evaluation results of RT channels without channel estimator (perfect CSI) were highly comparable to RT results with the estimator (with interpolation). This highlighted the accuracy of the currently used channel estimator. This would enable further tuning options in the estimator parameters depending on different channel types and number of involved UEs in the transmission. This is an extra effort that was not planed in the in the thesis initial proposal.

1.3.1 Thesis Related Publications

The below publications are the outcomes during my thesis research period in KFUPM:

Published papers (2012):

- **M. Amro**, M.A. Landolsi, and S.A. Zummo, "Practical Verifications for Coverage and Capacity Predictions and Simulations in Real-world Cellular UMTS Networks," in proceedings of the International Conference on Computer and Communication Engineering (ICCCE 2012), Kuala Lumpur, Malaysia, 2012.
- M. Danneberg, J. Holfeld, M. Grieger, **M. Amro**, and G. Fettweis, "Field Trial Evaluation of UE Specific Antenna Downtilt in an LTE Downlink," in proceedings of the 16th International ITG Workshop on Smart Antennas (WSA2012), Dresden, Germany, 2012.

Newly accepted papers (2013):

- M. Grieger, **M. Amro**, M. Danneberg, J. Voigt, M. A. Landolsi, S. A. Zummo, and G. Fettweis, "Uplink Coordinated Multi-Point in Field Trials and Ray Tracing Simulations," accepted on 18th December for publication in the 8th European Conference on Antennas and Propagation (EuCAP 2014)., the Hague - the Netherlands, 2014

Under preparation papers (2014):

- **M. Amro**, M. Grieger, M. A. Landolsi, S. A. Zummo, and G. Fettweis, "Ray-Tracing Wireless Channel Modeling and Verification in Coordinated Multi-Point Systems," under preparation to be submitted to a conference soon.

1.4 Thesis Outline

Chapter 1 presents a general overview for the recent growth of mobile telecommunication systems. Some important and basic wireless communications topics are being discussed such as channel modeling, propagation models, polarized antenna that are used in testbed BSs and MIMO introduction. Literature review, thesis contributions, and the outline are covered in Chapter 1. Chapter 2 describes the project environments involved in producing the thesis results. Field measurements, ray tracing simulator and UL CoMP tool chain simulators are described in detail. Chapter 3 covers the pre-processing of the RT channels before undergoing into the LTE-A tool chain signal processing. This includes additions and enhancements that increased the accuracy of the results. An example of these is simulating the two UEs transmission orders in the field measurements by shifting the CIR response by a similar delay offset. Chapter 4 presents verification results for different field measurements. Two experiments were based on RT simulations and one was based on empirical propagation model simulations. In this chapter multiple comparisons are summarized and evaluated. An evaluation of CoMP performance based on SNR, SINR, Spectral Efficiencies, and geometries like Symbol Time Offset (STO), Time Difference Of Arrival (TDOA) and DS are performed. At the end of the chapter, a short comparison between EPM and RT models in terms of accuracy or modeling real propagations and processing complexity is highlighted.

Chapter 5 provides a summary, conclusions and recommended future works that can be done based on this thesis work.

CHAPTER 2

DESCRIPTION OF CoMP TESTBED, MEASUREMENTS AND RT SIMULATION ENVIRONMENTS

2.1 Introduction

This chapter describes the project environments involved in producing the results. Section 2 is dedicated to describing the field measurements, explaining the UL transmission system model and the measurements collection scenario in the testbed. Section 3 is dedicated to the RT simulations and is divided into three subsections. The first subsection is describing the RT simulator that produces extended channel impulse responses (CIR) for the whole locations in the testbed. The required coordinates conversion from RT Cartesian system into WGS84 system is also shown. The second subsection is describing the extended CIRs components in order to prepare them to be processed in the LTE tool chain. The fourth section is describing the LTE tool chain, which is used for link level end-to-end simulations.

2.2 Measurements Environment Description

The field measurements were collected by researchers, students, and mobile operators in a large testbed that is an extension for the setup of the project Easy-C, namely, Enablers of Ambient Services and Systems Part C. The project is jointly led by many organizations from industry and academia in Germany and coordinated at the Vodafone Chain Mobile Communications Systems in Dresden University of Technology (TUD) [53].This project follows an integrated approach identifying the major obstacles, developing practical solutions, and showing realistic performance results for CoMP concepts supported by field trials.

The field trial setup is composed of 16 BSs deployed at seven UMTS co-sites in the downtown of the German city Dresden, as shown in Figure 2.1. The BSs are synchronized through Global Positioning System (GPS) fed reference normals. Each BS is equipped with a cross-polarized antenna, hence two antenna elements per BS, the co-polar, and the cross-polar components. Two types of antennas were used in the BSs, one with 58 degrees half-power beamwidth and 18-dBi gain, and the other is of 80 degrees half-power beamwidth and 16.5 dBi gain. More details about used antennas are in Table 2.1.

Table 2.1 Parameters of antennas used in testbed.

Antenna Type	Kathrein 800 105 41	Kathrein 800 106 29
Antenna Gain (dBi)	18	16.5
Downtilt (degrees)	6	6
Vertical half-power beam-width (degrees)	6.2	7.5
Horizontal half-power beam-width (degrees)	58	80

The UEs share the same resources in time and frequency. Each UE is using one dipole antenna; transmitting signals using orthogonal frequency division multiplexing (OFDM), and a sequence of different modulation and coding schemes (MCSs). Detailed transmission parameters are mentioned in Table 2.2. The received signals at all BSs are recorded for an offline evaluation [54].

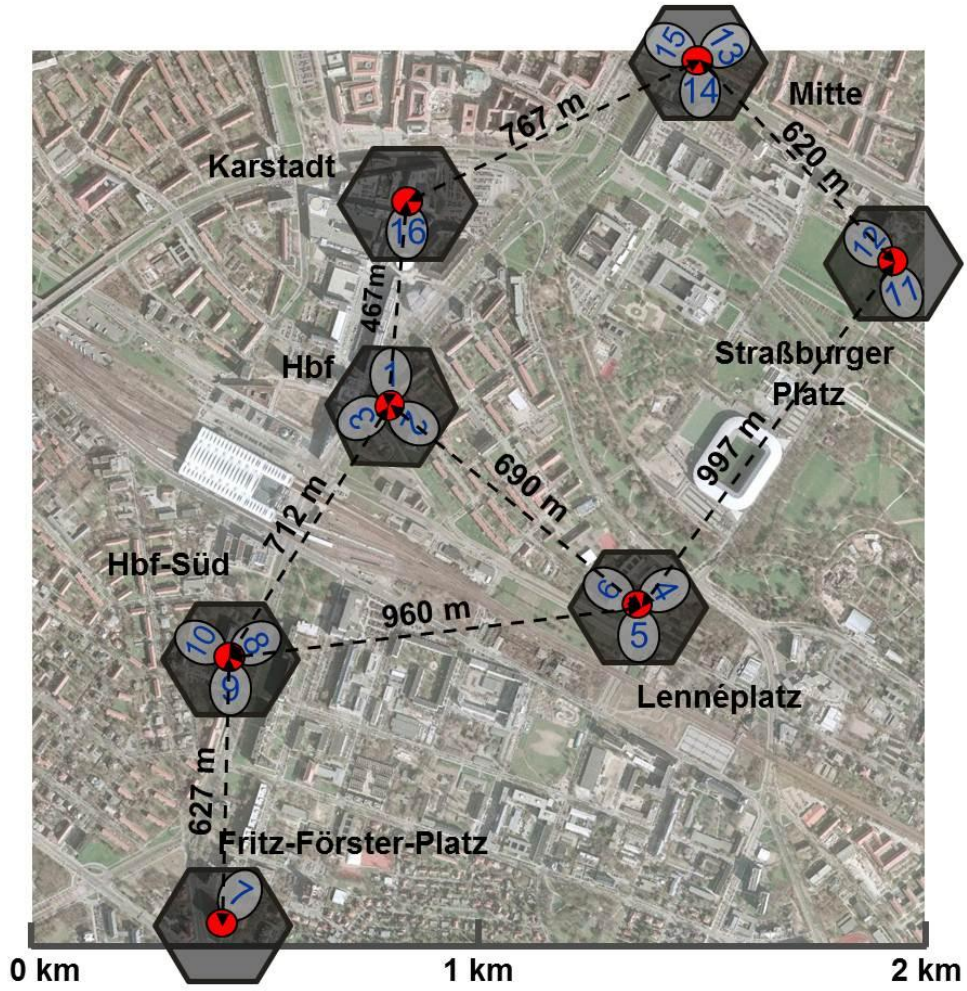

Figure 2.1 Field trial setup, BSs distribution, and measurements environment.

Table 2.2 Transmission parameters (see [54]).

Inter-BS average distance	750 m
BS antenna height	30-55 m
Distance between UEs	about 5 m
UE antenna height (over the ground)	1.5 m
Carrier Frequency	2.53 GHz
System Bandwidth	20 MHz
No. of Physical Resources Blocks (PRBs)	30
No. of Sub-carriers per PRB	12
UE Transmit Power	18 dBm
Quantization resolution	12 bits per real dimension

In contrast to 3GPP LTE Release 8 standard, the UEs used OFDM not Single Carrier (SC) FDMA during the uplink transmission, the reason is to simplify the multi-user equalization technique [55].

2.2.1 UL CoMP System Model

Figure 2.2 shows the CoMP schemes considered in this work. Mainly, two types of UL CoMP, which are Sectorized (SEC) CoMP with single and multiple users' scenarios are considered. SEC-CoMP deals with users under cooperating sectors of the same base station (intra-eNB). The other type is Network (NET) CoMP with single and multiple users' configurations. NET-CoMP deals with users under cooperating sectors connected to different bases stations (inter-eNBs). UL connections from UE can be of Line of Sight (LOS) or Non-Line Of Sight (NLOS). Backhauling for intra-site CoMP is not presented, as it is implicit in the base station itself. In case of inter-site CoMP, bold dashed rings connecting the eNBs present backhauling.

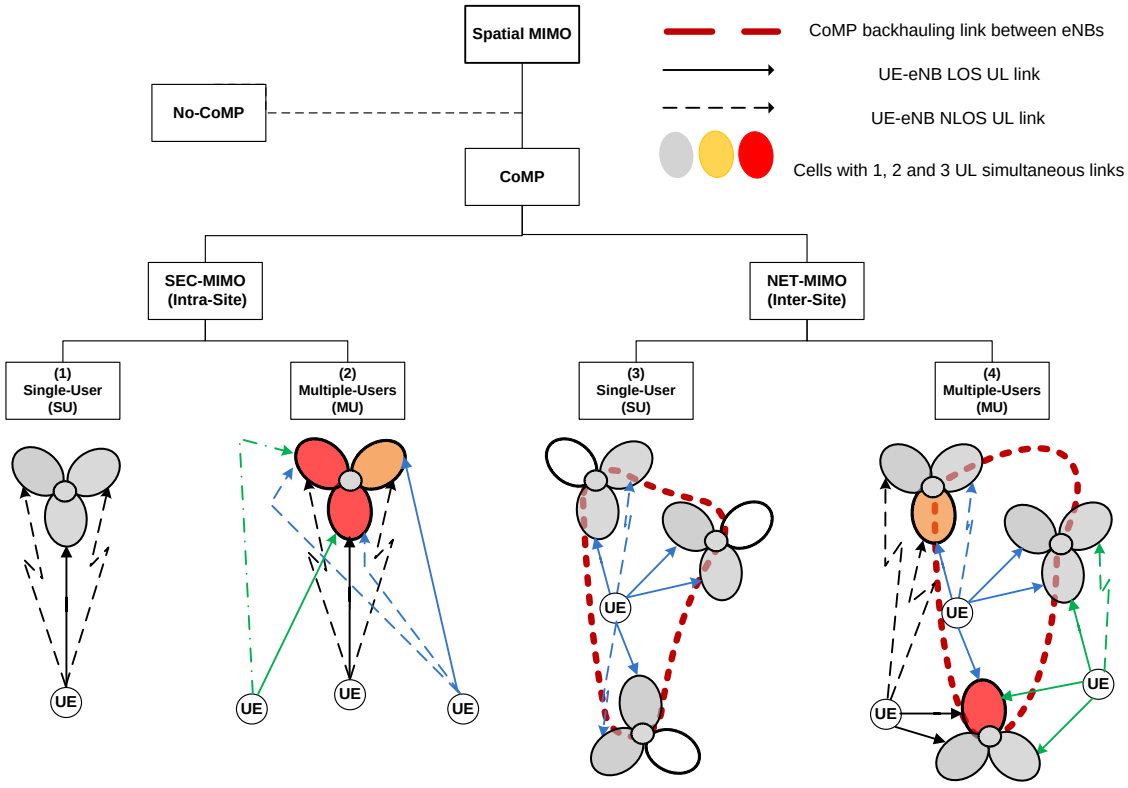

Figure 2.2 CoMP schemes system model. Adapted and modified from [39].

The transmission from UEs to eNBs for every single channel can be modeled as

$$Y(t) = H \cdot S(t) + N(t), \tag{2.1}$$

where Y: Received signals matrix at the base stations,

H: Channel matrix where every columns represents a UE

S: Symbols transmitted from the UEs

N: Additive Gaussian noise.

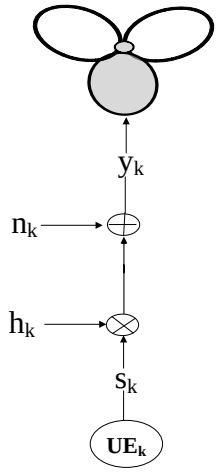

Figure 2.3 UL transmission model for single user.

Similarly, if we are considering two UEs sending signals to two eNBs (two cells), then we characterize the received signals by

$$y_1(t) = h_{1,1} \cdot s_1(t) + h_{1,2} \cdot s_2(t) + n_1(t), \quad (2.2)$$

$$y_2(t) = h_{2,1} \cdot s_1(t) + h_{2,2} \cdot s_2(t) + n_2(t), \quad (2.3)$$

where

y_i: Received signal vector at the base station i.

$h_{m,n}$: Channel matrix from UE n to eNB m.

s_i: Symbols transmitted from the UEi.

n_i: Uncorrelated additive Gaussian noise

In a CoMP MIMO setup there are set of BSs forming a cooperation cluster denoted by C with elements $\{c_1 \ldots c_C\}$. The cooperating cluster size is denoted by $C=|C|$. Therefore, the CoMP corresponding transmission model for the cluster is given by

$$y_c = \begin{bmatrix} h_{c_1,1} & h_{c_1,2} \\ \vdots & \vdots \\ h_{c_C,1} & h_{c_C,2} \end{bmatrix} \begin{bmatrix} s_1 \\ s_2 \end{bmatrix} + n_c \,, \tag{2.4}$$

where $y_c \in \mathbb{C}^{[Cx1]}$ are the signals received by the C antennas of the cluster.

The signal processing architecture shown in Figure 2.4 allows multiple cooperation and equalization schemes as:

- Independent decoding of both UEs by different BSs, using interference rejection combining (IRC) as shown in Figure 2.4.a.
- The same BS, using a linear detector (IRC) or successive interference cancellation (SIC) decodes both UEs as in Figures 2.4.b and 2.4.c.
- One BS forwards its received signal to another BS(s), where both UEs are detected jointly (JD), either using linear equalization or SIC (JD+SIC) as shown in Figures 2.4.d and 2.4.e.

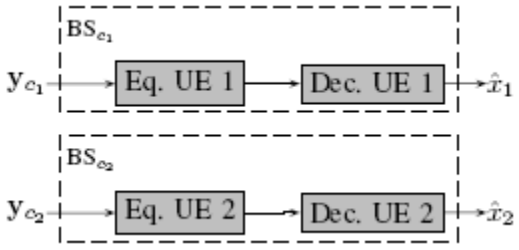

(a) Both UEs decoded by different BSs.

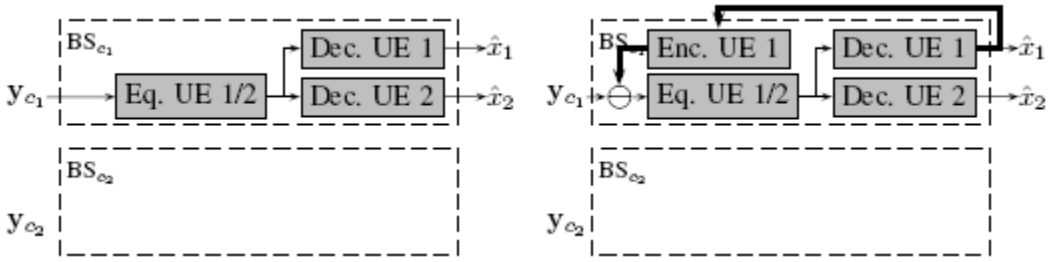

(b) Both UEs decoded by the same BS. (c) Both UEs decoded by the same BS + SIC.

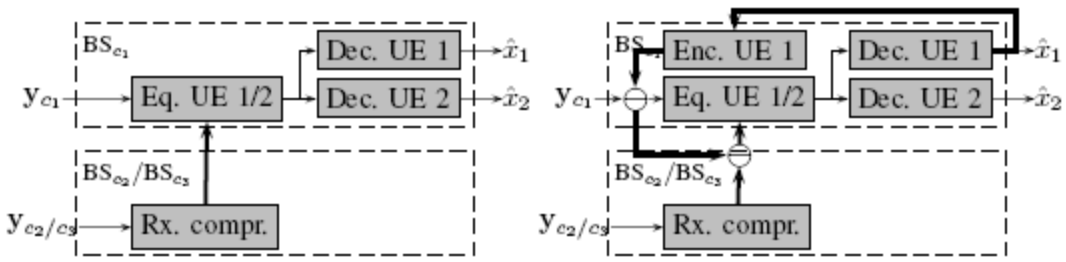

(d) Joint Detection among 2 or 3 BSs (e) Joint Detection among 2 or 3 BSs + SIC.

Figure 2.4 Signal processing setup for conventional MIMO schemes (a, b and c) and CoMP detection and cooperation schemes (d and e) [56].

The fundamental limits for achievable transmission rates are limited by Shannon's definition of channel capacity for the Gaussian multi-user MIMO channel with linear MMSE receivers.

For conventional MIMO when BSs do not cooperate, the achievable rates depend on the choice of the BS as shown in Figures 2.4 (a-c), detecting a particular UE. Assuming a channel realization that is flat in the frequency domain and static at least for one TTI, the rate of UE n that is detected at BS m (uplink)[55]

$$\mathrm{Rate}_{\mathrm{m,n}_{\mathrm{MIMO}}} = \log_2 \left| 1 + \mathrm{h}_{\mathrm{m,n}}^{\mathrm{H}} \left(\mathrm{h}_{\mathrm{m},\bar{\mathrm{n}}} \mathrm{h}_{\mathrm{m},\bar{\mathrm{n}}}^{\mathrm{H}} + \hat{\sigma}_{\mathrm{m}}^2 \mathbf{I} \right)^{-1} \mathrm{h}_{\mathrm{m,n}} \right| \quad , \qquad (2.5)$$

where $\mathrm{h}_{\mathrm{m,n}}$ is the channel response matrix between User Equipment (UE) n and BS m, **I** is the identity matrix, $\bar{\mathrm{n}}$ is the index of the interfering UE and $\hat{\sigma}_{\mathrm{m}}^2$ is the noise variance at BS m.

If multiple UEs (e.g. 2 UEs) are decoded jointly by multiple BSs (e.g. 2 BSs) in a CoMP scenario as in Figures 2.4 (d and e), the formula in (2.5) evolves, and the CoMP rate for UE n[55]

$$\mathrm{Rate}_{\mathrm{n}_{\mathrm{CoMP}}} = \log_2 \left| 1 + \mathrm{h}_{\mathrm{n}}^{\mathrm{H}} \left(\mathrm{h}_{\bar{\mathrm{n}}} \mathrm{h}_{\bar{\mathrm{n}}}^{\mathrm{H}} + \begin{bmatrix} \hat{\sigma}_1^2 \mathbf{I} & 0 \\ 0 & \hat{\sigma}_2^2 \mathbf{I} \end{bmatrix} \right)^{-1} \mathrm{h}_{\mathrm{n}} \right|, \qquad (2.6)$$

where $\mathrm{h}_{\mathrm{n}} = \begin{bmatrix} \mathrm{h}_{1,\mathrm{n}} \\ \mathrm{h}_{2,\mathrm{n}} \end{bmatrix}$, $\mathrm{h}_{\bar{\mathrm{n}}} = \begin{bmatrix} \mathrm{h}_{1,\bar{\mathrm{n}}} \\ \mathrm{h}_{2,\bar{\mathrm{n}}} \end{bmatrix}$, $\mathrm{h}_{1,\mathrm{n}}$ is the channel response between BS 1 and UE n, $\mathrm{h}_{2,\mathrm{n}}$ is the channel response matrix between BS 2 and UE n and $\hat{\sigma}_1^2$ and $\hat{\sigma}_2^2$ are the noise variance at BSs 1 and 2 respectively.

We see the difference between conventional MIMO and CoMP MIMO rate formulas is that both UEs and BSs are considered in calculating the rate for one particular UE. The BSs exchange information about the received UEs signals, either over a backhaul in case of inter-site CoMP or without it in case of intra-site CoMP. In [39], further information on equalization schemes and information theory performance analyses are presented.

2.2.2 Measurements Collection Scenario

A measurement car that is traveling at a speed of around 7 Km/h drives the route. The length of the measurement route is around 17 km in total. It passes through surroundings of very different building structures. The UEs transmitted a block of 80 codewords during 10 seconds. Each one TTI (duration of 1 ms) is switching cyclically through all eight MCSs. For each loop through all MCSs, the maximum achievable rate (MCS) is determined based on the assumption of a constant channel for at least the duration of one loop, emulating a perfect rate adaptation [54]. The achieved rate is obtained by averaging over all loops per one measurement location. The measurements are collected at 887 locations distributed all over the testbed.

2.3 RT Simulation Environments Description

2.3.1 Radiowave Propagation Simulator (RPS)

Radiowave Propagation Simulator (RPS) is a radio coverage and performance-planning tool for a variety of radio systems [57]. RPS provides 3D ray tracing simulations to predict the propagation of electromagnetic rays through communication channels. RPS is following the principles of geometrical optics (GO) and the uniform theory of diffraction (UTD).

The propagation environments database has many materials and objects that can be modeled in the simulation environment up on demand.

There are many types of antennas of the tool database such as dipole, isotropic, cross polarized and biconical antennas. The radio network is configured by placing base stations at particular positions, while mobiles are usually set in as grids at places where channel data shall be obtained, as shown in Figure 2.5. This placement of transmitters or receivers points is performed on an XY Cartesian grid. A proper grid area can be set by designing a proper grid diameter.

More parameters have to be configured at antennas, such as the antenna height (elevation over ground) for both transmitter and receiver, transmitting power parameter, and carrier frequency.

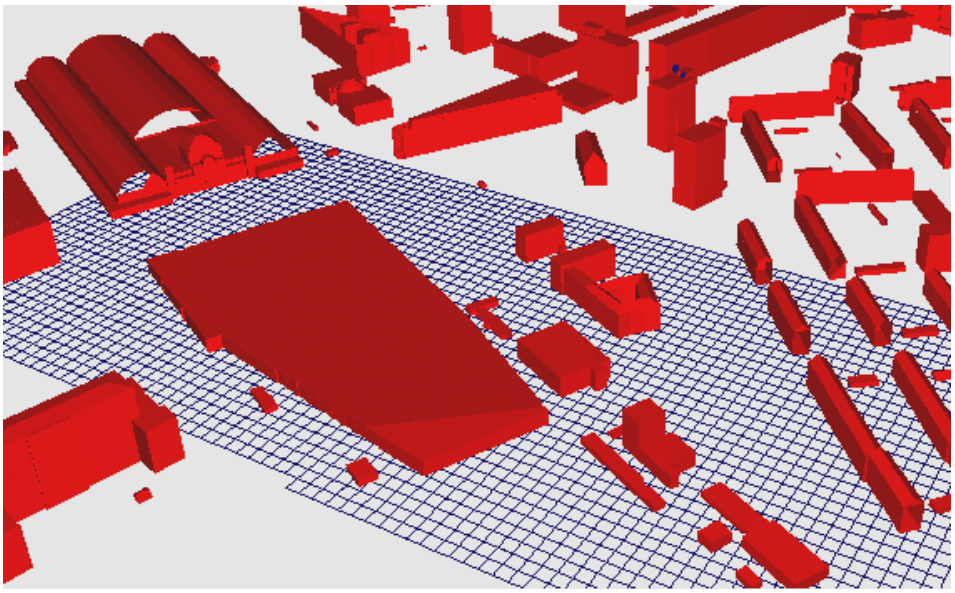

Figure 2.5 Example of receiver grids (blue squares) implemented in a 3D model.

A very important step in RT simulators is to configure the setup complexity. At this step, a trade-off between two key measures has to be decided, which are the accuracy of the results versus the speed of the simulations. In this step, two main algorithms are configured; the angular ray launching steps, and the RT limiting and cancellation thresholds.

The angular step size in angular ray launching algorithm determines the spacing between the rays that will be launched from a transmitter and eventually the total number of the transmitted rays. Two dimensions are considered here, a horizontal angle referred as theta (azimuth or orientation from north), and a vertical angle referred as phi (elevation or tilt from horizon).

The limiting and cancellation threshold is to set a pre-specified noise floor level, so that in the ray tracing process, rays are launched at the transmitter and propagate in the modeled environment until they hit the targeted receiver, or fall below the noise floor and are therefore cancelled. This way, RT is capable of simulating actual multi-path propagation.

More parameters related to GO and UTD algorithms can also be set, such as the maximum allowed number of reflections, penetrations, and diffractions that a ray can go through. The scattering model is configured depending on the simulated propagation environment. The maximum allowed delay that a ray can propagate could be limited, too.

Afterwards, network simulations can be performed and various outputs can be produced. Examples of RPS outputs are: complex channel impulse response (CIR), total received power, LOS, coverage area, DoD, DoA, best servers and delay spreads.

A very useful result from performing RPS ray tracing simulations is having complex radiation patterns and polarization from transmitting and receiving antennas. Storage of outgoing angles of arrivals and departures are transmitted from base stations and mobiles, which are used for the analysis of MIMO systems.

2.3.2 RT Extended CIR Components

CIR of an RT simulator consists of all MPCs and represents their temporal and angular properties. Hence, this CIR is called double directional, and is given for a static (time invariant) channel by

$$h(\vec{x}_{Tx}, \vec{x}_{Rx}, \tau, \phi, \psi) = \sum_{n=1}^{N} h_n(\vec{x}_{Tx}, \vec{x}_{Rx}, \tau, \phi, \psi) \quad , \tag{2.7}$$

$$\sum_{n=1}^{N} h_n(\vec{x}_{Tx}, \vec{x}_{Rx}, \tau, \phi, \psi) \quad = \sum_{n=1}^{N} \alpha_n \cdot \delta(\tau - \tau_n) \cdot \delta(\phi - \phi_n) \cdot \delta(\psi - \psi_n) \, , \tag{2.8}$$

where α_n, τ_n, ϕ_n and ψ_n represent the complex amplitude, delay, Direction of Departure (DoD) and Direction of Arrival DoA, respectively per MPC. The impulse response can also be extended to consider polarization effects by including a polarimetric matrix,

which describes the coupling between vertical (V) and horizontal (H) polarizations. The RT provides an extended CIR outputs which have 14 components cover the transmitting and receiving antennas polarity (cross or co-vertical), delay, DoD and DoA in two dimensions, the horizontal(ϕ) and the vertical (ψ).

2.3.3 Processing RT Channel Impulse Response

The output CIRs that resulted from RT simulations need to be pre-processed before being implemented in the UL receiver tool chain simulator. This processing is mainly utilizing the polarimetric output of the channel by splitting every single transmission between the UEs and the BSs. Each transmission has two impulse responses, one is between the UE and the co-polar antenna while the other one is between the UE and the cross-polar antenna. Therefore, the channel matrix is polarization dependent.

2.4 Uplink Receiver Simulator (Tool Chain)

As introduced, the UL transmitted field measurements and the simulated RT transmission results are processed in an offline processing tool representing a receiver built on LTE architecture. This is shown in Figure 2.6 as Matlab signal processing block.

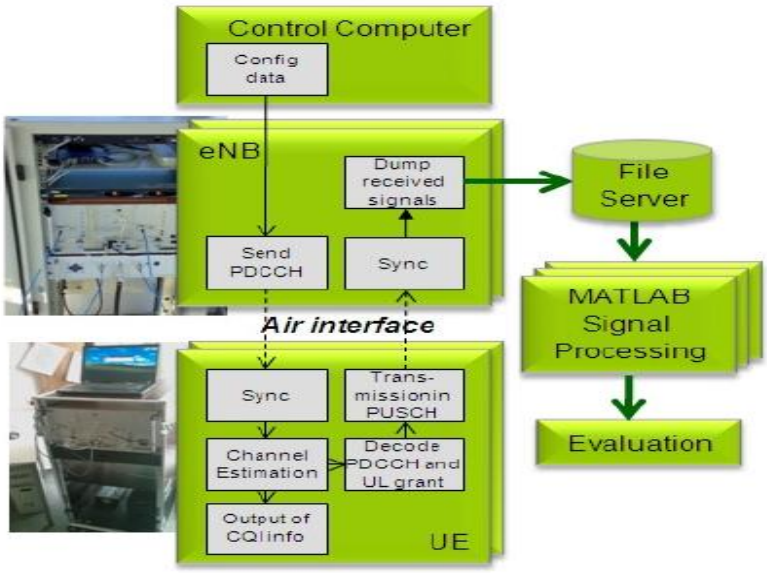

Figure 2.6 Overview of Receiver Processing Chain [55].

This receiver has an extra module in order to process the simulated RT channels in the receiver chain. The same signal transmissions that occurred during the field measurements is generated and transmitted through the RT simulated channels. In other words, the previously known codewords that were transmitted during field measurements will be generated and convolved with the RT channels to repeat the scenario that happened in the field measurements, before the signals are received and recorded by the UL receiver.

The UL receiver signal processing chain is depicted in Figure 2.7. The detailed signal processing architecture and evaluation concept are described in [54] and [55].

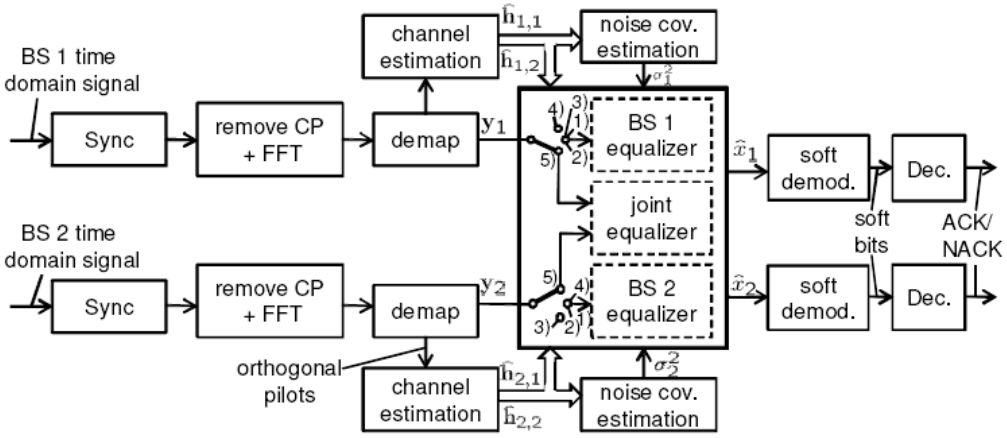

Figure 2.7 Receiver chain – adapted from [55].

2.4.1 Channel Estimation

A pilot based approach is used for channel estimation. Within each TTI, pilots are mapped on all sub-carriers of the 4th and 11th OFDM symbol. Interference between pilot symbols of different UEs is avoided by a code-orthogonal design. The channel of each UE is estimated for every second sub-carrier. Time and frequency interpolation and extrapolation are carried out separately to estimate the channel for all other sub-carriers.

As introduced, the system model has two UEs; each is having one antenna transmitting in uplink, therefore, M_T =2 and the BS has a cross polar antenna, that is two antenna elements, therefore, M_R = 2. The sampled received time domain signal at the receiver m antenna can be stated as [58]

$$y_n^m = \sum_{k=1}^{M_T} \sum_{\lambda=1}^{\Lambda^{m,k}} h_\lambda^{m,k} x_{n-\mu^{m,k}-\lambda}^k + v_n^m \quad , \tag{2.9}$$

where n denotes the discrete sample index, x^k representing a transmitted signal of antenna k and v_n^m is the added noise at antenna m. The variable $h^{m,k}$ =[$h_1{}^{m,k}$ … $h_\Lambda{}^{m,k}$] is the

sampled (unknown) CIR of length $\Lambda^{m,k} = \left\lceil \tau_c / T_s \right\rceil$ where τ_c is the channel delay spread and T_s is the sampling period. The integer valued Symbol Time Offset (STO) denoted by $\mu^{m,k} = \left\lceil \tau_d / T_s \right\rceil$ which is not known a-priori to the receiver and has to be estimated, too. Here τ_d represents the time delay. An STO can be caused by timing mis-synchronisation between UEs and BSs and Time Difference Of Arrivals (TDOAs) in the CoMP cooperating cluster.

The corresponding estimation model in frequency domain is approximated as [58]

$$Y_{o,q}^{m} = \sum_{k=1}^{M_T} \sum_{\lambda=1}^{\Lambda^{m,k}} H_{o,q}^{m,k} X_{o,q}^{k} \underbrace{e^{-\frac{j2\pi q \mu^{m,k}}{Q}}}_{\text{STO Phase}} + V_{o,q}^{m} \ , \qquad (2.10)$$

where $Q \subseteq \{1 \dots Q\}$ is a set of subcarriers allocated for data transmissions, q is the desired subcarrier and o is the OFDM symbol index, $H_{o,q}^{m,k}$ is the sampled interpolated channel transfer function at frequency bin q, $X_{o,q}^{k}$ is the transmitted symbol, m and k are the receiving and transmitting antennas respectively. Therefore, to recover the transmitted symbols $X_{o,q}^{k}$ over channel coefficients $H_{o,q}^{m,k}$, the STO ($\mu^{m,k}$) have to be estimated. Data symbols, frequency resources and references (or pilots) symbols are transmitted orthogonally in order to ensure accurate channel estimation, which is the basis for spatial decoupling of the data streams. In UL OFDM system, code orthogonal symbols are defined for training. We denote the set of pilot OFDM symbols by $\dot{p}_o$, the set of pilot subcarrier indices in the No. o OFDM symbol by p_o and the number of subcarriers per pilot OFDM symbol by $N_p = |p_o|, \ \forall_o \in \dot{p}_o$. The receiver knows all symbols $X_{o,q}^{m,k}$ transmitted on

subcarriers in this set. The channel estimation for time and frequency orthogonal pilots can be expressed as [58]

$$\widehat{H}_{o,q}^{m,k} = Y_{o,q}^{m,k} / X_{o,q}^{m,k} = H_{o,q}^{m,k} \underbrace{e^{-\frac{j2\pi q \mu^{m,k}}{Q}}}_{\text{STO Phase}} + V_{o,q}^{m} / X_{o,q}^{m,k} \quad \forall\ q \in p_o\ . \tag{2.11}$$

2.4.2 Channel Equalization

If residual synchronization errors are neglected, a flat fading channel is assumed on each subcarrier of bandwidth ΔF = 15 kHz, the received signal of each symbol on a single OFDM sub-carrier at BS m can be stated as [54]

$$y_m = h_{m,1} \cdot x_1 + h_{m,2} \cdot x_2 + n_m\ , \tag{2.12}$$

where $y_m \in \mathbb{C}^{[Nbs \times 1]}$ are the signals received by the N_{bs} antennas of BS m, $h_{m,k} \in C^{[Nbs \times 1]}$ denotes the channel gain vector from UE k to BS m, $x_k \in \mathbb{C}$ is a symbol transmitted by UE k, and $n_m \in \mathbb{C}^{[Nbs \times 1]}$ denotes additive, uncorrelated noise of covariance [54]:

$$E\{n_m\, n_m^H\} = {\sigma_m}^2\, \mathbf{I}\ . \tag{2.13}$$

In a CoMP case, if two BSs form a cooperation cluster (C) with elements {c1, c2}. The corresponding transmission model for C is given as [54]

$$\begin{bmatrix} y_{c_1} \\ y_{c_2} \end{bmatrix} = \begin{bmatrix} h_{c_1,1} & h_{c_1,2} \\ h_{c_2,1} & h_{c_2,2} \end{bmatrix} \begin{bmatrix} x_1 \\ x_2 \end{bmatrix} + \begin{bmatrix} n_{c_1} \\ n_{c_2} \end{bmatrix}\ . \tag{2.14}$$

As shown in Figure 2.4, equalization depends on the detection and cooperation scheme. In conventional MIMO scheme, a local equalization is performed (MMSE) shown in Figures 2.4 (b and c), the BS correct the scaling and phase rotation of the symbols as introduced by the channel. If UE n is locally detected at BS m, and subject to interference

from UE $\bar{n} \neq n$ (fig 2.4.b), the biased MMSE filter for a particular sub-carrier is given as [54]

$$G_{\text{biased}}^{[m,n]} = \hat{h}_{m,n}^{H} \left(\hat{h}_{m,n} \hat{h}_{m,n}^{H} + \hat{h}_{m,\bar{n}} \hat{h}_{m,\bar{n}}^{H} + (\hat{\sigma}_{m}^{2} \mathbf{I}) \right)^{-1}, \qquad (2.15)$$

where $\hat{h}_{m,n}$ and $\hat{\sigma}_{m}^{2}$ are the estimates of the channel and the noise.

If the interference of the other UE was cancelled (Figure 2.4.c), the MMSE filter in Equation (2.15) changes to [54]

$$G_{\text{biased}}^{[m,n]} = \hat{h}_{m,n}^{H} \left(\hat{h}_{m,n} \hat{h}_{m,n}^{H} (\hat{\sigma}_{m}^{2}) \right)^{-1} . \qquad (2.16)$$

In the case of CoMP JD as shown in Figure 2.4, an MMSE filter is used, which depends on whether interference subtraction (i.e. through SIC) has been performed in advance. If UE n is to be detected jointly (Figure 2.4.d), and still subject to the interference from UE $\bar{n} \neq n$, the biased MMSE filter for a particular sub-carrier is given as [54]

$$G_{\text{biased}}^{[n]} = \hat{h}_{C,n}^{H} \left(\hat{h}_{C,n} \hat{h}_{C,n}^{H} + \hat{h}_{C,\bar{n}} \hat{h}_{C,\bar{n}}^{H} + \text{diag}\left([\hat{\sigma}_{c1}^{2} \mathbf{I} \ldots \hat{\sigma}_{cC}^{2} \mathbf{I}] \right) \right)^{-1}, \qquad (2.17)$$

where $\hat{h}_{C,n}^{H} = \left[\hat{h}_{c1,n}^{T} \ldots \hat{h}_{cC,n}^{T} \right]^{T}$, and $\hat{\sigma}_{m}^{2}$ are the estimates of the noise.

If the interference of the other UE has been cancelled (Figure 2.4.e), the MMSE filter in Equation (2.17) changes to [54]

$$G_{\text{SIC,biased}}^{[n]} = \hat{h}_{C,n}^{H} \left(\hat{h}_{C,n} \hat{h}_{C,n}^{H} + \text{diag}\left([\hat{\sigma}_{c1}^{2} \ldots \hat{\sigma}_{cC}^{2}] \right) \right)^{-1}, \qquad (2.18)$$

where $\text{diag}(\cdot)$ takes a vector of size N to a diagonal matrix of size N × N, and $\text{diag}(\cdot)^{-1}$ maps the diagonal elements of any square matrix of size N × N to the entries of a size N vector. Hence, if $\text{diag}(\cdot)^{-1}$ and $\text{diag}(\cdot)$ are used successively, the off diagonal elements of the resulting matrix are all zero.

CHAPTER 3

APPLICATIONS OF RT IN THE RECEIVER CHAIN

3.1 Introduction

Chapter 3 covers the pre-processing of the RT channels before undergoing into the LTE-A tool chain signal processing. This includes additions and enhancements that increased the accuracy of the results. However, there will be errors due to differences between ray traced and measured channels and the impact of impairments happening in both environments. Few examples on these impairments are listed here:

Transmitter:

- IQ imbalance
- Non-linearity of Power Amplifiers (PA)

Channel:

- Estimation errors of CSI
- Simulation errors (in the receiver chain or RT simulators)

Receiver:

- Carrier Frequency Offset (CFO)
- Sampling Clock Offset (SCO)
- Phase Noise
- Analog to Digital Conversion (ADC) effect
- IQ imbalance

RT 3D map:

- Absence of small diffraction objects (e.g. balconies)
- Absence of small scattering objects (e.g. trees and cars)
- Absence of few big structures (e.g. a couple of buildings)

To compensate some of the errors that reduce accuracy of results, here are three introduced factors to enhance the setup and the results. These factors were trialled and proven to be working.

3.2 AWGN Noise Addition to RT Transmissions

Unlike field measurements, the RT transmission is not received by a real hardware (base station). Therefore, there is a need to add noise similar to the same noise caused by the real hardware in the field measurements.

A basic noise model is being adapted which is representing the thermal noise as AWGN and expressed as

$$AWGN = K \cdot T \cdot B \,, \tag{3.1}$$

where K: is the Boltzmann constant, T: is the thermal temperature, B: is the total bandwidth used for transmission.

An assumed noise Figure (NF) value is copied from the field receiver in order to imitate the loss of the transmitted signal power in the receiver.

Therefore, the total noise can be expressed as the sum of both thermal noise and NF as follows

$$\text{Total Noise} = AWGN + NF \,, \tag{3.2}$$

Table 3.1 shows the values used in the simulations.

Table 3.1 Noise design parameters.

Parameter	Value	Comments
K	1.3806504e-23	Boltzmann constant in dBm/degree K/Hz
T	290	Temperature in degree K
B	20	Bandwidth in MHz
NF	5	Base station Noise Figure in dB

3.3 Design of Sample Time Offset (SaTO) in RT Transmissions

During field measurements, UEs were not transmitting at the same time but with a delay interval that equals to 34 OFDM samples (about 1 μs). To introduce this behavior we padded 34 zeros to RT CIRs. This would guarantee that UE2 is idle for 34 samples while UE1 is transmitting. This adaptation is called as Sample Time Offset (SaTO). Figure 3.1 shows the design of SaTO offset. Statistical evaluation is shown in Table 3.2. It is shown that SaTO introduction improves the matching between measurements and RT simulated channels.

...	CIR_UE1	CIR_UE1	Padding zeros	CIR_UE1	CIR_UE1	Padding zeros	...
...	Padding zeros	CIR_UE2	CIR_UE2	Padding zeros	CIR_UE2	CIR_UE2	...

Figure 3.1 SaTO adaptation in RT resulting by padding zeros to the resulting CIR.

We observed during field measurements that the real hardware measured SNR values between -5 dB and 33 dB, while RT simulator could detect SNR values between -10 dB and 43 dB. The limitations in the field measurements was caused by the real hardware. This is shown in Figure. 3.2, which presents the SNR CDF results of field measurements and RT for the top 7 detected BSs. RT simulated SNR values were higher on almost all BSs. Figure 3.3 shows the SNR CDF comparisons for all 16 BSs for both field measurements and RT simulations. We can see that the introduction of SaTO improves the matching accuracy between field measurements and RT channels.

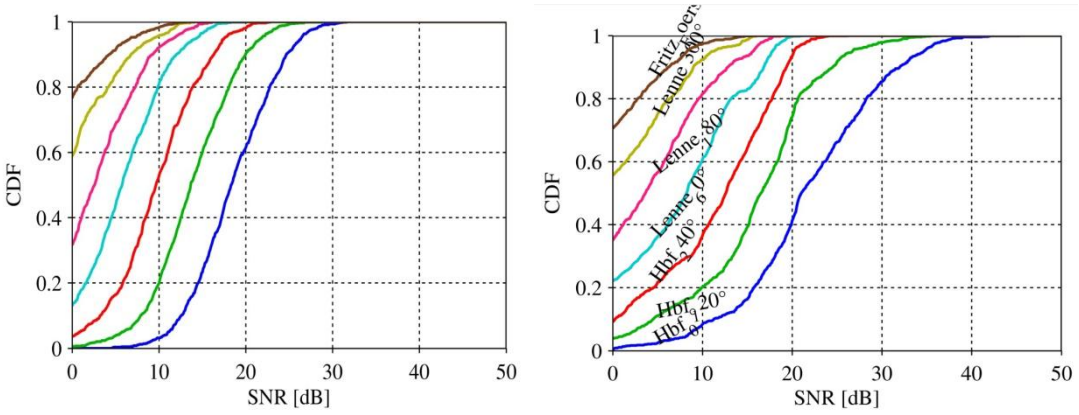

(a) (b)

Figure 3.2 SNR CDF for the highest SNR values at the top 7 BSs (a) field measurements (b) RT simulations.

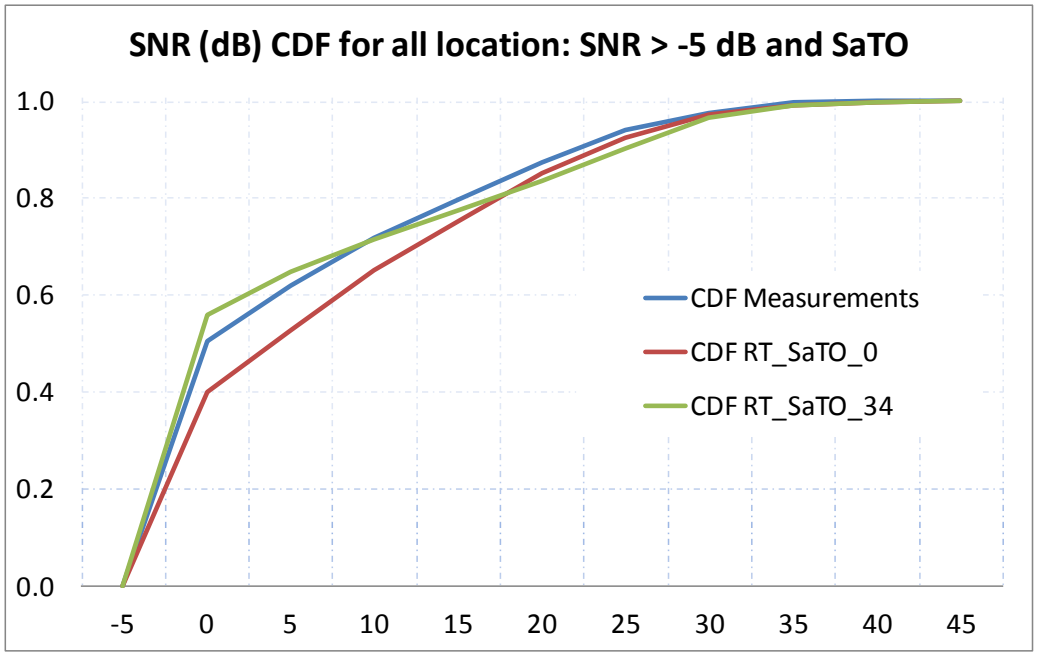

Figure 3.3 SNR CDF for three scenarios, without SaTO introduction (SaTO = 0), with SaTO introduction (SaTO = 34), and measurements.

Table 3.2 Statistical evaluation of SNR values.

	Field Measurements	RT Simulation with-out SaTO (zero)	RT Simulation with SaTO (34 samples)
Mean	0.45	-5.65	-1.05
Standard Deviation	15.05	15.65	16.80
Median	-0.20	-7.41	-2.45

An important observation from the SNR CDF comparison is that in the field measurements SNR values below -5 dB were not measured but considered as a noise. While in RT simulated channels (without SaTO introduction), low SNR values were detected even as low as -10 dB. Apparently, this is related to the limitation of the real-world hardware sensitivity of receiving values and very low SNR values, while this is not a concern in the RT simulation. In RT simulation, a threshold introduced earlier called RT limiting and a cancellation threshold is set to follow the real-world equipments sensitivity.

3.4 Verification of CoMP Channel Estimator Using RT Modeled Channels

3.4.1 Introduction of Channel Estimation in LTE System

Channel estimation plays necessary functionality in an OFDM system such as LTE. Accurate channel estimation increases the capacity of OFDMA systems by improving the system performance in terms of bit error rate. In a typical LTE receiver, pilot symbols that are known at the receiver are used to perform the channel estimation. Through interpolation, it is possible to estimate the channel across an arbitrary number of subframes.

3.4.2 RT Channels Signal Processing Simplification in the CoMP Chain

The signal processing in the CoMP tool chain includes channel estimation part for both measured and RT simulated channels. However, as we are completely aware of the RT simulated channels, we have available Channel State Information (CSI). Therefore, channel estimation is bypassed for RT channels and a low complexity CSI signal processing approach is achieved. The channel estimation ($\widehat{H}_{o,q}^{m,k}$) described in Section 2.4 for time and frequency orthogonal pilots in (21)

$$\widehat{H}_{o,q}^{m,k} = Y_{o,q}^{m,k}/X_{o,q}^{m,k} = \underbrace{H_{o,q}^{m,k}}_{\text{Interpolated CTF}} e^{-\frac{j2\pi q\mu^{m,k}}{Q}} + V_{o,q}^{m}/X_{o,q}^{m,k} \quad \forall\ q \in p_o \ ,$$

is simplified through the following three steps:

- Channel interpolation is removed for RT setup, which was used to estimate the channel across an arbitrary number of subframes. A direct Channel Transfer Function (CTF) is used instead of an interpolated one.
- The STO factor ($e^{-\frac{j2\pi q\mu^{m,k}}{Q}}$) is a known a priori to the receiver and does not need to be estimated.

Therefore, the channel estimation equation (2.11) can evolve as

$$\widehat{H}_{o,q}^{m,k} = Y_{o,q}^{m,k}/X_{o,q}^{m,k} = \underbrace{H_{o,q}^{m,k}}_{\text{Direct CTF}} \underbrace{e^{-\frac{j2\pi q\mu^{m,k}}{Q}}}_{\text{STO Phase}} + V_{o,q}^{m}/X_{o,q}^{m,k} \quad \forall\ q \in p_o \ . \qquad (3.3)$$

Noise estimation is kept the same for both RT and measured channels. Noise estimation for RT channels is now more accurate as we are obtaining it directly from the non-estimated channel (without any interpolation).

3.4.3 Comparisons between Perfect and Estimated CSI for RT Channels

SNR Results

Figure 3.4 shows the SNR delta between estimated channels and perfectly known channels depending on UE position and serving BS. The color bar shows that most of the SNR differences are in the range between -5 dB and +5 dB. SNR detailed analysis can be seen in Chapter 4.

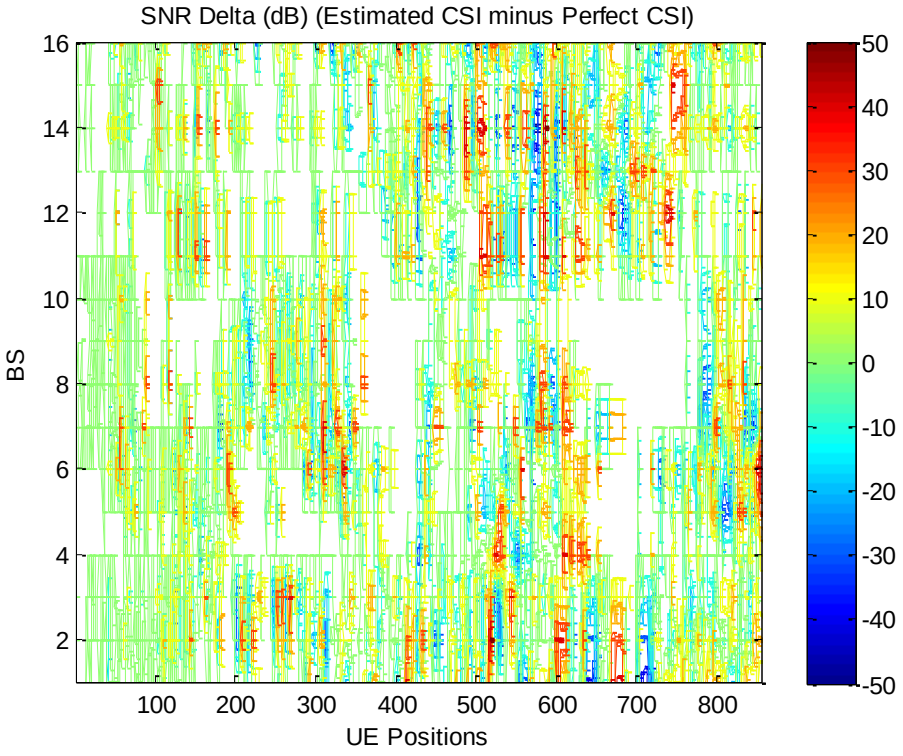

Figure 3.4 SNR map showing the delta between Estimated CSI vs. Perfect CSI per BS and per UE position.

SINR Results

SINR results are correlated to SNR results. The below histograms in Figures 3.5 (a-d) show how many samples have delta in SINR values when comparing perfect CSI channels with estimated channels. SINR detailed analysis can be seen in Chapter 4.

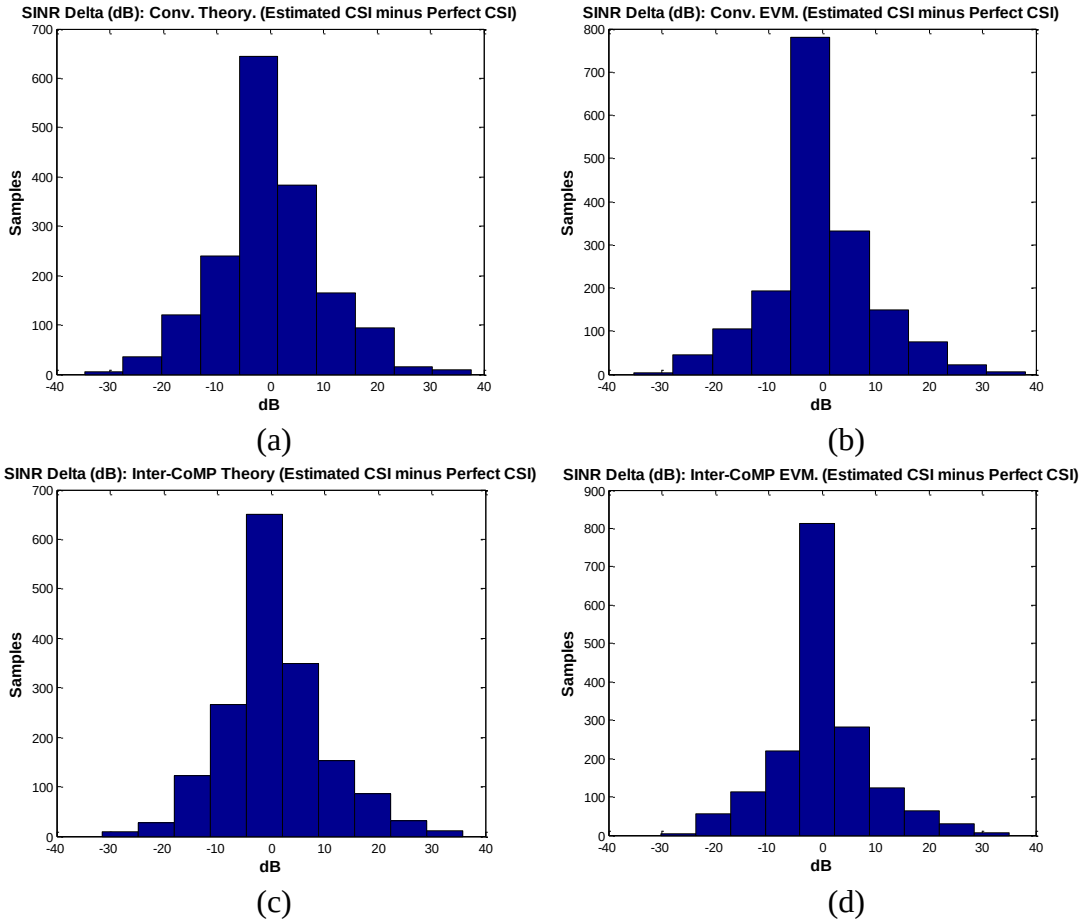

Figure 3.5 SINR histograms Comparison between Estimated CSI vs. Perfect CSI for CoMP scenarios Conv. MIMO (a and b) and Inter-CoMP (c and d).

Using a perfectly known CSI and STO gives a deviation by 3% in SINR CDF compared to estimated ones. An example here is the Inter-CoMP approaches shown in Figure 3.6.

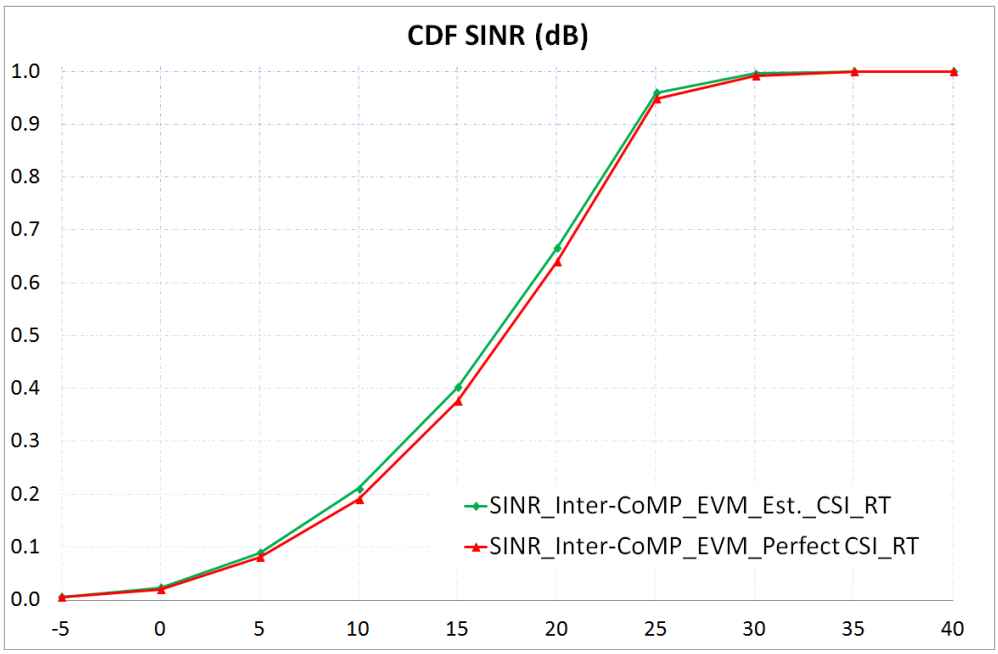

Figure 3.6 SINR CDF values comparison between Estimated CSI vs. Perfect CSI for Inter-CoMP scenario, EVM approach.

Symbol Time Offset (STO)

In a CoMP cooperating cluster, the timing mis-synchronisation between UEs and BSs and the delay spread is bigger than the values in conventional transmission. As explained earlier in (20) the STO ($\mu^{m,k}$) is estimated using the channels coefficients. When comparing the estimated STO with the known STO values we see that in both CoMP scenarios intra and inter there is no big delta in STO values and most of the samples are concentrated around the value zero microseconds (indicating no or very small delta). Positive samples indicate longer known STO values and negative samples indicate longer estimated STO values as shown in Figure 3.7 (a-b).

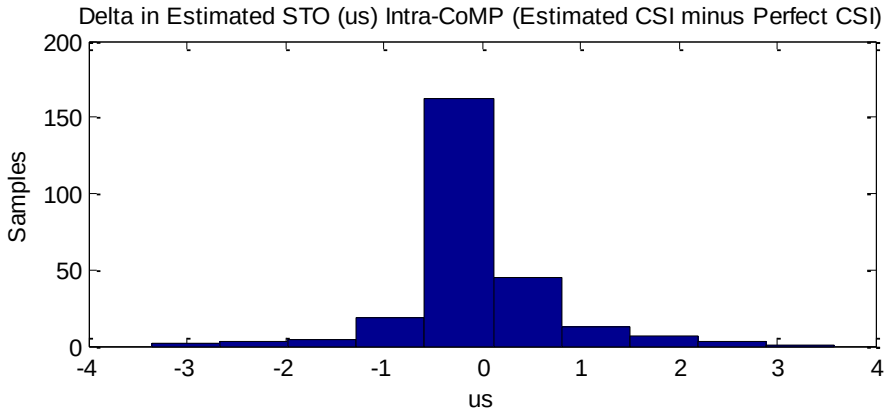

(a)

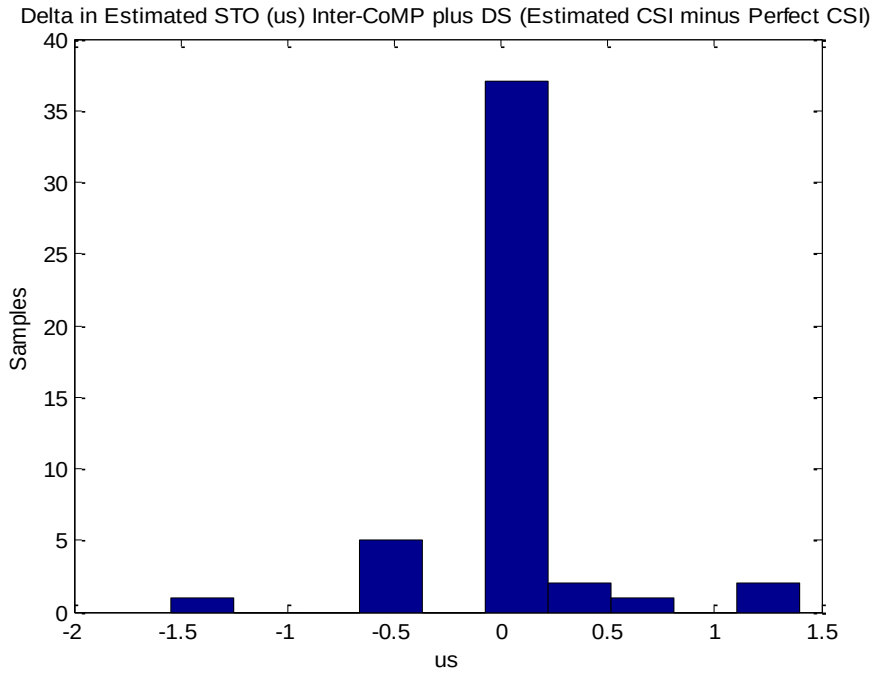

(b)

Figure 3.7 Estimated STO values comparison between Estimated CSI vs. Perfect CSI for CoMP scenarios (a) Intra-CoMP and (b) Inter-CoMP + DS.

Channel Estimator Evaluation

The channel estimation is based on:

- Linear interpolation LaGrange filter, which is depending mainly on the number of orthogonal pilots and the number of UEs
- A moving average window for the pilots symbols

Based on the comparison results show in Figures 3.4-3.7, we could see that the used estimation methods achieved accurate results.

CHAPTER 4

VERIFICATIONS OF RT CHANNEL MODELING AGAINST CoMP MEASUREMENTS

4.1 Introduction

Chapter 4 presents the verification results using RT modeling and simulations for two different field measurements in the described testbed. The first verifications case is based on considering three BSs. The second is considering all 16 BSs in the testbed. The verifications are done through comparisons of SNR, SINR, and spectral efficiency with field measurements in a CoMP receiver tool chain. The comparisons cover 24 conventional MIMO and CoMP MIMO scenarios. A short comparison between EPM and RT models in terms of accuracy and complexity is highlighted.

4.2 RT Simulations vs. First Field Measurements Campaign

In [59], RT simulator was modeled to calculate the received signal power at different receivers' locations and downtilts, under LOS and NLOS situations. An aspect of the work was to compare and verify the RT path loss and delay results with the field measurements. The most important RT parameters are summarized in Table 4.1. Table 4.2 provides the main parameters for the antenna system used in this test case.

Table 4.1 Key parameters used in RT model.

Parameter	Configurations
Noise Floor	-100 dBm
Angular ray launching step	1˚, (0.1˚)*
Max. number of reflections	Infinite
Max. number of penetrations	4
Max. number of diffractions	3
Scattering model	Directive
Depolarization method	Mean
Buildings permittivity coefficient (real part)	5
Surface effective roughness	0.3
UE Inter-Distance	5 meters
Downtilts: UE1 / UE2	-76˚/ +42˚
Azimuth UE1 / UE2	0˚/ +35˚
UE (Transmitter) Grid Area	5 m^2

* Launching step of value 0.1 degrees was used in particular simulations

Table 4.2 Parameters of antenna system in RT model.

Property	BS 1	BS 2	BS 3
Antenna height over ground [m]	54.5	50.1	32.5
Kathrein antenna type	800 105 41	800 106 29	800 106 29
Antenna gain [dBi]	18	16.5	16.5
Elect. Downtilt [°]	6-15	6-15	6-15
Half power beamwidth			
Vertical [°]	6.2	7.5	7.5
Horizontal [°]	58	80	80

4.2.1 Test Cases Description and Comparison Results

The first test case is performed under three base stations and at five receivers' locations. The second test case is performed under one base station and at seven different locations.

RT verifications for both cases showed that results were matching with field measurements except when field measurements had an issue at particular scenario [53].

The downtilt (DT) of each BS antenna is varying between 6 and 15 degrees. The analyses show that the signal maximum power is to be at a LOS location in the main lobe of a sector and dependent on DT value. Therefore, the term geometrical DT (geoDT) is introduced which indicates the optimal geometrical DT defined as the LOS propagation angle between BS and UE. This can be measured by the formula [53]

$$\phi_{geo}(i,j) = \arctan\left(\frac{h_j}{d_{i,j}}\right), \tag{4.1}$$

where $d_{i,j}$ is the distance between the UE (i) location and the BS (j), h_j is the height of the BS antenna. These two characteristics and the LOS/NLOS situations are all given in Table 4.3. If we assume a LOS situation, at this theoretical geometrical angle, the UE received power is supposed to be maximum [53].

Table 4.3 Test case 1: geometrical properties [53].

	Distance [m]			Geom. DT[°]			LOS/NLOS		
Location	BS 1	BS 2	BS 3	BS 1	BS 2	BS 3	BS 1	BS 2	BS 3
1	299	418	679	10.3	6.8	2.7	no	No	no
2	325	392	777	9.5	7.2	2.4	no	no	no
3	199	573	810	15.3	5	2.3	yes	no	no
4	214	710	461	14.3	4.0	4.0	no	yes	no
5	259	472	790	11.8	6.0	2.4	no	yes	no

During the evaluation, the Channel Transfer Function (CTF) $H_{s,t,r,i,j,\Phi_{tilt}}(n)$ of BSs was estimated. The average channel power $p_{i,j}$ is [53]

$$p_{i,j,\Phi_{tilt}} = \frac{1}{N_s N_t N_r} \sum_{s=1}^{N_s} \sum_{t=1}^{N_t} \sum_{r=1}^{N_r} \left(\sum_{n=1}^{N_p} \left| H_{s,t,r,i,j,\Phi_{tilt}}(n) \right|^2 \right), \tag{4.2}$$

where N_s is the number of measurements taken per location, N_t is the number of transmit antennas, N_r is the number of receiving antennas and N_p is the number of OFDM pilots transmitted in every slot. ($N_t = N_r = 2$), $N_s = 300$, $N_p = 200$. Φ_{tilt} is the downtilt angle [53].

The signal power results are expressed relatively to the highest average channel power.

While seeking accuracy improvements of the RT simulations, the ray launching step size was reduced from 1° to 0.1°, which gave better results for channels to BS2 at locations 1, 2, and 3, especially at higher DT values. The reason for this is because the transmitted signal is exposed to less free space propagation and more to the details of the terrains. Therefore, a more accurate modeling of the signal propagation using a larger number of rays achieved a more accurate channel propagation model. This increase in RT simulation complexity which is needed and significant at all locations where NLOS dominates, such as between BS2 and locations 1, 2 and 3, keeping in mind that the number of rays and the computation complexity increased 100 times when the step size is changed from 1° to 0.1°. This is a good example for the importance of the trade-off between accuracy and complexity in RT. Certainly, this is a drawback of RT because a large calibration effort is required to find proper settings for each individual study.

Figure 4.1.a shows two significant rays (channel taps) measured at the hardware-monitoring tool, which are about 0.63 μs apart (delayed). The more delayed path is stronger than the earlier one. These taps were exactly identified in the RT simulator as shown in Figure 4.1.b; the building to the right reflects the transmitted signal, which is stronger compared to the shorter signal, reflected from the upper building. Interestingly,

the results show that the longer path has higher received level and this draws attention to on how can building material cause loss of energy at a particular reflection point.

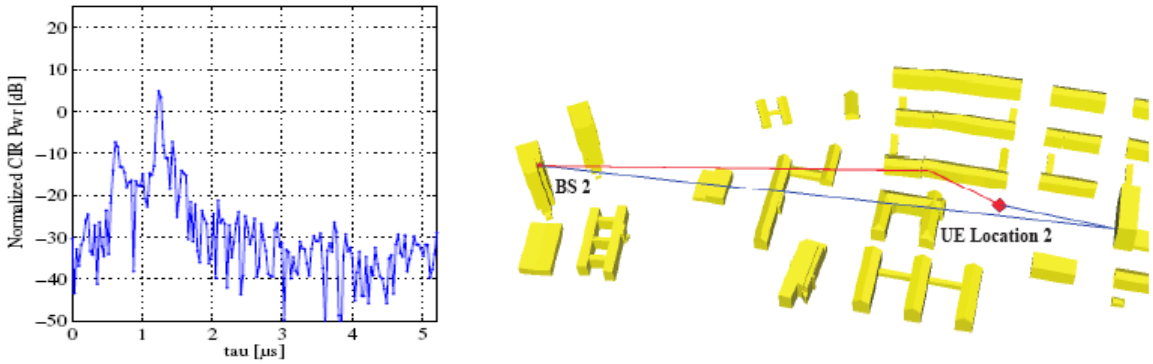

(a) (b)

Figure 4.1 Case 1, (a) Channel Impulse Response (CIR) between BS2 and UE2. (b) Rays distribution between BS2 and UE2. The Power-Delay-Profile (PDP) from RT is matching the field measurements.

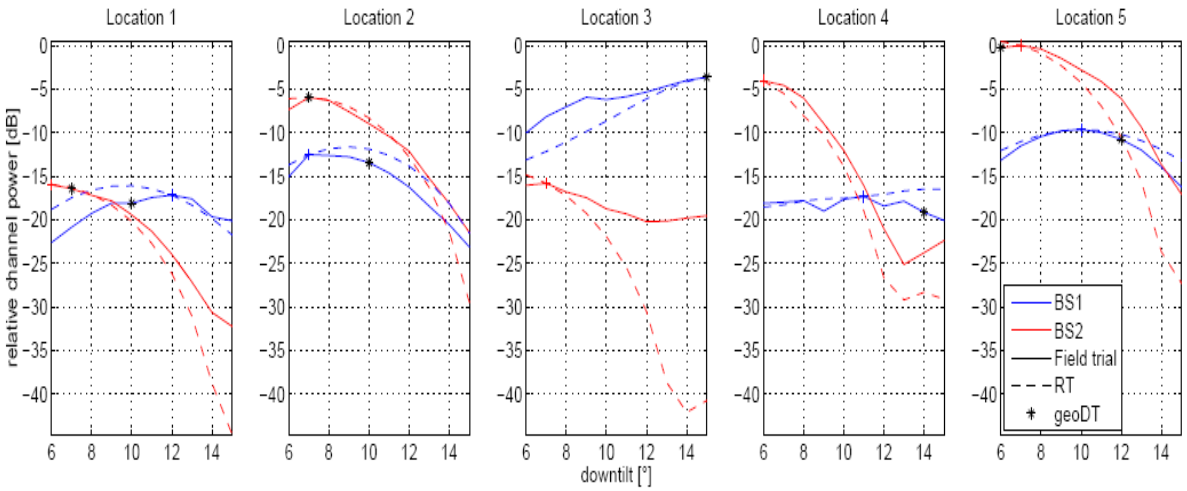

(a)

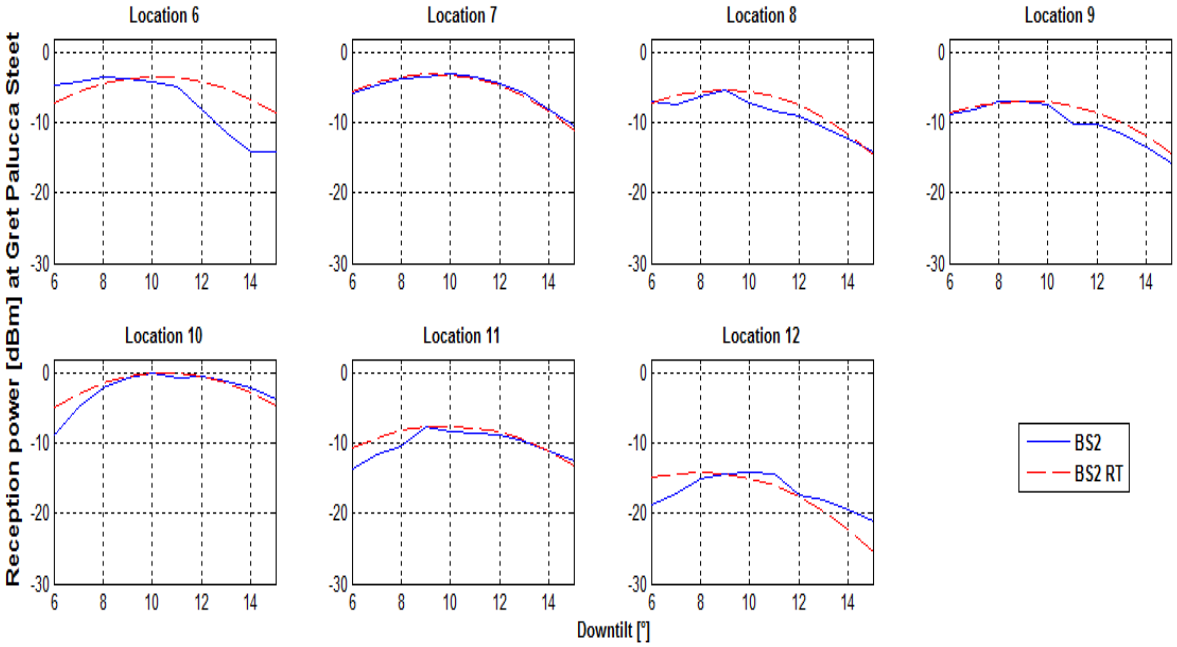

(b)

Figure 4.2 Measured UE relative channel power compared to results of the RT model

(a) Case 1: (b) Case 2

In case 1, RT results are matching the measurements very well at most locations and at different DTs. It can be noticed that at high DT values for BS2, some of the locations in RT model results have different power level trends than in field measurements (except location 3 which had an issue in the measurements).

One explanation for this observation could be the absence of small scattering details. Some of the chosen locations are located in vicinity of dense trees. A possible solution is to enhance the 3D map by various optimization techniques, e.g. by the pre-creation of different trees. Another reason for these slight differences is that the RT simulator at this test case used in these simulations an LTE antenna pattern that is similar but not using the exact pattern of the antennas used in the field measurements test bed. Another improvement technique might be by using the spatial averaging technique to avoid the inaccuracy of receiving antenna positions.

A problem observed during measurements after being highlighted by ray tracing simulations is the inter-carrier interference (ICI) impact on some measurements. This effect is certainly not severe when channels to BSs are of strong signal, but when channels differ by around 15 dB. This case is shown for measurements between BS2 and receiver at location 3, the difference between RT and measurements is not due to inaccuracy in the RT model but in the measurement. This case was also observed for multiple measurements with BS3.

In case2, locations are separated by 25 meters. The target of this case was to verify the geometrical impact on the maximum received power due to location change and at different downtilts (DT) values. The RT results are matching the measurements very well at most locations and DTs, as depicted in Figure 4.2.b. It was observed that there is a DT

dependency at all locations and the absolute values differ by up to 14 dB depending on the UE location

4.3 RT Simulations vs. Second Field Measurements Campaign

Second field measurement is performed under the complete 16 BSs in the test bed. Eight hundred and eighty-seven locations were measured. Two UEs are transmitting in UL at each location using one dipole antenna. Each receiving BS is having a cross-polarized antenna, that is, two antennas. The target is to verify and analyze the performance using RT simulations compared to field measurements. Many results are presented, mainly SNR, SINR and spectral efficiency rates. These results are the output of multiple MIMO decoding schemes. The first decoding scheme is the conventional MIMO, which will be referred to later on as Conv. MIMO, where two UEs are transmitting and only one BS with two antennas is receiving. Conventional scheme (Conv.) is a non-CoMP scheme and there is no cooperating cluster defined. The second MIMO scheme is decoding both UEs by more than one BS. This scheme is representing CoMP and having cooperating clusters composed of two BSs. CoMP covers both intra-CoMP and inter-CoMP schemes. Intra-CoMP scheme represents decoding UEs at cooperating BSs belonging to the same site. Inter-CoMP scheme represents decoding UEs at cooperating BSs belonging to different sites. A linear detection scheme will be used and sometimes followed by SIC signal processing. Moreover, after equalization, SINR values are estimated using theoretical approaches or EVM approach. EVM can offer insightful infor-

mation on the various transmitter imperfections, including carrier leakage, IQ mismatch, nonlinearity, local oscillator (LO) phase noise and frequency error [60].

4.3.1 Signal to Noise Ratio (SNR)

The SNR depends on the average channel power $\widehat{H}^{m}$. Therefore, estimated SNR value per UE (k) at BS (m) can be expressed as

$$\widehat{SNR}_{m,k} = \frac{E_{o,q}\left\{\left|\widehat{H}^{m}(k)\right|^{2}\right\}}{\widehat{\sigma}^{2}_{V,m}} \quad . \tag{4.3}$$

Therefore, estimated SNR values per BS (m) which are the sum of SNR values from all UEs, can be expressed as

$$\widehat{SNR}_{m} = \frac{E_{o,q}\left\{\sum_{k=1}^{K}\left|\widehat{H}^{m}(k)\right|^{2}\right\}}{\widehat{\sigma}^{2}_{V,m}} \quad , \tag{4.4}$$

where $\widehat{H}^{m}$ is the estimated channel, k is the number of UEs transmitting under the BS and $\widehat{\sigma}^{2}_{V,m}$ is the estimated noise power over all OFDM symbols. $E_{o,q}\{\cdot\}$ averages over all sub-carriers (q) and OFDM symbols (o).

Figure 4.3 shows the $\widehat{SNR}_{m,k}$ values for each BS and locations, for measurements (a) and RT simulations (b). From this plot, we can notice big matching for $\widehat{SNR}_{m,k}$ value per location between both setups measurements and RT. One main observation is that $\widehat{SNR}_{m,k}$ for RT simulations in general is higher than the ones in field measurements.

In conventional cellular system, the strongest BS server, the one with the highest SNR value, would serve each UE. This is denoted in fig. 4.3 as the largest SNR BS. As seen in previous experiment [59], the BS antenna downtilt has a great impact on results; therefore, downtilt was fixed here to all BSs antennas at 6 degrees.

The largest and second largest SNRs values at any BS for each location are depicted in the upper part of the figure. In CoMP scenarios, cooperation clusters exist between more than one BS. If the criterion of forming CoMP cooperation cluster is based on BSs with the highest received SNR, then, if the two highest SNR values belong to the same site, the term “intra” is used to indicate that these BSs can be forming an intra-site cooperation cluster of size two. This can be seen in the upper part of the plots. If the largest two SNR values belong to BSs of different sites, then the cooperation cluster is formed as “inter” site, this is not shown on the figure. All results shown in Figure 4.3 are based on cooperation cluster of size two. We can observe that more locations can have second largest inter-site SNR values than intra-site. Inter-site CoMP requires additional resources called backhauling to exchange data between BSs, while intra-site CoMP does not need that.

Based on Figure 4.3, a cluster of size three does not seem to be very beneficial for intra-site CoMP, because the SNR values at the strongest BS (largest) is much larger than the SNR of the third strongest BS under the same site. A third strongest BS under a different site with high enough SNR will be beneficial to form an inter-site CoMP cluster of size three. A CoMP cluster is formed based on the strongest SNR values to achieve highest possible spectral efficiency.

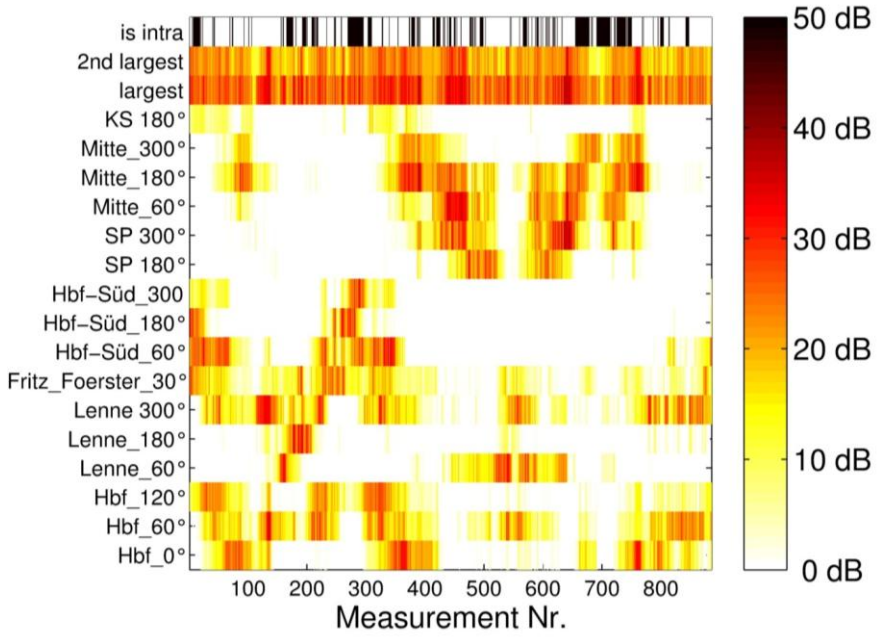

(a)

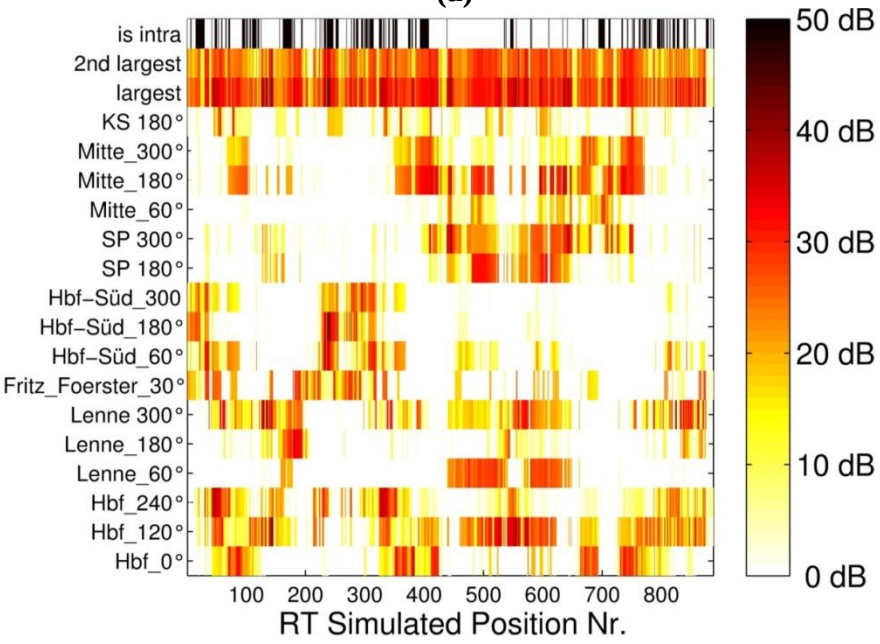

(b)

Figure 4.3 SNR distributions over all BSs and locations. (a) Measurements and (b) RT simulations.

To analyze the reason behind that SNR values of RT results are higher than field measurements, SNR CDF plotted in Figure 4.4. Based on the CDFs in Figure 4.4, it can be ob-

served that in field measurements, no SNR values below -5 dB were measured due to real hardware limitations, while in RT simulator all SNR values until -10 dB were detected.

Figure 4.4 shows SNR CDFs when considering the outage samples in measurements (SNR <-5 dB) compared to RT SNR CDF. Another important indicator that can be seen is the impact of the transmission sequence on the received SNR values. As introduced earlier in chapter 3, in field measurements both UEs were not transmitting at the same time, but there was a delay of around 34 samples, which is equivalent to around 1 micro-second (sampling rate was $30.72*10^6$). Interestingly, when this delay was introduced to RT simulation CIR matrix, it caused worse SNR values by around 5 dBs for 10% of SNR CDF values compared to not considering any SaTO delay. This made RT simulated SNR values closer to the measured SNR values. Therefore, the emulation of UE transmission order by introducing this SaTO gave a higher matching between field measurements and simulation.

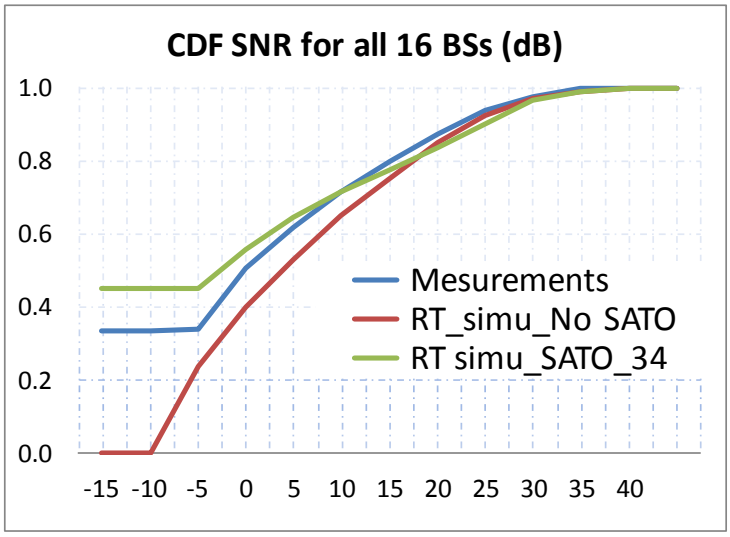

Figure 4.4 CDF for SNR values with different scenarios

In Table 4.4, we present the statistical mean, standard deviation and median values for SNR values resulting from both field measurements and RT simulations. The table covers

three scenarios, field measurements, RT simulations without SaTO introduction (SaTO=0) and with SaTO introduction (SaTO=34). Apparently, SaTO introduction makes the results more matching and differences are of around 2 dB in terms of mean value and around 1 dB in terms of standard deviation, which is a very good matching.

Table 4.4 Statistical evaluation for SNR values with different scenarios.

Scenario	Mean (dB)	Standard Deviation (dB)	Median (dB)
Field Measurements	0.45	15.05	-0.20
RT_Simulations with SaTO =0	-5.65	15.65	-7.41
RT_Simulations with SaTO =34	-1.05	16.80	-2.45

Based on comparing signal to noise ratio (SNR) values between field measured and RT simulated transmissions, some differences were observed at some locations. 3D model impairments such as missing objects are, mainly but not exclusively, building, cars, and bushes. These will influence also the scattering behaviour of the rays.

An example therefore is shown in Figure 4.5, which is for SNR values distribution per location, comparing both field measurements (blue), and RT simulations (green) at all 887 positions in the testbed. It is shown that RT simulated SNR values are higher than the measured ones at locations varying between 440 and 600. These locations are mainly those of NLOS transmissions where terrain and 3D play a big role in the results accuracy. The SNR values for LOS locations such as from 810 till 887 are having a similar or a comparable level between measurements and simulations as shown in Figure 4.5.

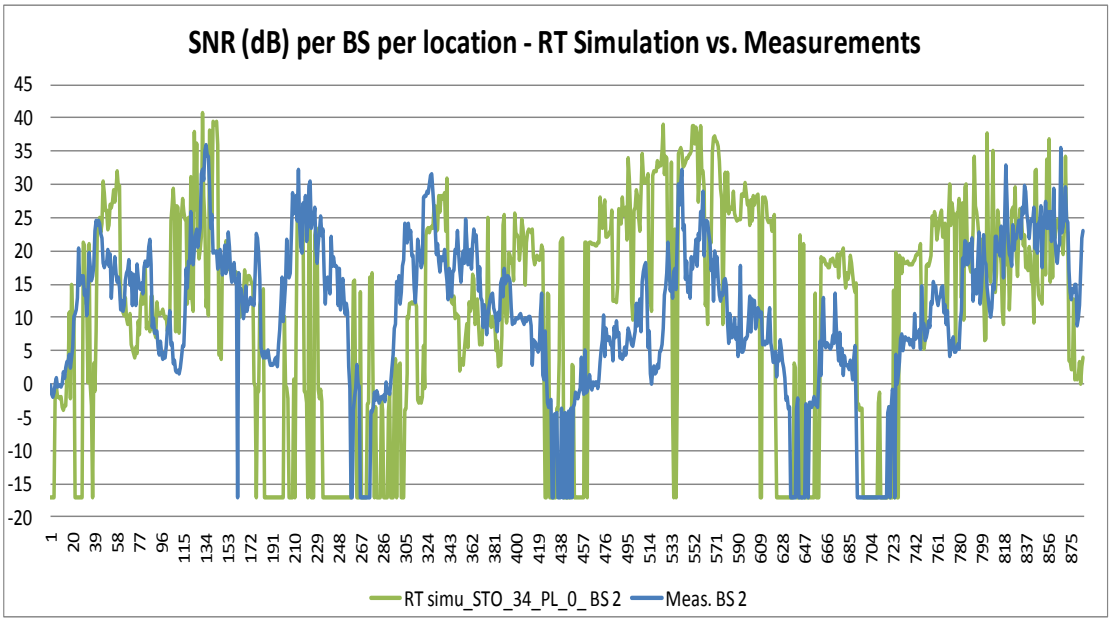

Figure 4.5 An example case where RT simulations and measurements do not match in NLOS scenarios and match in LOS scenarios

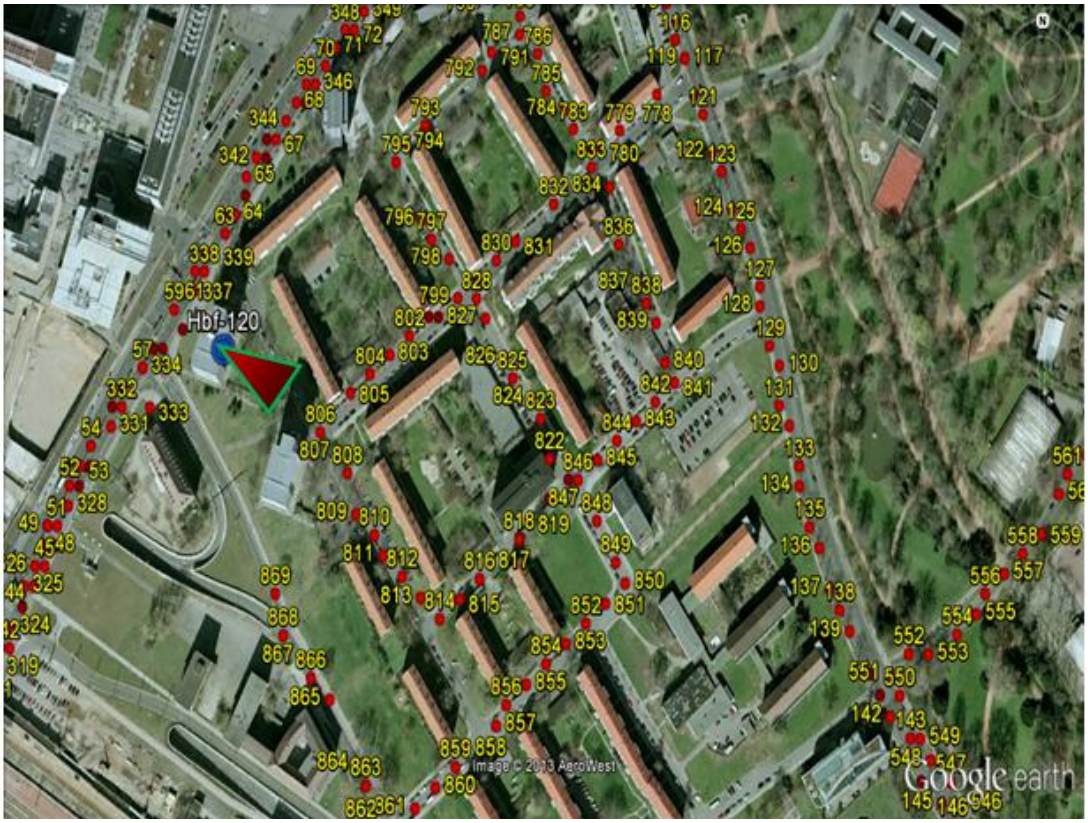

Figure 4.6 An example case transmission locations distribution around the site Hbf120 where the SNR values are matching between field and RT.

4.3.2 Signal to Interference plus Noise Ratio (SINR)

Linear filters were used in order to obtain post equalization SINR values in order to estimate the maximum achievable system capacity. Using the same transmission model in Equation (2.1), for an instantaneous channel realization we get

$$Y_{o,q} = \hat{H}_{o,q} X_{o,q} + V_{o,q}\,, \tag{4.5}$$

where $\hat{H}_{o,q} = \left[\hat{H}^{1}{}_{o,q} \ldots \hat{H}^{M}{}_{o,q}\right]^{T}$, M is the maximum number of receiving antennas.

The transmitted symbols $X_{o,q}$ are estimated by multiplying a linear filter matrix $G_{o,q}$ to the available observation vector

$$\hat{X}_{o,q} = G_{o,q} Y_{o,q} = G_{o,q}\left(\hat{H}_{o,q} X_{o,q} + V_{o,q}\right). \tag{4.6}$$

The filter minimizes the mean square error (MSE) given by the Linear Mean Square Error (LMMSE) as

$$G_{o,q} = \left(\mathbf{I} + \hat{H}^{H}{}_{o,q}\ \Phi^{-1}{}_{VV}\ \hat{H}_{o,q}\right)^{-1} + \hat{H}^{H}{}_{o,q}\ \Phi^{-1}{}_{VV,o\dot{q}}\ , \tag{4.7}$$

where $\Phi_{VV} = \mathrm{diag}\left(\left[\sigma^{2}_{V,1} \ldots \sigma^{2}_{V,M}\right]\right)$ is the diagonal noise variance matrix of all M receiving antennas.

The post equalization SINR for the k^{th} user at the equalizer output used as a performance measure can be stated as

SINR =

$$\Gamma^{k}_{o,q} = \frac{\left(\widetilde{G}^{k}{}_{o,q}\right)^{H} \widehat{H}^{k}{}_{o,q} \left(\widehat{H}^{k}{}_{o,q}\right)^{H} \widetilde{G}^{k}{}_{o,q}}{\sum_{i=1,i\neq k}^{K} \left(\widetilde{G}^{k}{}_{o,q}\right)^{H} \widehat{H}^{k}{}_{o,q} \left(\widehat{H}^{k}{}_{o,q}\right)^{H} \widetilde{G}^{k}{}_{o,q} + \left(\widetilde{G}^{k}{}_{o,q}\right)^{H} \Phi_{VV} \widetilde{G}^{k}{}_{o,q}} \quad , \quad (4.8)$$

where $\widetilde{G}^{k}{}_{o,q}$ is the kth column vector of matrix $\widetilde{G}_{o,q} = G^{H}{}_{o,q}$

Since the transmitted signal is known under field measurements and RT simulations, EVM estimation of the post-equalization SINR can be determined as

$$\Gamma^{k}_{EVM} = E_{o,q}\left\{\left|X^{k}_{o,q} - \widehat{X}^{k}_{o,q}\right|^{2}\right\} \quad . \quad (4.9)$$

In contrast to (41), EVM SINR in (42) includes impairments such as channel estimation errors. Both SINR and Rates will be comparing measurements with RT simulations for 12 scenarios shown in table 4.5.

Table 4.5 Second field measurements comparison scenarios.

Scenario No.	Conv. MIMO &	Intra-CoMP &	Inter-CoMP &
1, 2, 3	EVM	EVM	EVM
4, 5, 6	Theoretical	Theoretical	Theoretical
7, 8, 9	EVM_SIC	EVM_SIC	EVM_SIC
10, 11, 12	Theoretical _SIC	Theoretical _SIC	Theoretical _SIC

The above table shows all possible combinations that were evaluated for both field measurements and RT simulations. They are composed of conventional (Conv.) MIMO and Cooperative MIMO (CoMP). Theoretical (Theo.) approach is using linear detectors as shown in Equation (4.8). EVM approach is also implemented as in Equation (4.9) and is to be compared with the theoretical approach. SIC processing is implemented on all approaches and the gain is presented, too.

The SINR detection is only processed for BS that have a higher received SNR than 5dB.

Based on SINR CDF plots in Figures 4.7 and 4.8, and statistical evaluation Table 4.6, we see that RT results are in general having higher values. This difference is explained partially in Chapter 3 and in Chapter 4. The differences are mainly caused by real hardware limitation and missing objects in 3D RT model. An important observation is that SINRs resulting from field measurements are having a bigger difference than EVM SINRs resulting from RT simulations. As the offline signal processing is similar for both approaches, this can be explained by the real-world synchronization errors as well as estimation errors.

The SINRs results are used to calculate the spectral efficiency rates in the following section and will be analyzed thoroughly in terms of spectral efficiencies.

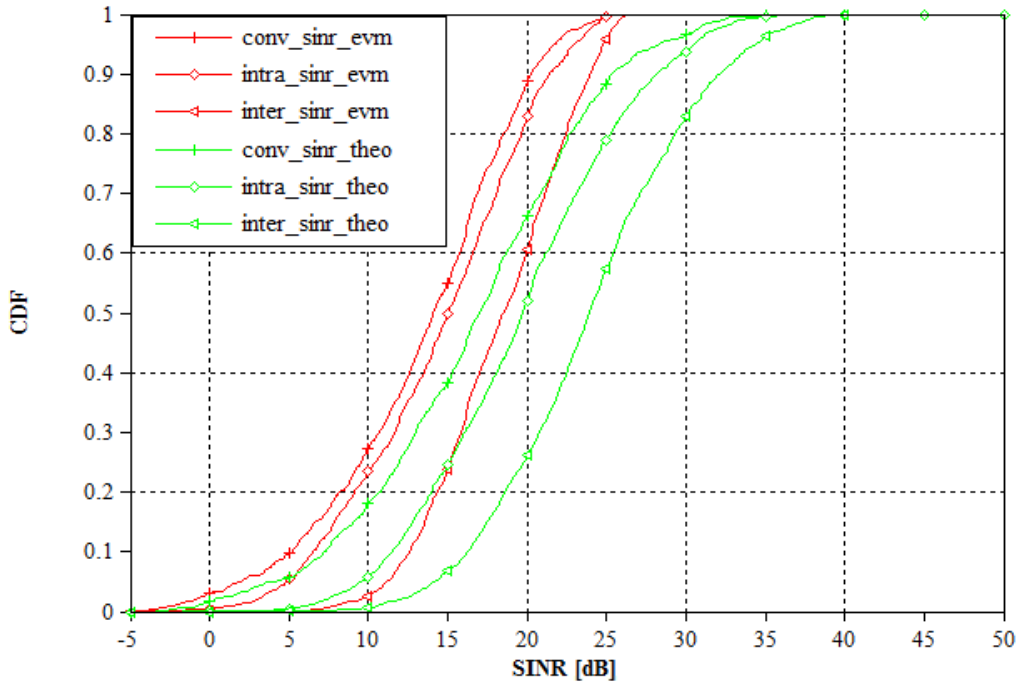

(a)

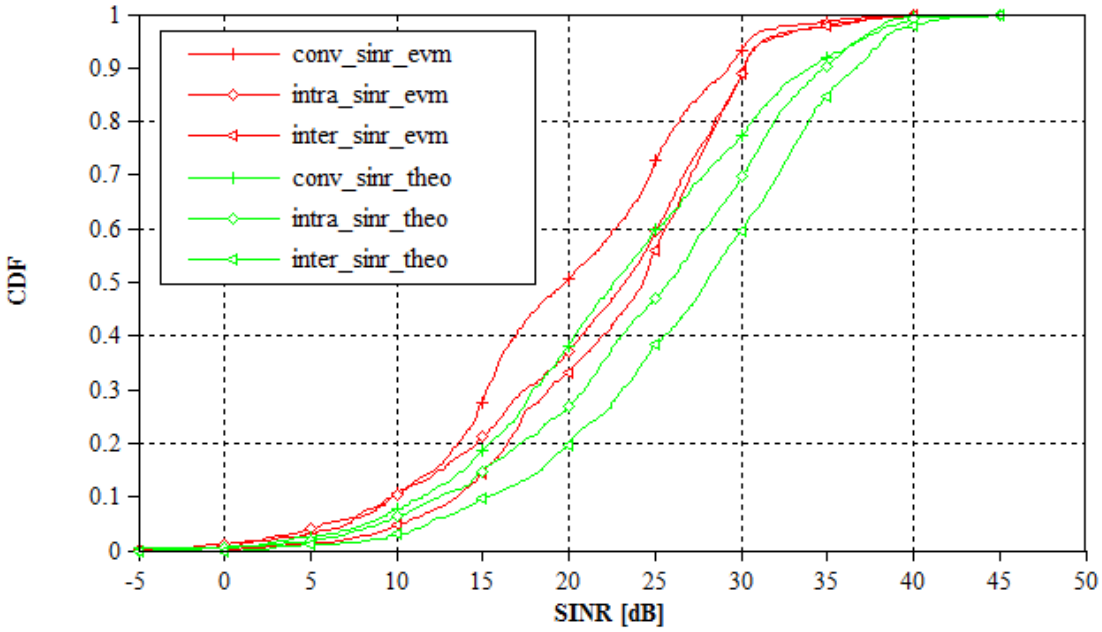

(b)

Figure 4.7 CDF for SINR values with different scenarios using linear detection scheme. (a) Measurements. (b) RT simulations.

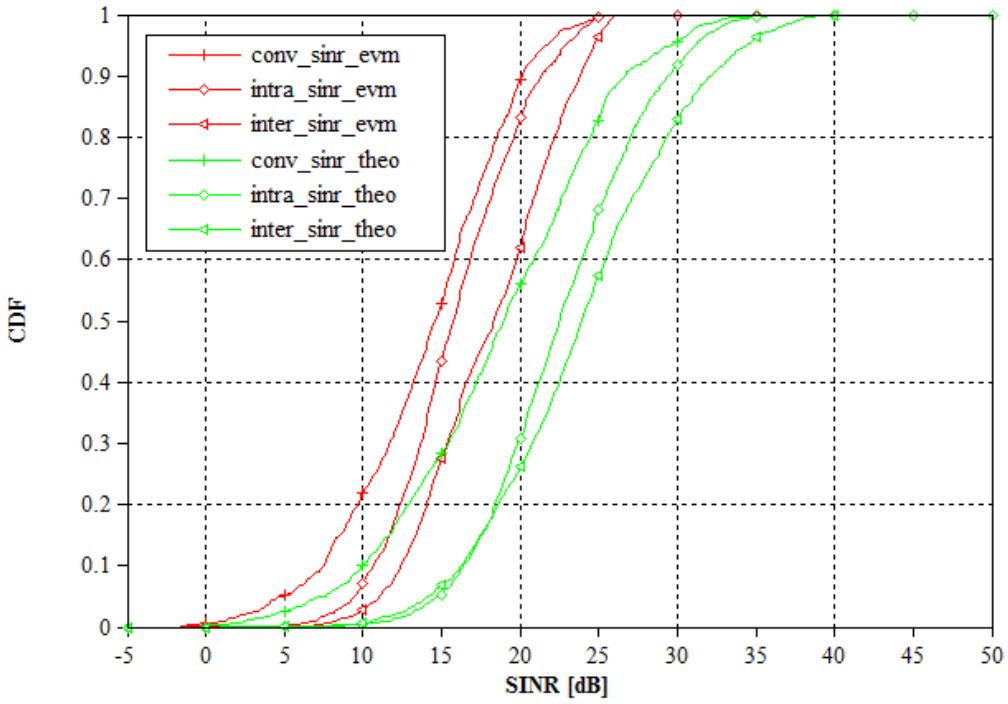

(a)

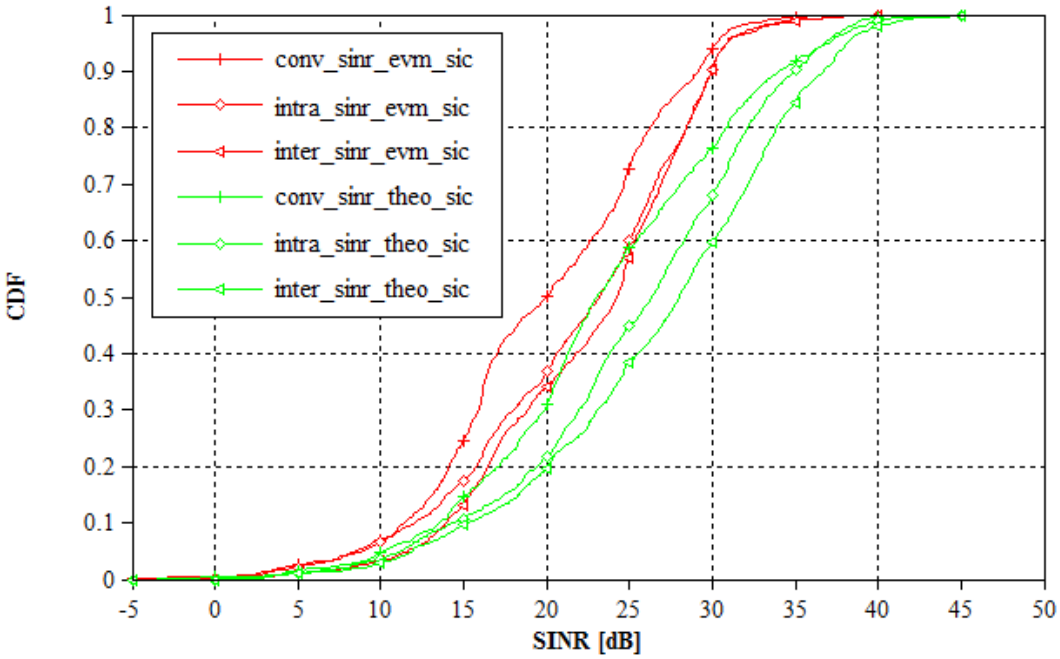

(b)

Figure 4.8 CDF for SINR values with different scenarios implementing SIC scheme.

(a) Measurements. (b) RT simulations.

Table 4.6 Statistical evaluation for SINR values with different MIMO scenarios.

No.	MIMO Scenario	Field Measurements	Mean (dB)	STD. Dev. (dB)	Median (dB)	RT Simulations	Mean (dB)	STD. Dev. (dB)	Median (dB)
1	Conv_Theo_MIMO		14.37	12.93	15.78		16.73	7.21	17.06
2	Intra_Theo_CoMP		19.75	6.33	19.75		24.68	8.55	25.79
3	Inter_Theo_CoMP		24.07	6.08	23.92		26.75	8.39	27.98
4	Conv_Theo_MIMO_SIC		14.91	13.00	17.41		18.75	6.61	19.02
5	Intra_Theo_CoMP_SIC		22.73	4.99	22.51		25.55	7.81	26.41
6	Inter_Theo_CoMP_SIC		24.07	6.08	23.92		26.75	8.39	27.98
7	Conv_EVM_MIMO		12.43	11.25	13.83		13.37	5.97	14.14
8	Intra_EVM_CoMP		14.53	5.61	15.06		21.51	8.15	23.38
9	Inter_EVM_CoMP		18.35	4.33	18.60		22.59	7.17	24.32
10	Conv_EVM_MIMO_SIC		12.61	11.11	14.36		14.13	5.07	14.67
11	Intra_EVM_CoMP_SIC		15.93	4.07	15.81		21.90	7.17	23.25
12	Inter_EVM_CoMP_SIC		18.11	4.31	18.38		22.53	6.75	24.24

4.3.3 Spectral Efficiency (Rate)

Based on SINR values the maximum achievable spectral efficiency assuming Gaussian noise is

$$\text{Rate} \quad = \sum_{k=1}^{n_t} \log_2(1 + \text{SINR}_\text{k}) \ , \tag{4.10}$$

where SINR_k is as in Equation (4.8) for theoretical rates and EVM approach is using Equation (4.9) and where n_t is the number of transmitting antennas (2 UEs each having 1 antenna). SINR_k is the signal to interference plus noise ratio for the MIMO stream K [16]. The rate formula in (4.10) represents the Shannon rate and therefore, the results form an upper bound to the actual rates.

Figures 4.9-4.12 show spectral efficiencies CDF plots for all possible combinations mentioned previously for conventional MIMO, CoMP, with and without using SIC, and EVM

approaches. As expected, the inter-site CoMP achieved higher spectral efficiencies for both field measurements and RT followed by intra-site CoMP and at last by the Conv. MIMO results. RT simulation rates could achieve higher rates than the ones resulting from field measurements. An important observation is that the rates gap between Theo and EVM approaches in field measurements is bigger than the one in RT. Apparently the field measurements got more errors caused by real-world synchronization and estimation errors as well as hardware impairments at both transmitter and receiver sides.

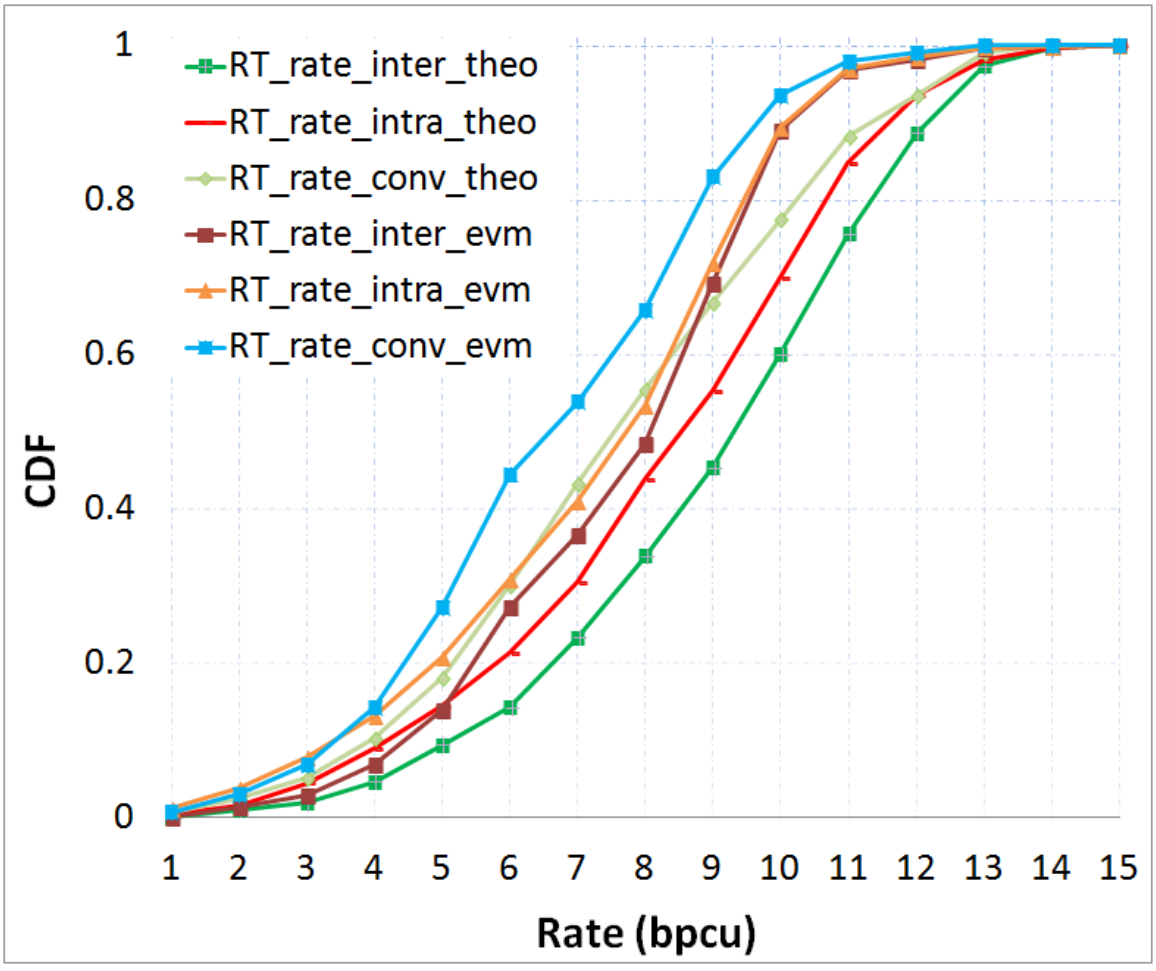

Figure 4.9 RT CDF for Spectral efficiencies with different MIMO scenarios (Conv. and CoMP) and both Theo and EVM approaches.

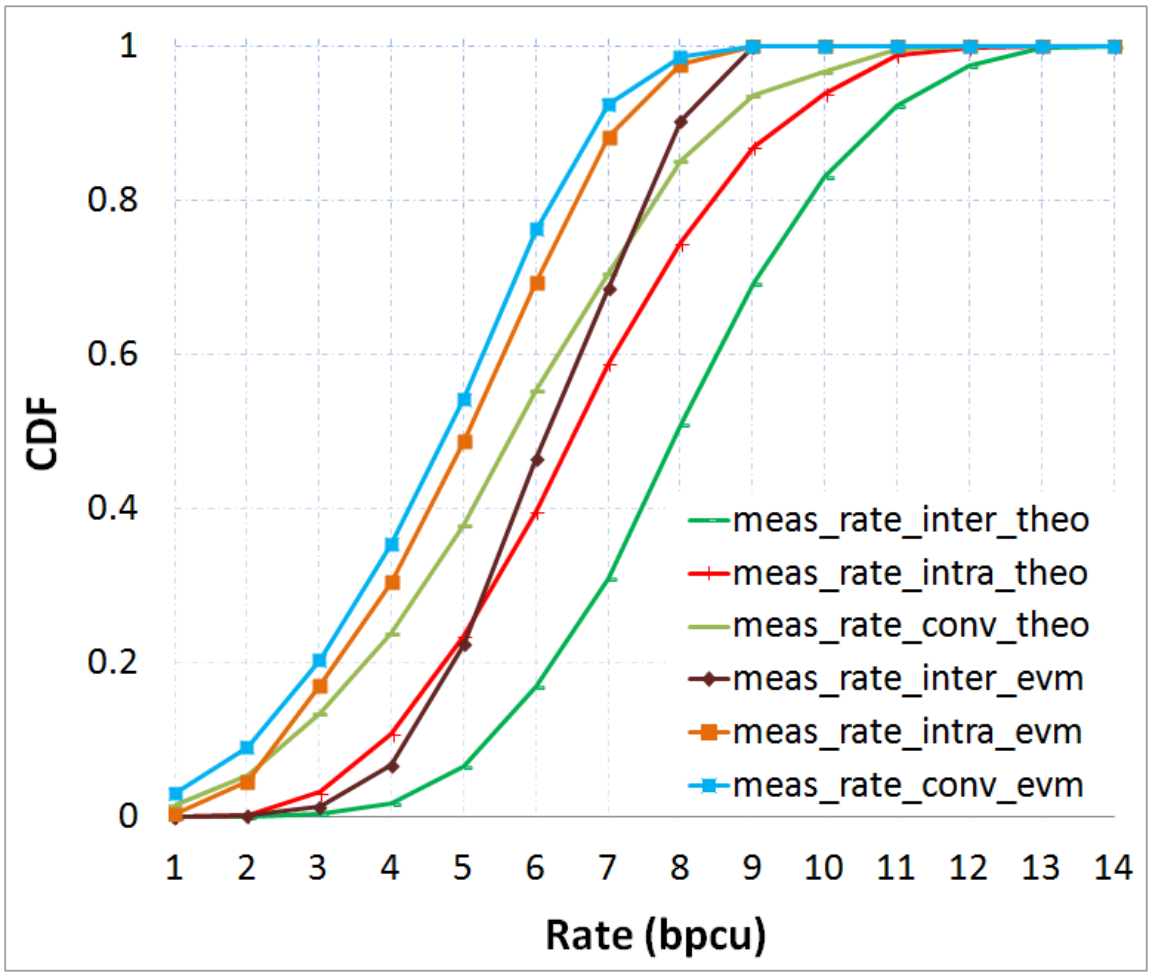

Figure 4.10 Measurements CDF for Spectral efficiencies with different MIMO scenarios (Conv. and CoMP) and both Theo and EVM approaches.

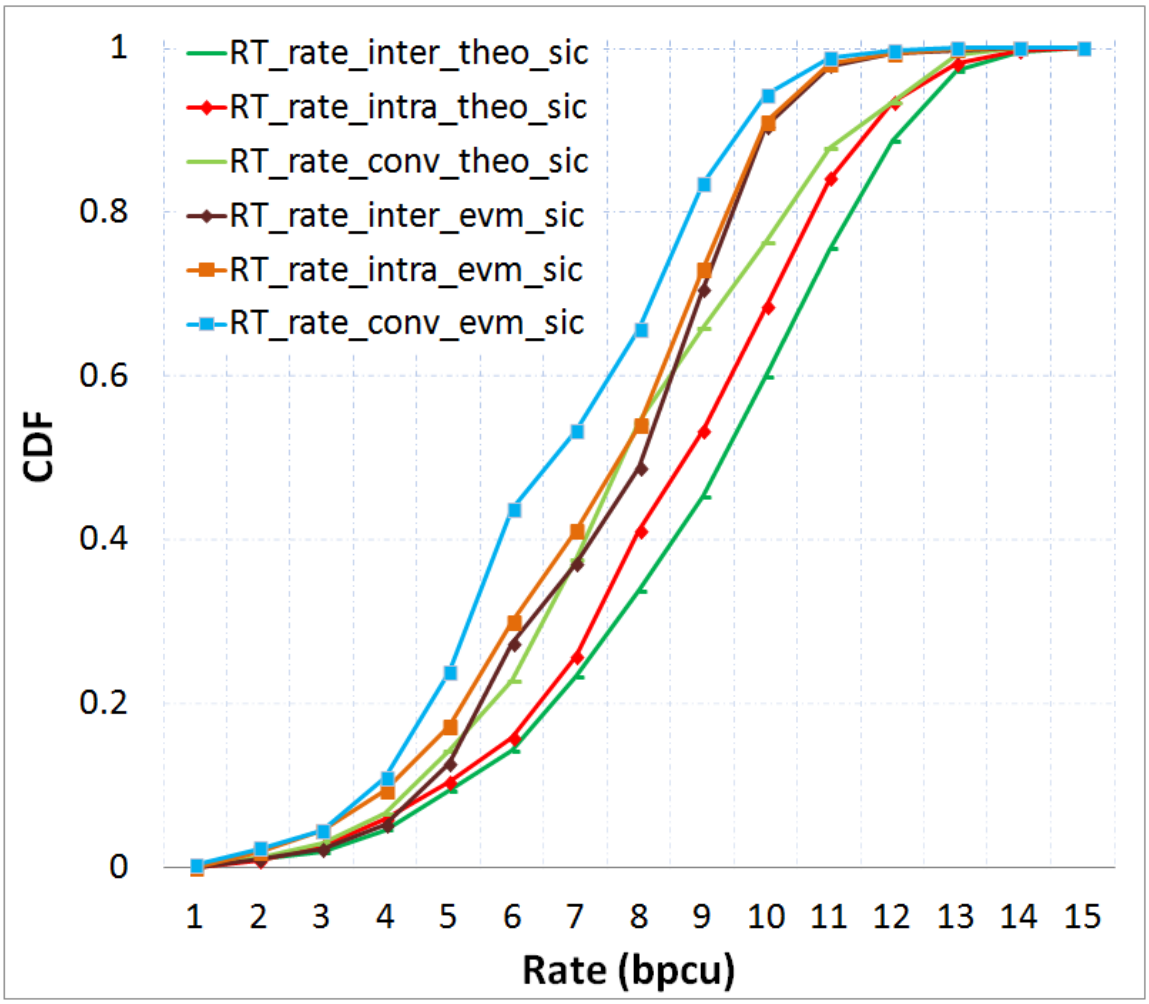

Figure 4.11 RT CDF for Spectral efficiencies with different MIMO scenarios (Conv. and CoMP) and both Theo and EVM approaches adding SIC technique.

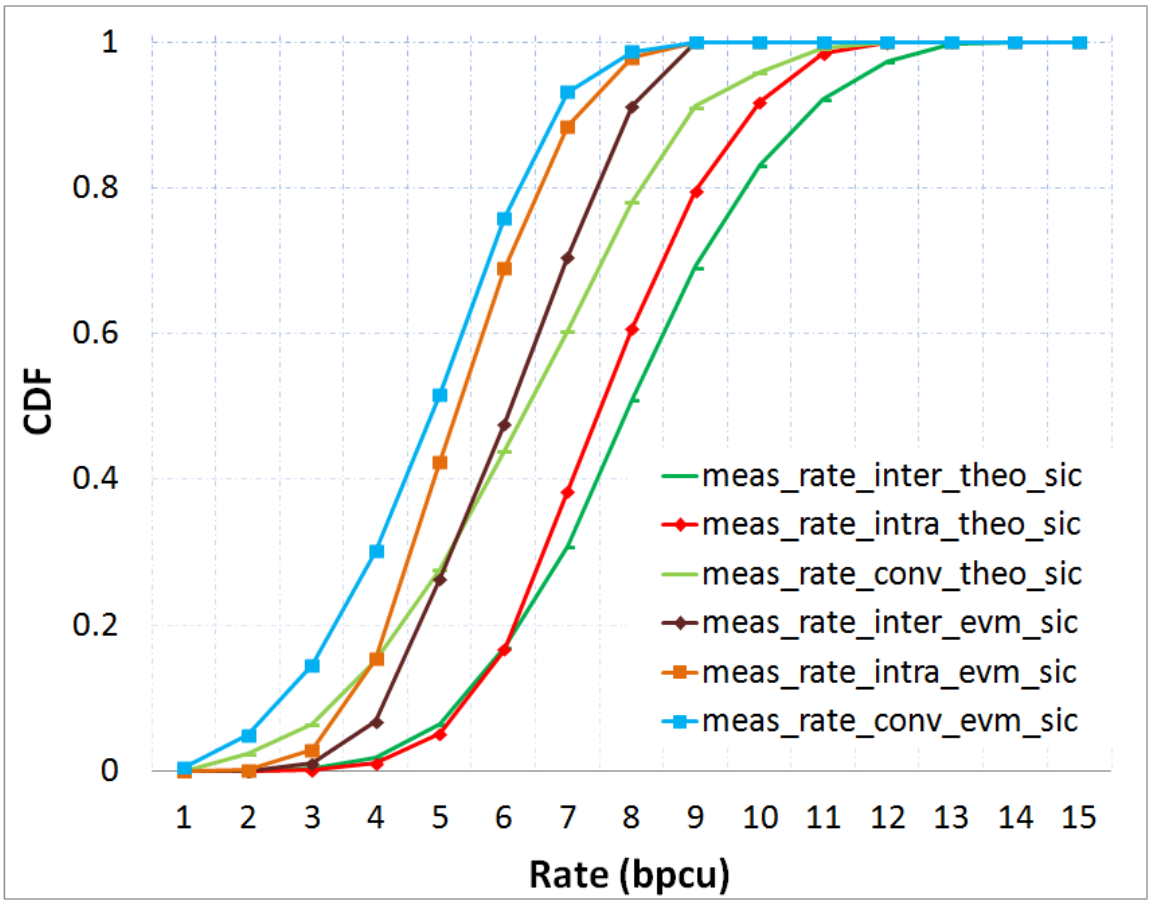

Figure 4.12 Measurements CDF for Spectral Efficiencies with different MIMO scenarios (Conv. and CoMP) and both Theo and EVM approaches adding SIC technique.

Table 4.7 Statistical evaluation for spectral efficiency values with different MIMO Scenarios.

No.	MIMO Scenario	Rate Field Measurements	Mean (bpcu)	STD. Dev. (bpcu)	Median (bpcu)	Rate RT Simulations	Mean (bpcu)	STD. Dev. (bpcu)	Median (bpcu)
1	Conv_Theo_MIMO		5.66	2.25	5.70		7.60	2.78	7.55
2	Intra_Theo_CoMP		6.60	2.06	6.57		8.23	2.77	8.57
3	Inter_Theo_CoMP		8.01	2.00	7.95		8.97	2.66	9.31
4	Conv_Theo_MIMO_SIC		6.29	2.12	6.34		7.86	2.57	7.69
5	Intra_Theo_CoMP_SIC		7.57	1.64	7.49		8.51	2.55	8.78
6	Inter_Theo_CoMP_SIC		8.01	2.00	7.95		8.97	2.66	9.31
7	Conv_EVM_MIMO		4.60	1.77	4.75		6.60	2.42	6.60
8	Intra_EVM_CoMP		4.93	1.74	5.05		7.21	2.58	7.77
9	Inter_EVM_CoMP		6.13	1.40	6.20		7.59	2.25	8.09
10	Conv_EVM_MIMO_SIC		4.80	1.56	4.92		6.68	2.24	6.65
11	Intra_EVM_CoMP_SIC		5.35	1.30	5.29		7.31	2.31	7.73
12	Inter_EVM_CoMP_SIC		6.05	1.40	6.13		7.56	2.12	8.07

To measure how much gain can CoMP techniques bring over the Conv. MIMO techniques, a gain factor in terms of average spectral efficiencies (rates) as

$$\text{CoMP Gain} = \frac{\text{E}\{\text{Rate}_{\text{CoMP}}\} - \text{E}\{\text{Rate}_{\text{Conv}}\}}{\text{E}\{\text{Rate}_{\text{Conv}}\}} . \tag{4.11}$$

We defined also a matching factor comparing the average spectral efficiencies (rates) as the percentage ratio of the complement of the difference between the achieved rates using RT simulations and the rates using field measurements

$$\text{Matching Factor} = 1 - \left[\frac{\text{E}\{\text{Rate}_{\text{RT}}\} - \text{E}\{\text{Rate}_{\text{Meas}}\}}{\text{E}\{\text{Rate}_{\text{Meas}}\}}\right] . \tag{4.12}$$

Figure 4.13 shows the rate gain ratios for CoMP scheme over Conv. MIMO scheme. Interestingly, the rates gain for RT simulations is similar regardless which approach was used, Theo or EVM. In field measurements, the rates gain ratios where higher when we used the Theo approach compared to the EVM approach (due to the unavoidable errors

appearing during real-world field measurements). Field measurements rates are showing a high CoMP gain of around 43%, while RT CoMP gain is around 18%. The rates gain difference between Theo and EVM approaches was 10% for field measurements and 5% for RT. The higher differences for measurements come from hardware error and estimation errors during the field measurements.

Figure 4.14 shows the matching factor, which reflects how close RT matched field measurements rates results for both CoMP and Conv. MIMO schemes. RT simulations rates mostly matched with field measurements rates at the inter-site CoMP scenario with 88%. This high matching can be explained by the fact that in the inter-site CoMP scenario the received signals are more diversified and coming from different non-collocated BSs. The major objects in the propagation environment mainly influence these signals. On the contrary, the lowest matching scenario with 53% was the intra-site CoMP. This low matching could be explained by the fact that in the intra-site CoMP scenario the received signals have less diversity and come from collocated BSs. In such scenario, the small details in the propagation environment such as trees, cars, and people influence the propagation; these details were missing in the RT simulator. Moreover, comparing the SNR values for both field measurements and RT simulations for the 887 transmitter locations, we could see that around 15% of RT results did not match the field measurements. These locations are in reality located at trees alleys and heavy foliage but not modeled in the RT simulator. Nevertheless, unmatched percentage might sound too high but in terms of spectral efficiencies, the delta varies between fractions of bit per channel use (bpcu) to less than three bpcu.

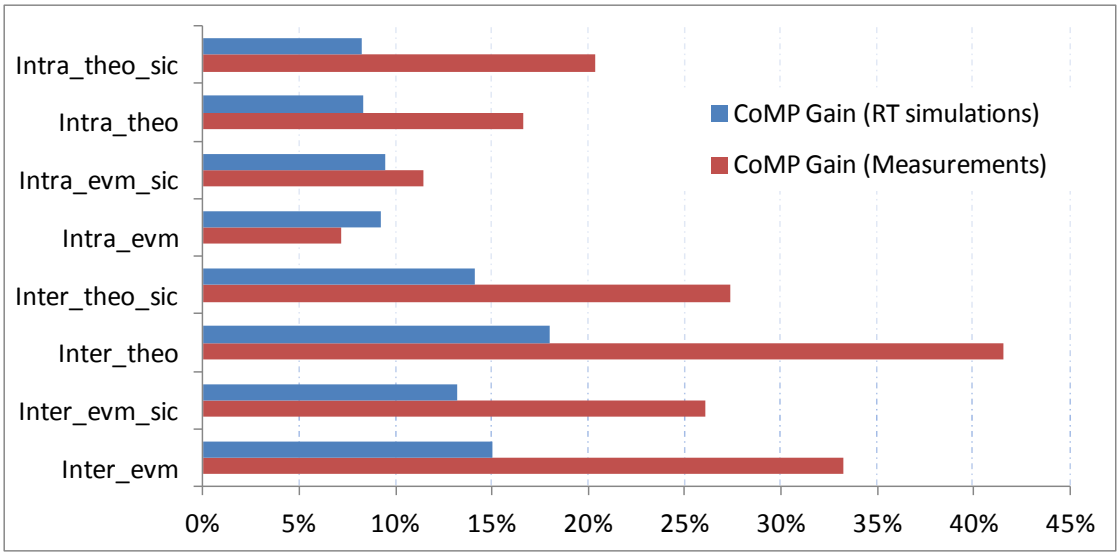

Figure 4.13 Spectral efficiency gain using different MIMO scheme for both field measurements and RT simulations.

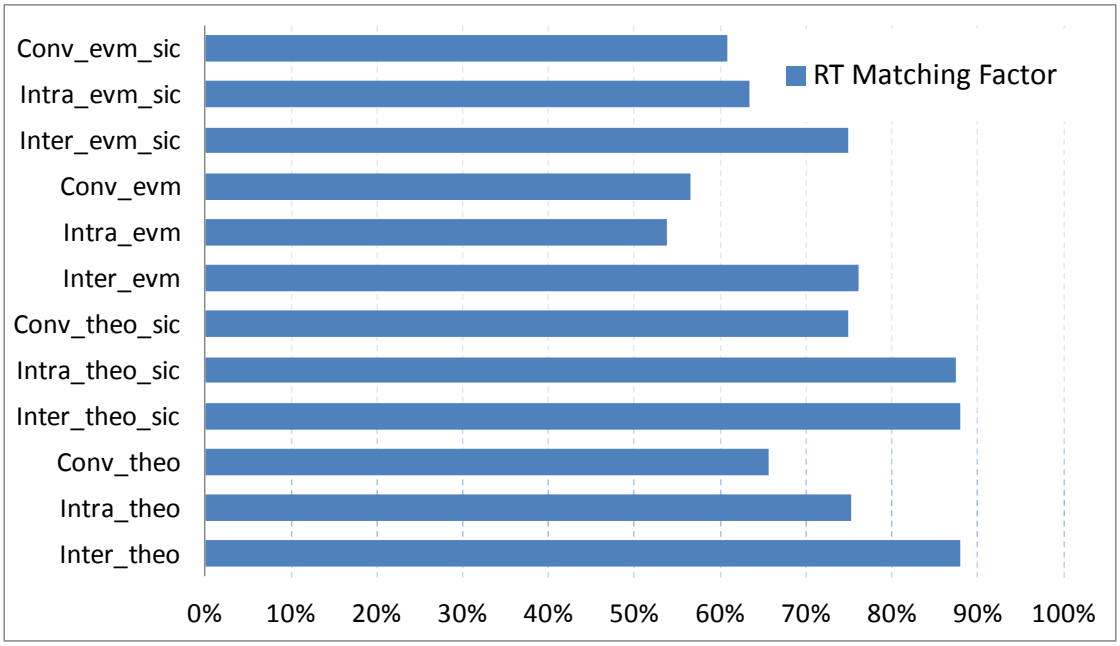

Figure 4.14 Spectral efficiency matching factor between RT simulations and field measurements using the different MIMO scheme and equalization approach.

4.4 Geometrical Analyses

As introduced earlier, RT simulation allows observing bidirectional characteristics of propagation channels. These are both the temporal and the angular domain characteristics. Here, we look at some properties of the channels and compare them between field measurements and RT simulations.

4.4.1 Direction of Arrival (DoA)

In Figure 4.15, the SNR of rays received by BS antenna within 120 degrees DoA were plotted. The difference between BS and UE locations in terms of distance was calculated and presented as the deltas in meters in the graph. Δ x presents the difference in longitude and Δy presents the difference in latitude. Based on comparing field measurements SNR values and RT simulations, we can observe that in most cases RT values have higher SNR values by 5 to 10 dB, which could be due to the less scattering environment.

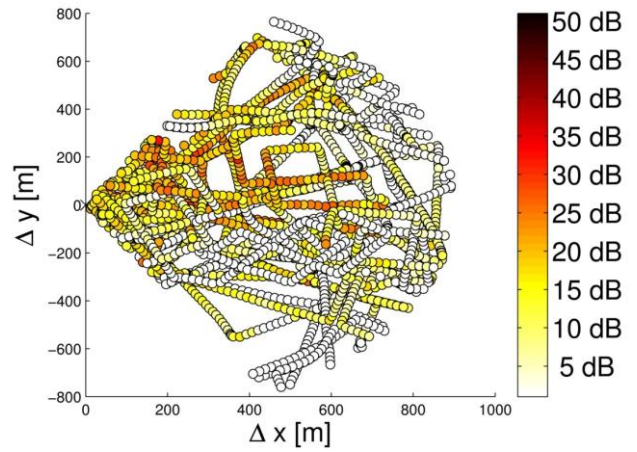

(a)

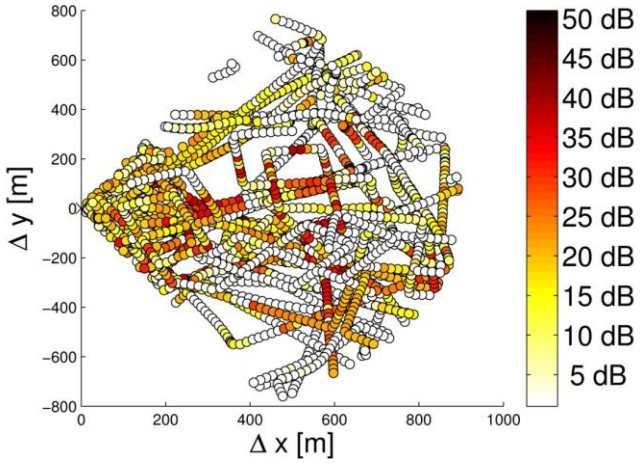

(b)

Figure 4.15 SNR distribution over distances for received rays with DoA within ±60 degrees of BSs azimuth (a) Measurements and (b) RT simulations.

4.4.2 Geometrical Distribution of SNR Samples

Figure 4.16 shows the SNR values distributed over distances from BSs. RT simulations had a higher SNR peaks reaching above 40 dB while measured SNR values were below that. This could be due to the hardware (BS) limitation in real field measurements. The absence of objects in 3D RT model leads to a higher signal level and to less absorption and scattering effect. RT results are concentrated in the first 1200 meters distance from

the BS while in field measurements the concentration goes up to 1500 meters. RT simulation results have very less samples beyond 2000 meters while field measurements have plenty of samples beyond 2000 meters. This can observed at low SNR values, which usually come from scattering elements.

An issue that can appear is the Inter Symbol Interference (ISI) and Inter Carrier Interference (ICI) when the cooperation clusters are formed of samples with high SNR values and faraway from cooperating BSs.

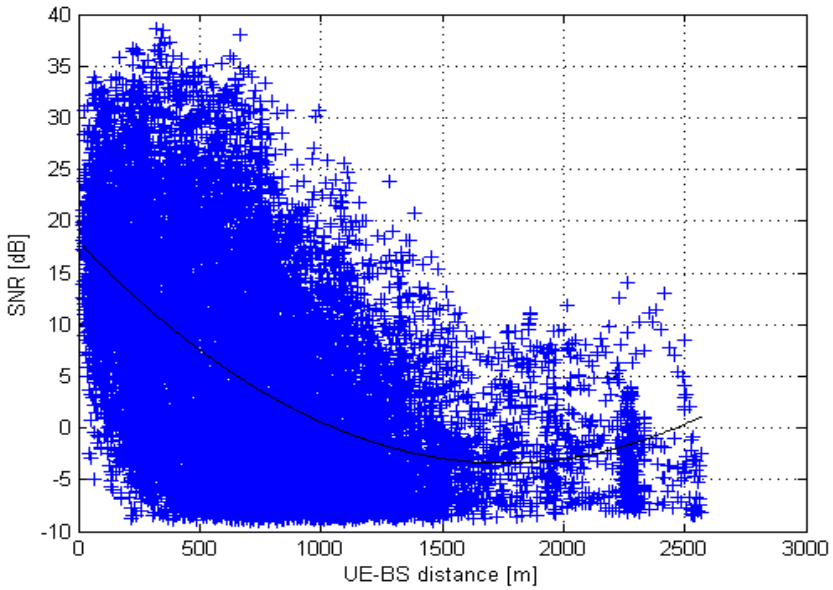

(a)

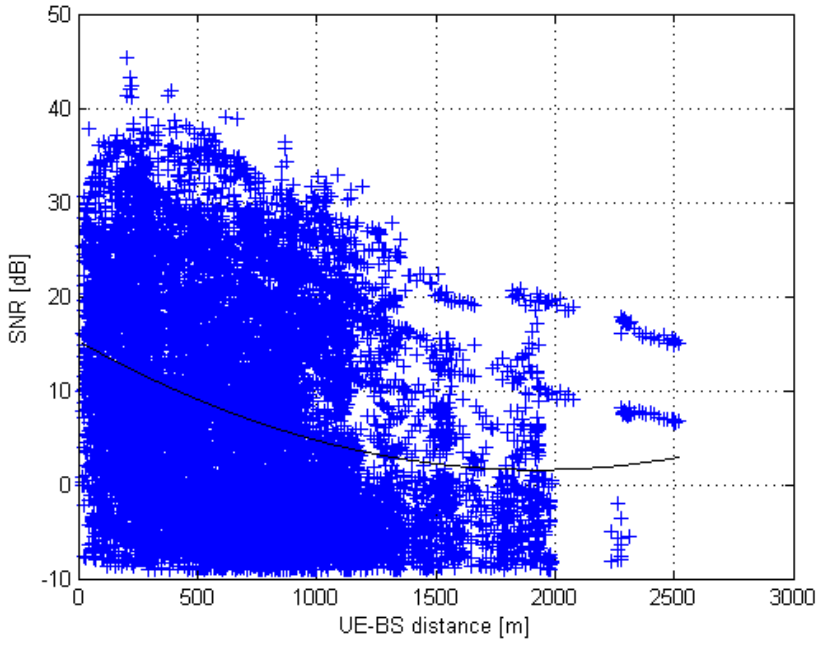

(b)

Figure 4.16 SNR Distributed over Distance from BSs, (a) Measurements and (b) RT simulations.

4.4.3 Symbol Time Offset (STO)

As per 3GPP standards, UEs should be able to align their timing to all BSs of an intra-site cluster using conventional LTE timing advance. This is not possible if the cooperation cluster is formed across sites (inter-site CoMP). Thus, larger symbol timing offsets (STOs) are expected. It should be noted that the maximum delay should not exceed the cyclic prefix of 4.7μs in order to avoid ISI.

$$\text{Symbol Timing Offset} = [\tau_d / T_S] \ , \tag{4.13}$$

where τ_d is the propagation delay and T_S is the sampling period.

When considering an OFDM system (or SC-FDMA in LTE), usually a cyclic prefix (CP) is used to ensure a circular convolution and, thus, to allow detection in the frequency domain. Therefore, we assume that the STOs should be always less or equal than the cyclic prefix length (T_{CP}) minus propagation delay (τ_d).

$$\text{STO} \leq (T_{CP} - \tau_d) \ , \tag{4.14}$$

where T_{CP} is the cyclic prefix duration.

The CDF of the STO in the field trial and RT simulations for cooperation clusters of two BSs are shown in Figure 4.17. The STO values for intra-site cooperation (blue curve) are as expected lower than the ones for inter-site cooperation (green curve).

Furthermore, the results indicate that a large percentage of the STOs are within the CP so that no ISI occurred. As shown in Figure 4.17 the STO for intra-site clusters is shorter than STO for inter-site clusters by around one microsecond. This was for both measurements and RT simulations.

4.4.4 Time Difference of Arrival (TDoA)

Due to the relatively small inter-site distances within the testbed, it can be expected that the occurring Time Differences Of Arrival (TDOA) do not exceed the CP length.

This is validated and compared between field measurements and RT simulations. The geometrical TDOA is the difference in propagation time to all BSs in the cooperation cluster. A simplified TDOA formula can be expressed as

$$\mathrm{TDOA} = \frac{\max(\mathrm{D}) - \min(\mathrm{D})}{\mathrm{C}_{\mathrm{light}}} \quad , \tag{4.15}$$

where $\mathrm{D} = [\mathrm{d}_1\ \mathrm{d}_2]$, $\mathrm{d}_k = \left[\mathrm{d}_{c1,k}\ \mathrm{d}_{c2,k}\right]$ is the distance between UEs and BSs at any time, $\mathrm{d}_{c1,1}$ is the distance between UE1 and BS c_1. $\mathrm{C}_{\mathrm{light}}$ is the speed of light.

Assuming e.g. channel lengths of: $\tau_d \approx 2$ µs, the maximum TDOA must not exceed ($T_{CP} - \tau_d \approx 2.7$µs), which corresponds to a distance of [$2.7\mu s \times c\_{light} \approx 810$ m].

As shown in Figure 4.16, SNR distributions between BSs and UEs, most high SNR values that are candidates to form a cooperating cluster are located nearby BSs. Therefore, an arriving signal with TDOA bigger than 810 m is less expected. This was verified and shown in Figure 4.17 where almost all LOS TDOA were within the CP time.

A CP is one of the key parameters in LTE system. However, in bigger sizes of cooperating clusters (C > 2), CIR can be very long compared to CP length due to TDOAs in the cooperation cluster that can lead to ISI and ICI.

4.4.5 Delay Spread (DS)

An estimated DS has to be considered and added to the STO is shown in Figure 4.17 to assess whether the CP is of sufficient length that can prevent ISI.

The total channel length including STOs and delay spread for inter-site cooperation is shown in Figure 4.17 as well (light brown). At this worst case, an ISI effect can be avoided by 95% of the cases. We observe a longer STO in RT simulations than in field measurements for the inter-site case.

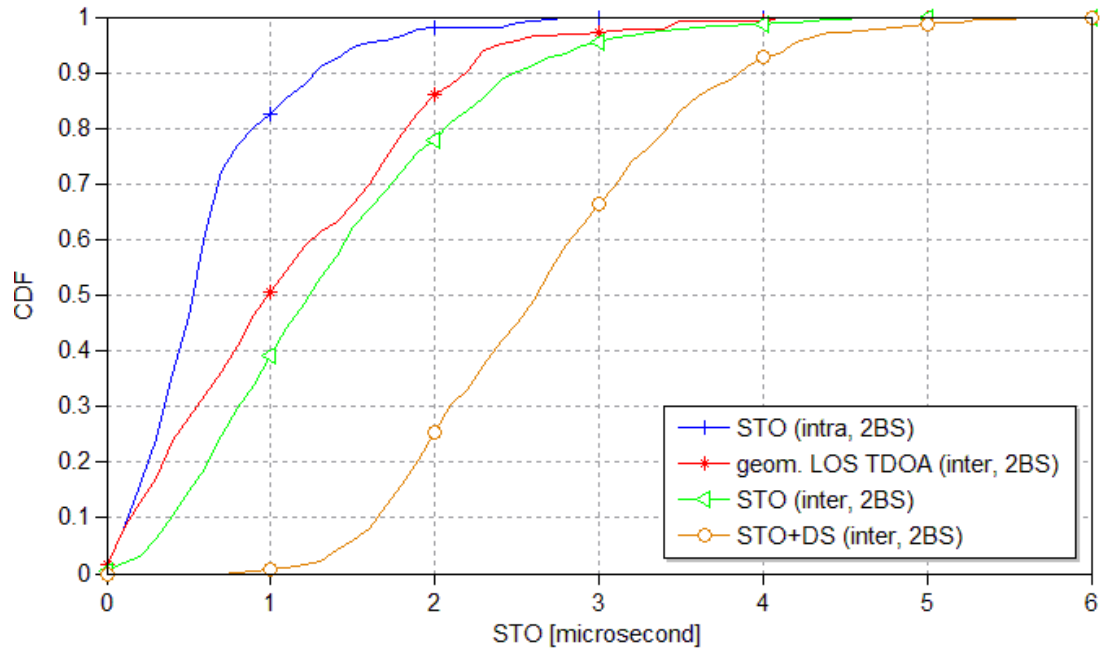

(a)

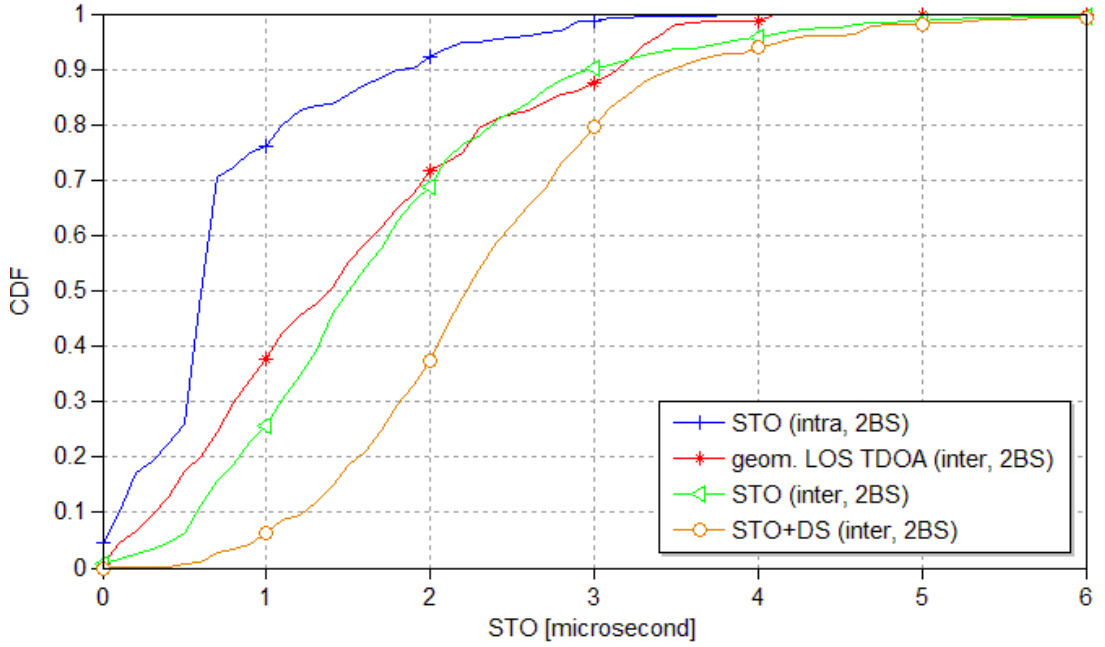

(b)

Figure 4.17 CDFs for STO (intra-site and inter-site), Geometrical TDOA and DS (inter-site), (a) Measurements and (b) RT simulations.

4.4.6 3D Map Accuracy Impact on Results

In Figure 4.18, spectral efficiency for both UEs for inter-site CoMP is shown over all testbed measurements locations. The graph is showing a good matching between field measurement rates and RT ones. Those were calculated based on received SINR values. An exception to this matching is around locations 480 and 600, where it was observed that SNR, SINR, and CoMP values were less.

Based on SNR values per location shown in Figure 4.19, it can be observed that RT SNR values are higher at these locations by 15 dB and consequently, this leads to have a difference in spectral efficiency by up to 10 bpcu.

In Figures 4.20 and 4.21, the CoMP rate is broken down per UE in attempting to see if the impact is related to one particular UE, but it is clear that both UEs got a lower rate at field measurements and higher rates at RT simulations for the same locations.

After looking into the details of the 3D map in the RT simulator and comparing it to the real propagation environments, this loss results from two missing objects:

1- Both locations are situated and surrounded by tree alleys, which existed in measurements but not in simulations. As these locations are situated in the shadow of the nearest site, absorption and scattering played an important role in the transmitted signals.

2- For both locations, two neighboring buildings are not modeled in the 3D map as shown in Figure 4.22. These missing objects caused to have much less absorption and scattering of RT simulated signals. In Figure 4.22, measurement route is shown in dots (light blue), modeled buildings in the RT simulator (yellow build-

ings), two missing buildings are highlighted by two red arrows and surrounding sites as red circles. All these are imposed on Google Earth © snapshots.

In Figures 4.20 and 4.21 we observe that the UE1 has almost always lower rate values than UE2. This is because UE1 was down-tilted by around 35 degrees more than UE2 during both measurements and RT simulations. Another reason is that UE2 was placed at higher point than UE1 in the setup. The rates differences are more obvious in measurements than in RT results.

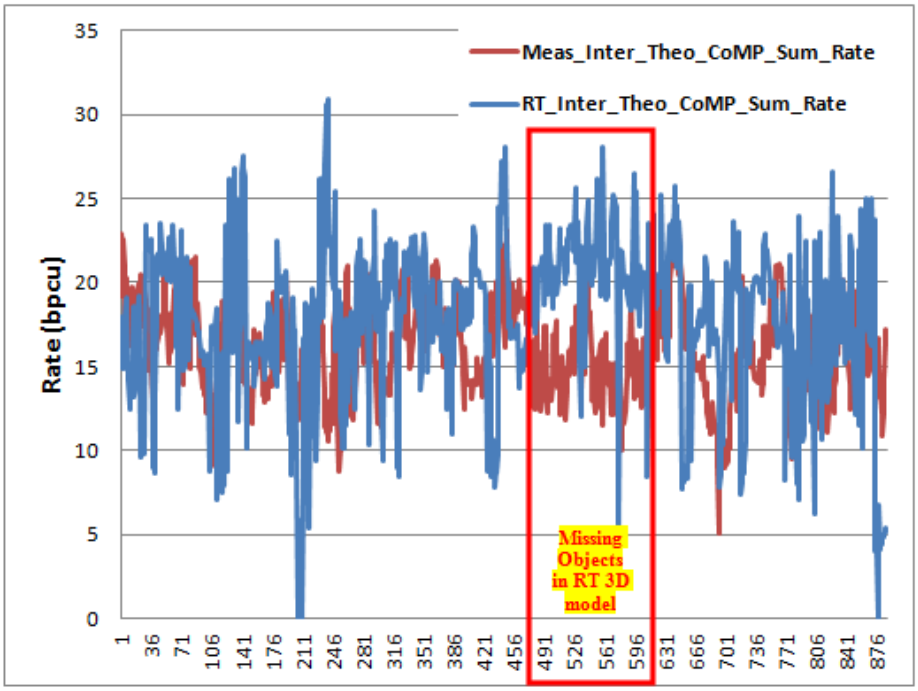

(a)

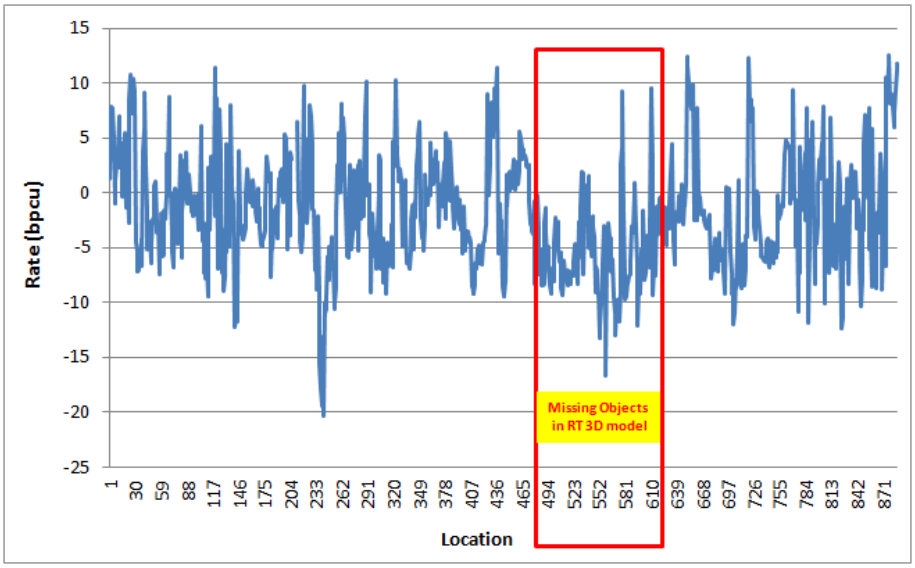

(b)

Figure 4.18 (a) Spectral Efficiency Sum Rate Delta (for both UEs) Distributed over transmission locations (b) Delta rates between measurements and RT.

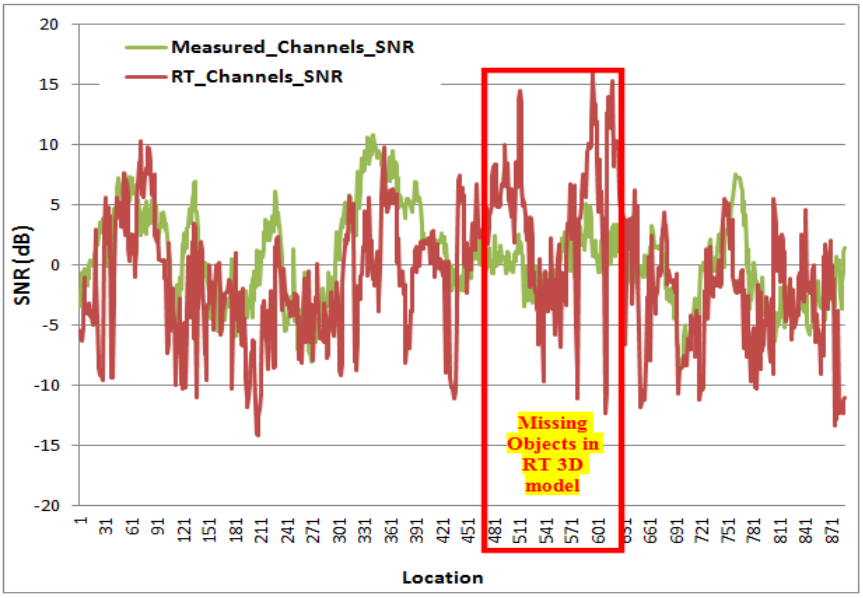

(a)

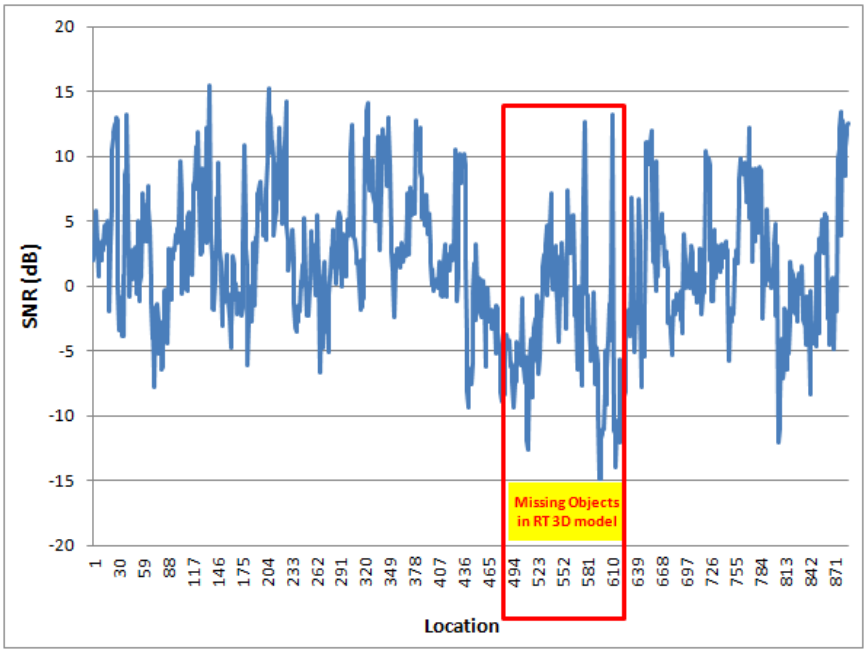

(b)

Figure 4.19 (a) SNR Distributions over Locations for Measured Channels (red) and RT Simulated Channels (green). (b) Delta SNR between measurements and RT.

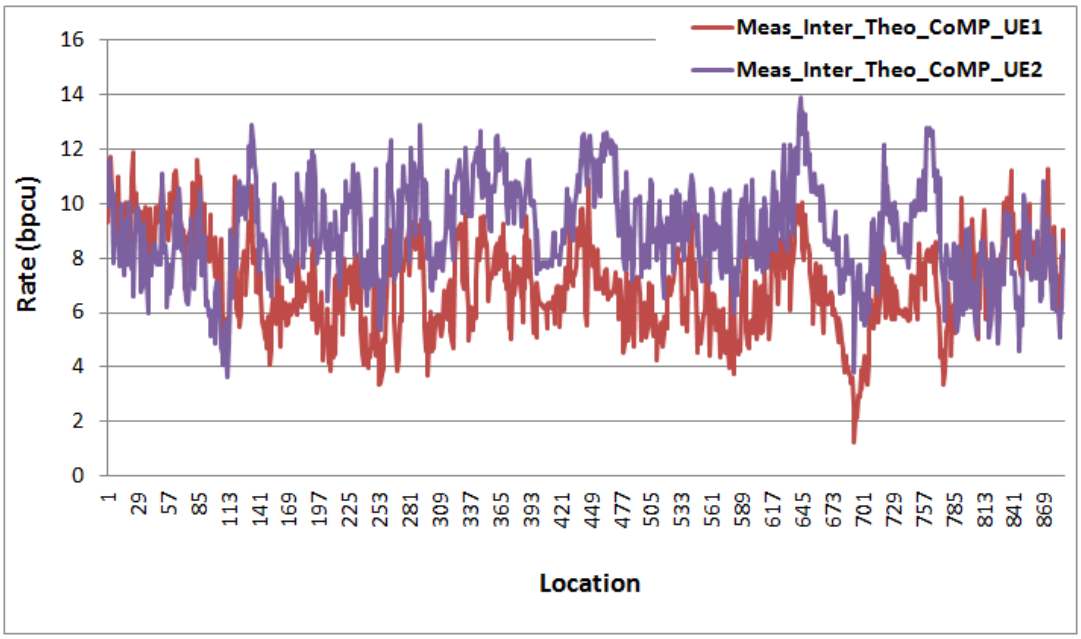

Figure 4.20 Measured Channels Spectral Efficiency Rate (per UE) Distribution over Locations for UE1 (red) and UE2 (violet).

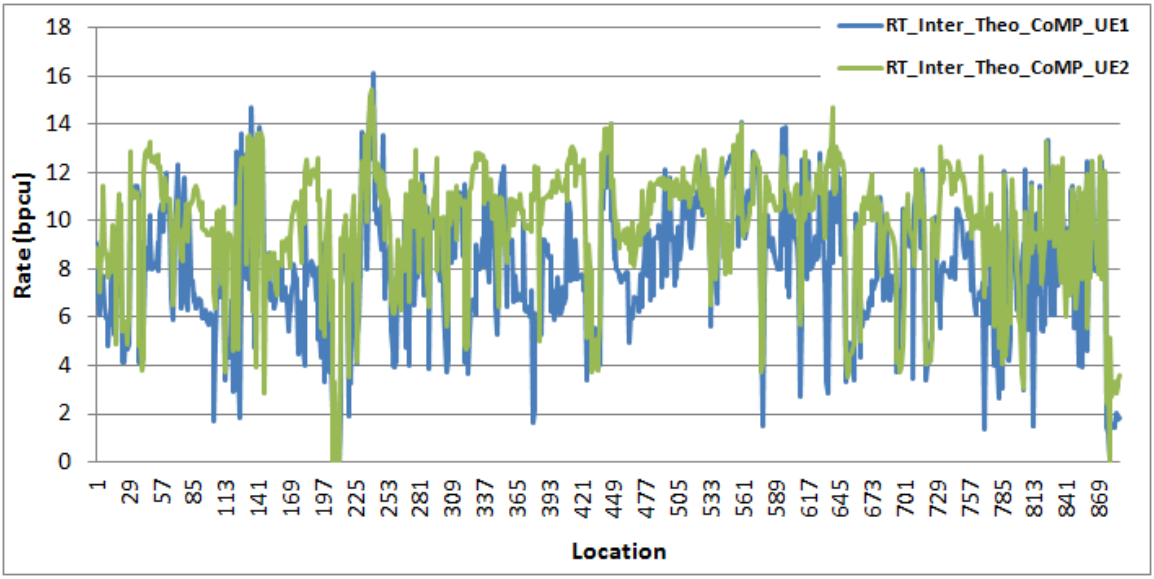

Figure 4.21 RT simulated Channels Spectral Efficiency Rate (per UE) Distribution over Locations for UE1 (blue) and UE2 (green).

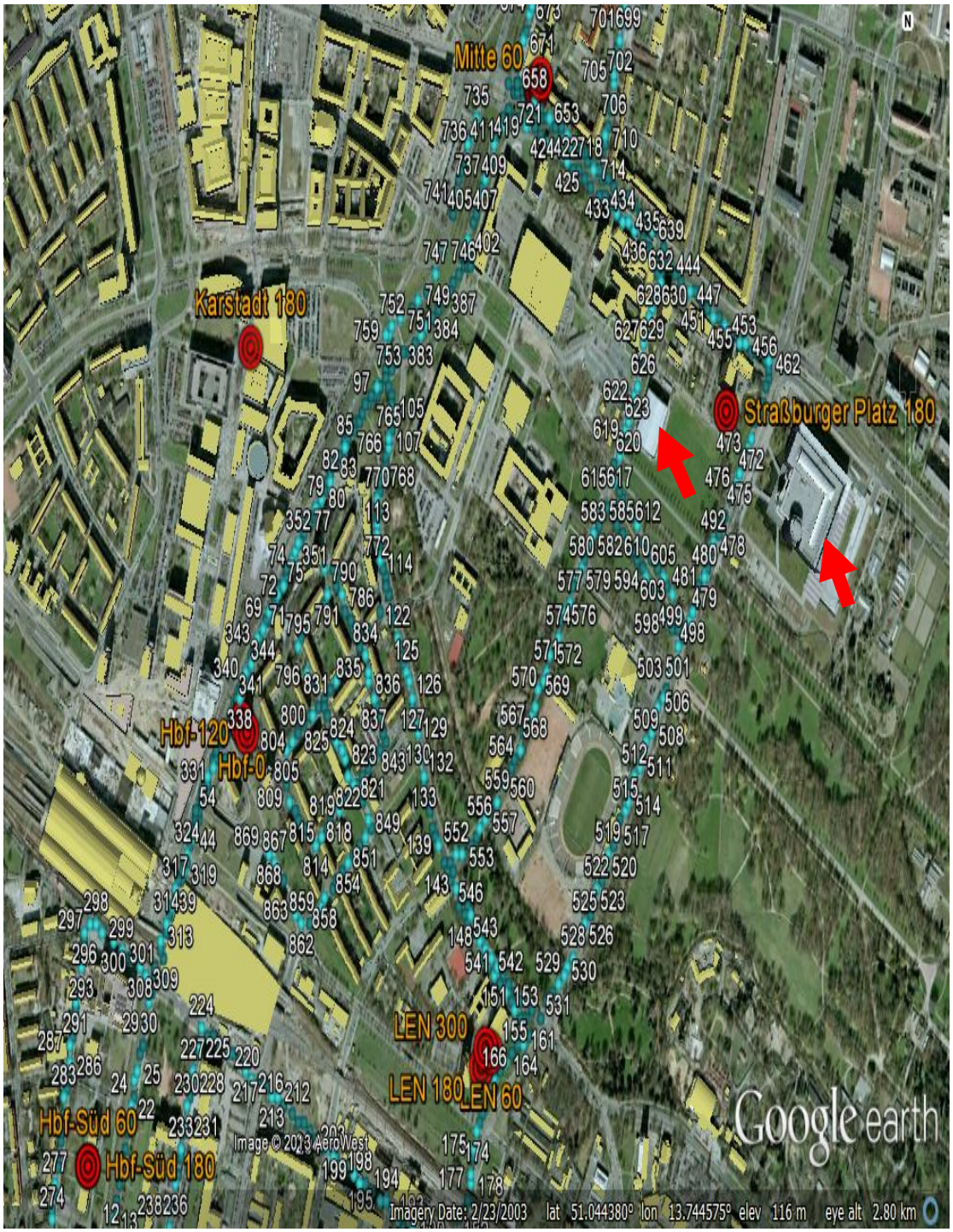

Figure 4.22 3D map in RT module. Modeled Buildings are shown in yellow. Missing buildings are shown in grey and are indicated with red arrows. Route and transmission position are the dotted blue points. Trees Alleys are shown in the environment.

4.5 EPM Simulations vs. Field Measurements

In [12], a calibrated simulation model was used to predict the coverage and the capacity of a cellular UMTS network. The network studied was chosen to be large enough in order to obtain representative results not biased due to insufficient number of samples or dominance of a particular radio environment. The terrain varies from hilly areas with foliage and water surfaces, to suburban housing neighborhoods and downtown commercial buildings. A tuned empirical propagation model (EPM) derived from Cost-231 Hata model was used. Tuning for the model was done by using continuous wave (CW) tests to improve the accuracy of the coverage predictions. Traffic maps were designed based on the area and population profile. Field measurements were collected through drive testing for a benchmark with coverage simulations.

In this section, the focus will be concentrated on part of the results to present the performance of EPM and compare it later on with the Ray Tracing simulation model.

4.5.1 Measurements and Predictions Setups

In order to verify the network coverage from the field, a drive test (DT) is performed at a designed route that has to be followed in order to receive signals from all cells (coverage). Table 4.8 demonstrates key parameters of the case study.

Table 4.8 Key parameters of the EPM case study.

Number of sites	11
Number of cells	28
Inter-Site distance (m)	400-2500
Carrier Frequency (MHz)	2100
Spectrum bandwidth (MHz)	5
Antenna type	Kathrein 742264
Max. transmit power (dBm)	43
CPICH pilot power (dBm)	33
Max. Number of HS-PDSCH codes	5
Number of channel elements (CE) per base station (NodeB)	128
User profiles	Standard and business
Traffic environments	Urban, suburban and rural
Drive test mobile	Sony Ericsson W995
Drive test air interface software	TEMS Investigation
Drive test GPS	Garmin nüvi 1690
Drive test car average speed	50 Km/h

4.5.2 Simulated Area, Simulated Route vs. Measured Route

Figure 4.23 shows the network area-level predictions for RSCP coverage levels. As it is not possible to drive through all the points in the simulation area of the case study, a main DT route was designed to be driven through while measuring. RSCP coverage levels results from the measured route is shown in Figure 4.24.

4.5.3 EPM Simulations vs. Field Measurements Comparison

To compare the results, the cumulative distribution functions (CDF) and histograms were plotted for all predictions and measurements. The RSCP CDFs and histograms (showing lognormal type of distribution) in Figures 4.25 and 4.26 show that the area predictions underestimate the route measurements. The difference reaches up to 20 dBs when compared to the area level that covers much more terrains compared to the designed driven

route highlighted as a dark route in Figure 4.23. This difference can be explained because the route passes under the coverage of antennas main lobes. A realistic benchmark should only consider predictions for a similar route followed in the measurements. Therefore, route predictions that were performed on a similar route followed in the drive test measurement were closer to the measurements with an underestimation less than 10 dBs.

The Ec/Io histograms and CDFs in Figures 4.27 and 4.28 show very good matching between the predicted route and the measured route. This perfect matching indicates that the designed traffic models, which were used by the MC simulations, have reflected the real cellular users' behavior and their generated load in the network, i.e., interference. The area level predictions show worse Ec/Io for the same reasons mentioned in RSCP part as Ec/Io can be defined in terms of RSCP.

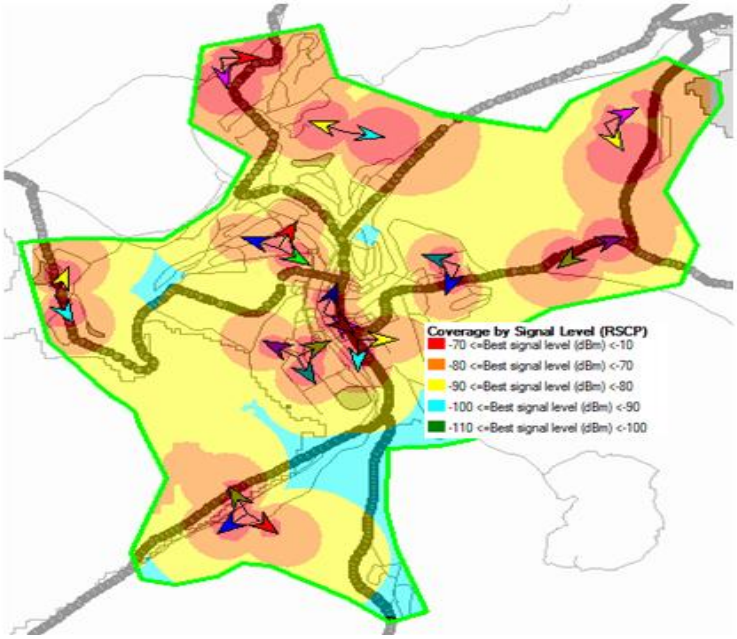

Figure 4.23 Case study coverage prediction results RSCP (dBm) – the designed route is in the background (dark road).

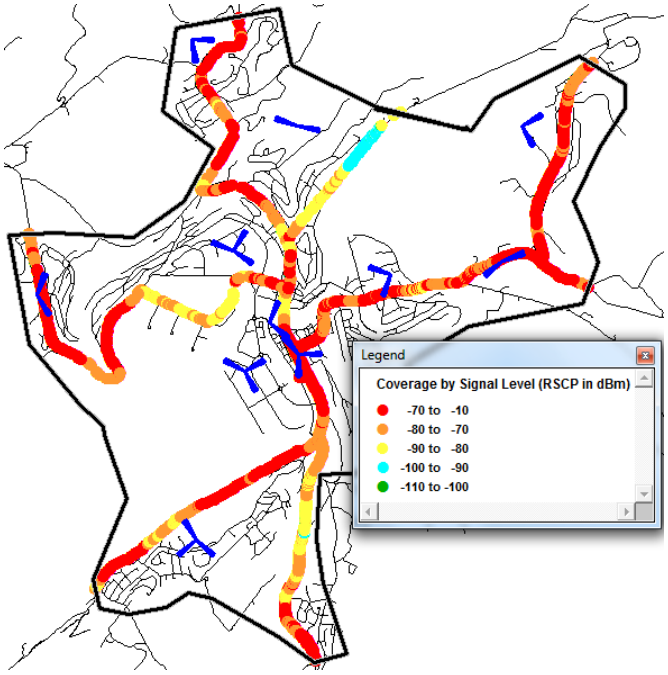

Figure 4.24 DT measured route coverage CPICH RSCP (dBm).

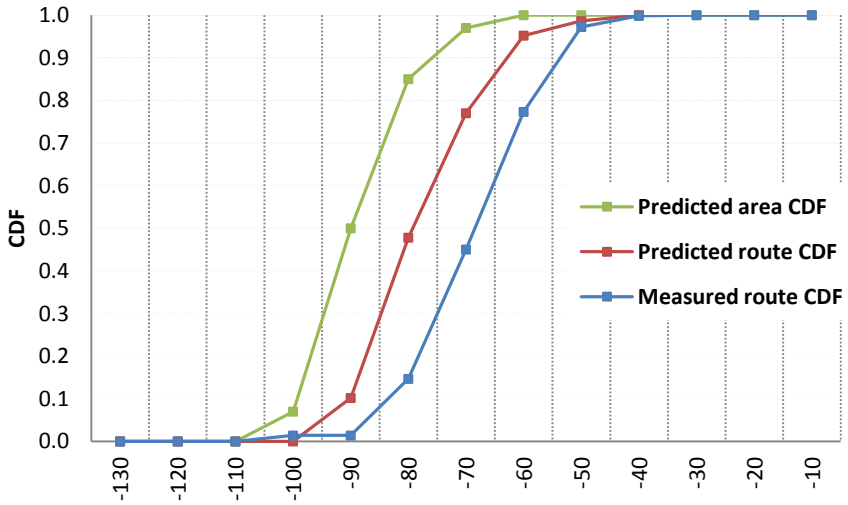

Figure 4.25 CDFs for predicted and measured RSCP values (dBm).

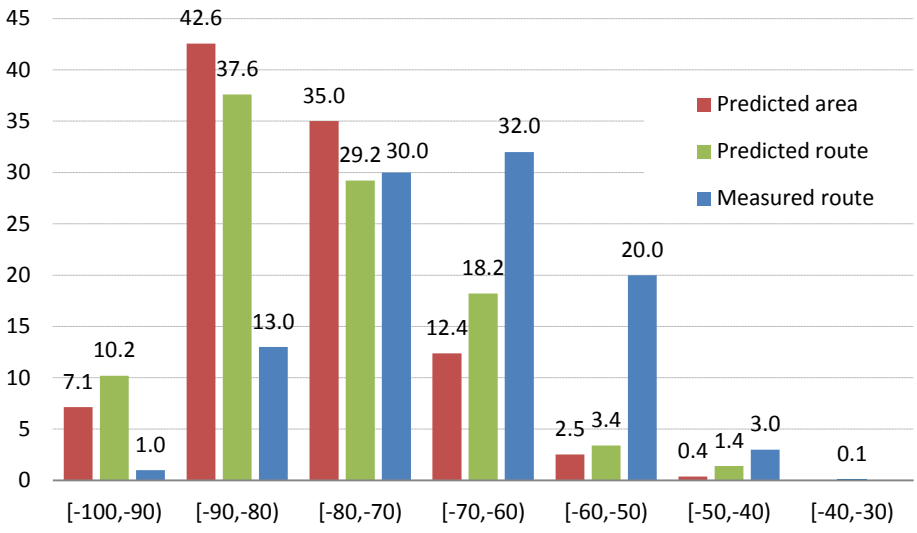

Figure 4.26 Histograms for coverage verifications scenarios - RSCP (dBm).

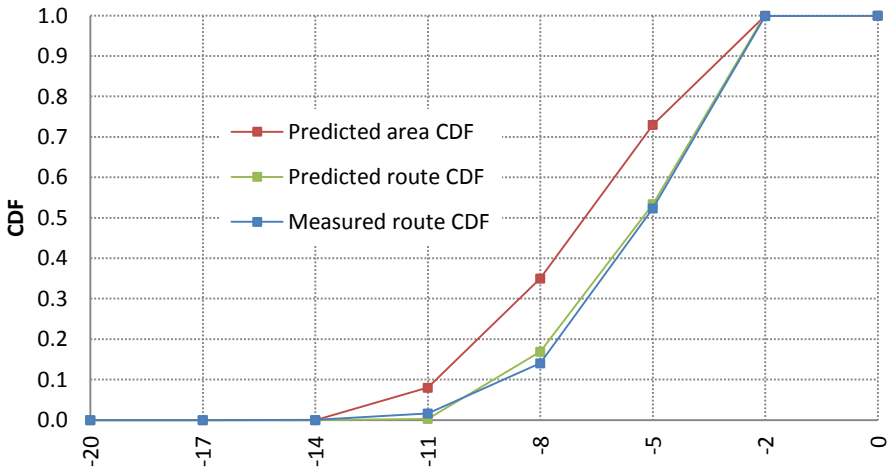

Figure 4.27 CDFs for predicted and measured Ec/Io values (dB).

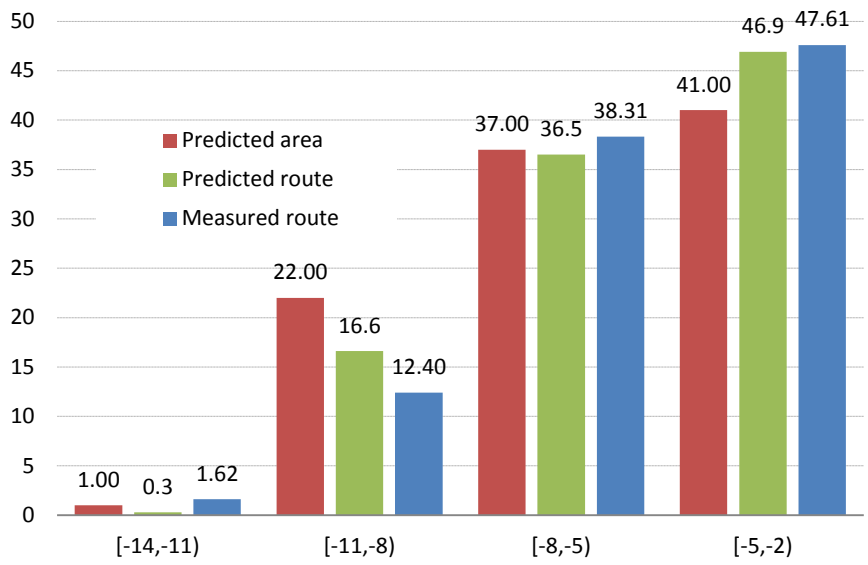

Figure 4.28 Histograms for coverage verifications scenarios - Ec/Io (dB).

Table 4.9 Statistical measures for route predictions and measurements.

Scenario	Mean		Standard Deviation	
	RSCP (dBm)	Ec/Io (dB)	RSCP (dBm)	Ec/Io (dB)
Predicted route	-73.8	-5.4	7.31	1.19
Measured route	-65.4	-5	5.11	1.05

Table 4.9 shows high statistical correlations between measured and predicted routes.

The results of the predictions using the tuned EPM are far better than the ones presented for the non-tuned Cost-231 Hata model (the most similar empirical model to EPM) presented in [61]), where the path loss predictions are overestimating the measurements by about 40 dBs. Differences can result from multiple causes such as that the CW tuning test did not cover all the terrains, especially in complex environments where different buildings, streets and foliage are present. Another reason is the almost impossible job of pre-

dicting the losses resulting from cables, connectors …etc. Antenna patterns slight differences play a role as well. Achieved results are highly matching and therefore these models can be used in the same live network in similar areas and traffic profiles.

4.6 Comparison between EPM and RT Simulation Models

Based on the previous experiments in modeling and comparing field measurements in EPM and RT simulation models, we could conclude that EPM models were easier and faster to use. Accuracy was good especially in environments where the needed result are mainly to show the coverage and capacity calculations. EPM are accurate for environments with the same characteristics (not too complicated terrains). The input parameters for the EPM models are usually qualitative and not very specific, (e.g. a dense urban area, a rural area, and so on). One of the main drawbacks of empirical models is that they cannot be used for different environments without modification through a continuous wave (CW) tuning test.

The Ray Tracing (RT) model is a multidimensional characterization of radio propagation environment including time delay, Direction of Arrival (DoA), Direction of Departure (DoD) profiles and time variance of the radio channel such as the Delay Spread (DS). This implies that RT propagation models are more capable of simulating the actual multipath propagation environment than EPM models.

The computation time for ray tracing simulations is its main disadvantage compared to EPM simulations. The RT simulations provide a more accurate path loss and more accurate channel characteristics compared to EPM, which is also confirmed in [62]. Table

4.10 summarizes few measures comparing EPM and RT models based on experimental field measurements and simulation works.

Table 4.10 Quantitative & qualitative measures for the experienced simulation models.

Model	Modeling Complexity	Computation Speed	Path Loss Prediction Accuracy	Ideal for
EPM	Medium	Very fast (12 sites in urban areas in couple of hours)	Medium (deviation within less than 10 dB) if CW is performed	Rural & Suburban Non-MIMO Systems
RT	Difficult	Extremely slow (16 sites in urban area in 21 days)	High (deviation within less than 5 dB)	Urban & Dense Urban, MIMO Systems

It is advisable to use EPM in cases where the radio environment is more homogeneous and the results are supposed to provide approximate coverage plots and capacity simulations. EPM accuracy increases significantly by using CW tests, which is radio environment dependent. This increases the complexity of EPM simulations [12].

The difference between the EPM prediction and the ray-tracing simulator may be explained on the basis that the EPM model was obtained by fitting the experimental data measured by Okumura and using only a few parameters to describe the environment. On the other hand, the ray-tracing simulator accounts for the actual geometry of the environment [62].

GSM and UMTS do not much benefit from RT simulations as MIMO and CoMP based systems used in LTE and WiMAX systems.

CHAPTER 5

SUMMARY, CONCLUSIONS AND RECOMMENDED FUTURE WORK

5.1 Introduction

Chapter 5 provides a summary; conclusions and recommended future work that can be done as an extension to this work.

5.2 Summary and Conclusions

An ongoing work in one of the biggest LTE testbeds worldwide is the evaluation of potential rate gains through different uplink CoMP schemes by using field trials to develop methods and schemes based on real field measurements [63]. This research was established to answer the open question of how close these measured channel conditions can be simulated using cutting-edge ray tracing (RT) technology and how we can correlate and evaluate their performance.

In chapter 2, we described the environments of field measurements, RT simulations, and UL CoMP processing tool chain. The steps and the procedures to establish this research were described, too. An example of that is the integration of RT simulator output with the CoMP tool chain.

In Chapter 3, few enhancements to increase the RT simulation accuracy were proposed and implemented. The AWGN term was introduced to RT channels due to the lack of hardware in effect in RT simulations. Emulation to real-world transmitted channel was introduced and denoted as Sample Time Offset (SaTO) and proven to have improved the accuracy of results. Signal Processing Simplification in the CoMP Chain for the RT channels improved the accuracy by a small value.

In Chapter 4, experimental work and numerical results were presented and analyzed. In the first experimental work, we modeled part of the testbed in the RT simulator. Received signal or path loss was compared for measurements and RT simulations when changing downtilt values at different locations in the testbed and under different radio conditions. The work showed good matching results between field measurements and RT simulations and highlighted measurements ICI errors. In a co-publication, the results shown that vertical beamforming through UE downtilting can improve SINR values by 5-10 dB. This work gave confidence in the RT simulator in terms of the predicted path loss that is essential for SNR and further results.

The second experimental work was the main part of this thesis and covered the complete testbed modeled in the RT simulator. An extended CIR was processed in a CoMP tool chain. SNR, SINR, and spectral efficiencies were evaluated and analyzed for 12 MIMO scenarios for both RT simulations and field measurements. These scenarios were combinations of conventional MIMO and CoMP (inter-site and intra-site) and signal processing approaches. Results showed that RT traces match field measurements at some scenarios such as inter-site CoMP and mismatch under other scenarios. Signal processing schemes such as SIC and EVM were applied and their influence was highlighted.

Field measurements rates are showing a high CoMP gain around 43%, while RT CoMP gain is around 18%. SIC improved the performance of conventional and CoMP schemes by around 10% at low spectral efficiencies. SIC had a smaller improvement over inter-site CoMP compared to other schemes.

Field measurements had 10% higher rates when using theoretical post-equalization schemes compared to EVM rates. In RT simulations, rates had around 5% higher values than rates when applying EVM approach. EVM approach is possible as in this study the transmitted signal is known.

RT simulation is a promising radio planning and propagation prediction technique that captures CoMP real-world measurements. RT simulations require proper modeling for RT algorithms and high accuracy 3D maps. A key parameter in RT modeling is the design of the ray launching step size that requires a compromise between accuracy and simulations time.

CoMP spectral efficiency (rate) gain over conventional MIMO was presented as a gain factor per MIMO scheme and a matching factor showing the differences between RT simulations and field measurements. RT rates have shown to form an upper bound to field measurements. RT simulations rates matched mostly with field measurements rates at the inter-site CoMP scenario with 88%.

Because we have available RT Channel State Information (CSI), the channel estimation part is by-passed for RT channels and a low complexity CSI signal processing approach is achieved. The signal processing simplifications could increase accuracy by a small ratio less than 5%. This showed that the current implemented estimators have high accuracy.

Geometrical analyses covered DoA, SNR per location, Symbol Time Offset (STO), TDOA and DS for both measurements and RT simulations. These geometrical properties showed that an ISI or ICI is unlikely due to a short inter-site distance in the test bed. STO plus DS was within the cyclic prefix time.

3D map missing objects and their impact on overall results is presented on particular locations. At these locations, two big buildings and trees alleys were missing from the RT 3D map. This leads to higher SNR values in RT simulations and higher spectral efficiencies compared to field measurements.

Inter-site CoMP showed less sensitivity to RT modeling errors while Conv. MIMO and Intra-Site CoMP were more sensitive. RT Simulations showed less CoMP gain compared to field measurements gain.

The real hardware and the measurements setup influenced the accuracy of field measurements and its matching with RT simulations results. The rates delta between Theo and EVM approaches emphasized that more errors occurred in field measurements. Inter-Site CoMP showed higher gain compared to intra-site CoMP.

Analyses based on both EPM and RT simulation models showed that EPM model is easier to model, and takes less simulation time to simulate measurements but requires some field measurements to tune the model. RT model is more difficult to model and requires longer simulation times and very accurate 3D digital maps but does not require field measurements for tuning.

5.3 Recommended Future Work

- In the field measurements, two UEs were transmitting at the same time and therefore causing interference towards each other. It is difficult to run more UEs in the testbed and reproduce the actual scenario in live networks due to hardware limitation. But this is possible using RT by placing as many as desired number of UEs to simulate the interference impact on the spectral efficiencies and how could CoMP and signal processing approaches could cope with it. Also in RT, simulation environment BS antenna patterns and other parameters can be controlled easily.
- For RT channels, channel estimation was removed. Channel interpolation was replaced by using the CTF of the simulated channels. In addition, the estimated STO was replaced by a known STO phase. Comparison results showed that the implemented estimators are quite accurate. It would be an interesting work to look further into the estimator implementation and parameters such as averaging window and the number of UEs to analyze their impact in terms of performance.

APPENDIX

CHANNEL IMPULSE RESPONSE MAGNITUDE for LINEAR ANTENNA ELEMENTS:

Simulation	Radio Path	Polarization	Co-polarized-element (CIR complex magnitude in mW)	Cross-polarized-element (CIR complex magnitude in mW)
Test 1	1	L+45	-0.000021155763368 + 0.000024665032705i	-0.00001063495221 + 0.000012170051348i
	2	L+45	0.000002199483917 + 0.000009499392371i	0.000003771947878 + 0.000017963785453i
	3	L+45	-0.000559985767562 - 0.001469249799479i	0.000102149879709 + 0.000260854525925i
Test 2	1	L-45	-0.00001063495221 + 0.000012170051348i	-0.000021155763368 + 0.000024665032705i
	2	L-45	0.000003771947878 + 0.000017963785453i	0.000002199483917 + 0.000009499392371i
	3	L-45	0.000102149879709 + 0.000260854525925i	-0.000559985767562 - 0.001469249799479i
Test 3	1	LH	-0.000007439336913 + 0.000008835286049i	-0.000022479430564 +

				0.000026046337719i
	2	LH	-0.00000111189993 - 0.000005985229747i	0.000004222439916 + 0.000019419399273i
	3	LH	-0.000468200606251 - 0.001223368500653i	-0.000323738860971 - 0.000854464492284i
Test 4	1	LV	-0.000022479430564 + 0.000026046337719i	-0.000007439336913 + 0.000008835286049i
	2	LV	0.000004222439916 + 0.000019419399273i	-0.00000111189993 - 0.000005985229747i
	3	LV	-0.000323738860971 - 0.000854464492284i	-0.000468200606251 - 0.001223368500653i

REFERENCES

[1] International Telecommunication Union (ITU). (2013, February) ICT Facts and Figures. http://www.itu.int/ITU-D/ict/facts/material/ICTFactsFigures2013.pdf

[2] M.C. Necker, "Towards frequency reuse 1 cellular FDM/TDM systems," in *9th ACM/IEEE International Symposium on Modeling, Analysis and Simulation of Wireless and Mobile Systems (MSWiM 2006)*, Malaga, Spain, 2006.

[3] Y. Peng, G. Mandyam, and D. Rajan, "CDMA vs. OFDM for wideband cellular systems," in *IEEE Signals, Systems and Computers, 42nd Asilomar Conference*, California, USA, 2008.

[4] A. Sibille, C. Oestges, and A. Zanella, *MIMO: From Theory to Implementation*. Oxford: Academic Press, 2010.

[5] S-H. Oh and N-H. Myung, "MIMO channel estimation method using ray-tracing propagation model," *IEEE Electronics Letters*, vol. 40, no. 21, pp. 1350-1352, 2004.

[6] 3GPP. (2009, October) RP-090939 (3GPP Submission Package for IMT-Advanced). http://www.3gpp.org/ftp/tsg_ran/TSG_RAN/TSGR_45/Documents/RP-090739.zip

[7] S. Parkvall et al., "LTE-Advanced - Evolving LTE towards IMT-advanced," in *The 68th IEEE Vehicular Technology Conference*, Calgary, Canada, 2008.

[8] S. Parkvall, J. Skold E. Dahlman, *4G: LTE/LTE-Advanced for Mobile Broadband: The 4G Solution for Mobile Broadband*.: Academic Press, 2011.

[9] H. Droste , P. Marsch , M. Grieger , G. Fettweis , S. Brueck , H.-P. Mayer , L. Thiele

and V. Jungnickel R. Irmer, "Coordinated multipoint: Concepts, performance, and field trial results," *IEEE Communications Magazine*, vol. 49, no. 2 , pp. 102 - 111 , 2011.

[10] N. Lebedev, J. M. Gorce V. Garcia, "Capacity-Fairness Trade-Off Using Coordinated Multi-Cell Processing," in *IEEE Vehicular Technology Conference (VTC Fall)*, San Francisco, USA, 2011.

[11] M.F. Iskander and Z. Yun, "Propagation prediction models for wireless communication systems," *IEEE Journal for Microwave Theory and Techniques*, vol. 50, no. 3, pp. 662 - 673, 2002.

[12] M. Amro, M.A. Landolsi, and S.A. Zummo, "Practical verifications for coverage and capacity predictions and simulations in real-world cellular UMTS networks," in *International Conference on Computer and Communication Engineering*, Kuala Lumpur, Malaysia, 2012.

[13] V. Degli-Esposti, F. Fuschini, E. Vitucci, and G. Falciasecca, "Speed-Up Techniques for Ray Tracing Field Prediction Models," *IEEE Transactions on Antennas and Propagation*, vol. 57, no. 5, pp. 1469-1480, 2009.

[14] Y. Corre and Y. Lostanlen, "3D urban propagation model for large ray-tracing computation," in *International Conference on Electromagnetics in Advanced Applications (ICEAA'07)*, Torino, Italy, 2007.

[15] T. Fugen, J. Maurer, W. Sorgel, and W. Wiesbeck, "Characterization of multipath clusters with ray-tracing in urban MIMO propagation environments at 2 GHz," in *IEEE Proceedings of the International Symposium on Antennas and Propagation*,

Washington, USA, 2005.

[16] D. Tse and P. Viswanath, *Fundamentals of Wireless Communication*.: Cambridge University Press, 2005.

[17] G. Stuber, *Principles of Mobile Communications*. Norwell, USA: Kluwer Academic Publishers, 2001.

[18] A. Goldsmith, *Wireless Communications*. New York: Cambridge University Press, 2005.

[19] J.W. Schuster and R. J Luebbers, "Comparison of GTD and FDTD predictions for UHF radio wave propagation in a simple outdoor urban environment," in *IEEE Antennas and Propagation Society International Symposium*, Montreal, Canada, 1997.

[20] David Jenn. Radiowave Propagation, Department of Electrical and Computer Engineering, Naval Postgraduate School. http://www.dcjenn.com/EC3630/GO&GTD%28v1.5%29.pdf

[21] I. Sen, "5 GHz Channel Characterization for airport surface areas and vehicle to vehicle communication systems," Electrical Engineering & Computer Science, Ohio University, Ohio, USA, Doctor of Philosophy (PhD) dissertation 2007.

[22] C. Cerasoli, "The Use of Ray Tracing Models to Predict MIMO Performance in Urban Environments," in *IEEE Military Communications Conference*, Washington, USA, 2006.

[23] H. Ling, R. Chou, and S. Lee, "Shooting and bouncing rays: Calculating the RCS of

an arbitrarily shaped cavity," *IEEE Transactions on Antennas and Propagation*, vol. 37, no. 2, pp. 194 - 205, 1989.

[24] G. Durgin, N. Patwari, and T. S. Rappaport, "Improved 3D ray launching method for wireless propagation prediction," *Electronics Letters*, vol. 33, no. 16, pp. 1412 - 1413, 1997.

[25] J. O'Rourke, *Computational Geometry in C.*: Cambridge University Press, 1993.

[26] M. F. Catedra, J. Perez, and F. S. de Anana, "Efficient ray-tracing techniques for three-dimensional analyses of propagation in mobile communications: application to picocell and microcell scenarios," *IEEE Antennas and Propagation Magazine*, vol. 40, no. 2, pp. 15 - 28, 1998.

[27] R. Ibernon-Fernandez, J-M. Molina-Garcia-Pardo, and L. Juan-Llacer, "Comparison Between Measurements and Simulations of Conventional and Distributed MIMO System," *IEEE Antennas and Wireless Propagation Letters*, vol. 7, pp. 546 - 549, 2008.

[28] J-M. Molina-Garcia-Pardo, J-V. Rodríguez, and L. Juan-Llacer, "Parametric MIMO Model for Ray Tracing/Launching Simulations," in *IEEE Vehicular Technology Conference*, Los Angeles, USA, 2004.

[29] K. H. Ng, E. K. Tameh, and A. R. Nix, "Modelling and performance prediction for multiple antenna systems using enhanced ray tracing," in *IEEE Wireless Communications and Networking Conference*, New Orleans, USA, 2005.

[30] R. Fritzsche, J. Voigt, C. Jandura, and G. Fettweis, "Comparing Ray Tracing Based

MU-CoMP-MIMO Channel Predictions with Channel Sounding Measurements," in *European Conference on Antennas and Propagation (EuCAP)*, Barcelona, Spain, 2010.

[31] A. Ludwig, "The definition of cross polarization," *IEEE Transactions on Antennas and Propagation*, vol. 21, no. 1, pp. 116-119, 1973.

[32] IEEE Antennas and Propagation Society. (1993) 145-1993 - IEEE Standard Definitions of Terms for Antennas.

[33] kathrein Scala Division. Dual Polarized Base Station Antennas For Polarization Diversity Systems. http://www.kathrein-scala.com/tech_bulletins/DualPolarized.pdf

[34] Kathrein Scala Division. Advanced X-POL Antenna Standards. http://www.kathrein-scala.com/tech_bulletins/AdvancedXpol.pdf

[35] G. J. Foschini and M. J. Gans, "On limits of wireless communications in a fading environment when using multiple antennas," *IEEE Wireless Personal Communications*, vol. 6, no. 3, pp. 311-335, 1998.

[36] A.F. Naguib, N. Seshadri, and A.R. Calderbank, "Increasing data rate over wireless channels," *IEEE Signal Processing Magazine*, vol. 17, no. 3, pp. 76 – 92, 2000.

[37] J. Xuehua and C. Peijiang, "Research and Simulation of MIMO-OFDM Wireless Communication System," in *International Forum on Information Technology and Applications*, Chengdu, China, 2009.

[38] R. Hoppe, J. Ramulu, H. Buddendick, O. Staebler, and G. Woelfle, "Comparison of MIMO Channel Characteristics Computed by 3D Ray Tracing and Statistical

Models," in *2nd European Conference on Antennas and Propagation (EuCAP 2007)*, Edinburgh, UK, 2007.

[39] P. Marsch and G. Fettweis, "Uplink CoMP under a Constrained Backhaul and Imperfect Channel Knowledge," *IEEE Transactions on Wireless Communications*, vol. 10, no. 6, pp. 1730 - 1742, 2011.

[40] P. Baier, M. Meurer, T. Weber, and H. Troeger, "Joint transmission (JT), an alternative rationale for the downlink of time division CDMA using multi-element transmit antennas," in *IEEE International Symposium on Spread Spectrum Techniques and Applications (ISSSTA)*, Parsippany, NJ, USA, 2000.

[41] S. Shamai and B. Zaidel, "Enhancing the cellular downlink capacity via co-processing at the transmitter end," in *IEEE Vehicular Technology Conference (VTC'01 Spring)*, Atlantic City, NJ, USA, 2001.

[42] S. Venkatesan, "Coordinating base stations for greater uplink spectral efficiency in a cellular network," in *IEEE Personal Indoor and Mobile Radio Communications*, Athens, Greece, 2007.

[43] G.J. Foschini, K. Karakayali, and R.A. Valenzuela, "Coordinating multiple antenna cellular networks to achieve enormous spectral efficiency," *IEE Communications*, vol. 153, no. 4, pp. 548 - 555, 2006.

[44] 3GPP, "Report of 3GPP TSG RAN WG1 #59bis," Valencia, Spain, 2010.

[45] A. Müller and P. Frank, "Performance of the LTE Uplink with Intra-Site Joint Detection and Joint Link Adaptation," in *IEEE Vehicular Technology Conference*

(VTC 2010-Spring), Taipei, Taiwan, 2010.

[46] M. Necker, "Interference Coordination in Cellular OFDMA Networks," *IEEE Network: The Magazine of Global Internetworking*, vol. 22, no. 6, pp. 12-19, 2008.

[47] S. Jaeckel et al., "Intercell Interference Measured in Urban Areas," in *IEEE international conference on Communications (ICC09)*, Dresden, Germany, 2009.

[48] V. Jungnickel et al., "Capacity measurements in a cooperative multicell MIMO network," *IEEE Transactions on Vehicular Technology*, vol. 58, no. 5, pp. 2392 - 2405, 2009.

[49] S. Jaeckel et al., "Correlation properties of large and small scale parameters from multicell channel measurements," in *European Conference on Antennas and Propagation (EuCAP'09)*, Berlin, Germany, 2009.

[50] Z. Yun, Z. Zhang, and M. F. Iskander, "A ray-tracing method based on the triangular grid approach and application to propagation prediction in urban environments," *IEEE Transactions on Antennas and Propagation*, vol. 50, no. 5, pp. 750-758, 2002.

[51] T. Fuegen, S. Knoerzer, M. Landmann, R. Thomae, and W. Wiesbeck, "A 3d ray tracing model for macrocell urban environments and its verification wih measurements," in *2nd European Conference on Antennas and Propagation (EuCAP)*, Edinburgh, Scotland, 2007.

[52] E. M. Vitucci, V. Degli-Esposti, and F. Fuschini, "MIMO channel characterization through ray tracing simulation," in *European Conference on Antenna and Propagation*, Nice, France, 2006.

[53] R. Irmer et al., "Multisite field trial for LTE and advanced concepts," *IEEE Communications Magazine*, vol. 47, no. 2, pp. 92 - 98, 2009.

[54] M. Grieger, G. Fettweis, and P. Marsch, "Large Scale Field Trial Results on Uplink CoMP with Multi Antenna Base Stations," in *IEEE Vehicular Technology Conference (VTC Fall)*, San Francisco, USA, 2011.

[55] P. Marsch , Z. Rong and G. Fettweis M. Grieger, "Field trial results for a coordinated multi-point (CoMP) uplink in cellular systems," in *ITG/IEEE Workshop on Smart Antennas (WSA\'10)*, Bremen, Germany, 2010.

[56] P. Marsch, M. Grieger, and G. Fettweis, "Large scale field trial results on different uplink coordinated Multi-Point (CoMP) concepts in an urban environment," in *IEEE Wireless Communications and Networking Conference (WCNC '11)*, Cancun, Mexico, 2011.

[57] J. Deissner, J. Huebner, D. Hunold, and J. Viogt. (2011) RPS Radiowave Propagation Simulator.

[58] M. Grieger, V. Kotzsch, and G. Fettweis, "Comparison of intra and inter site coordinated joint detection in a cellular field trial," in *IEEE 23rd International Symposium Personal Indoor and Mobile Radio Communications (PIMRC)*, Sydney, Australia, 2012.

[59] M. Danneberg, J. Holfeld, M. Grieger, M. Amro, and G. Fettweis, "Field Trial Evaluation of UE Specific Antenna Downtilt in an LTE Downlink," in *16th International ITG Workshop on Smart Antennas (WSA2012)*, Dresden, Germany, 2012.

[60] Y. Li R. Liu, H. Chen, and Z. Wang, "EVM estimation by analyzing transmitter imperfections mathematically and graphically," *Analog Integrated Circuits and Signal Processing*, vol. 48, no. 3, pp. 257-262, 2006.

[61] J. Chebil, A. K. Lwas, M. R. Islam, and A. Zyoud, "Comparison of empirical propagation path loss models for mobile communications in the suburban area of Kuala Lumpur," in *International Conference On Mechatronics (ICOM)*, Kuala Lumpur, Malaysia, 2011.

[62] D. Erricolo and P.L.E. Uslenghi, "Propagation path loss-a comparison between ray-tracing approach and empirical models," *IEEE Transactions on Antennas and Propagation*, vol. 50, no. 5, pp. 766-768, 2002.

[63] German Federal Ministry for Education and Research; Deutsche Telekom; Vodafone; Fraunhofer Institute for Communications; Vodafone Chair Mobile Communications Systems; Heinrich-Hertz Institute (HHI). (2011) Easy-C. http://www.easy-c.de/index_en.html

VITAE

Name: Mohammad Hasan Suleiman Amro

Nationality: Jordanian

Date of Birth: 6/20/1981

Email: mohammad.amro@ieee.org

Address: Riyadh - King Faisal District - Prince Saud bin Abdulaziz Al-Saud Al-Kabir Road, Building 166

Academic Background: A holder of a BSc. in Electronics and Communication Engineering (ECE), University of Aden, Faculty of Engineering. Graduated in 2004 with a CGPA 4.46/5.00 as the top class student.

Industry Experience: Worked for around 10 years in the field of Radio Network Planning and Optimization (RNP & RNO) engineering. Worked for Huawei Technologies and Etihad Etisalat (Mobily) in many positions and currently as a Senior Engineer in Huawei Technologies. Projects experiences covered roll out, swap and live network operations for GSM, UMTS and LTE cellular systems.

Publications :

- **M. Amro**, M.A. Landolsi, and S.A. Zummo, "Practical Verifications for Coverage and Capacity Predictions and Simulations in Real-world Cellular UMTS Networks," in proceedings of the International Conference on Computer and Communication Engineering (ICCCE 2012), Kuala Lumpur, Malaysia, 2012.

- M. Danneberg, J. Holfeld, M. Grieger, **M. Amro**, and G. Fettweis, "Field Trial Evaluation of UE Specific Antenna Downtilt in an LTE Downlink," in proceedings of the 16th International ITG Workshop on Smart Antennas (WSA2012), Dresden, Germany, 2012.
- M. Grieger, **M. Amro**, M. Danneberg, J. Voigt, M. A. Landolsi, S. A. Zummo, and G. Fettweis, "Uplink Coordinated Multi-Point in Field Trials and Ray Tracing Simulations," accepted on December for publication in the 8th European Conference on Antennas and Propagation (EuCAP 2014)., the Hague - the Netherlands, 2014.